

FINAL REPORT

**ADVANCED COMPOSITE SOLDERS
FOR MICROELECTRONICS**

SBIR PHASE II

CONTRACT No. DAAL01-93-C-0056

SUBMITTED

TO

**ARMY RESEARCH LABORATORIES
2800 POWDER MILL ROAD
ADELPHI, MD 20783-1197**

BY

**HIGH PERFORMANCE MATERIALS INC
500 W, NINTH STREET
HERMANN, MO-65041**

FEBRUARY 1997

DISTRIBUTION STATEMENT A
Approved for public release;
Distribution Unlimited

19970219 051

FINAL REPORT
ADVANCED COMPOSITE SOLDERS
FOR MICROELECTRONICS
SBIR PHASE II
CONTRACT No. DAAL01-93-C-0056

SUBMITTED
TO
ARMY RESEARCH LABORATORIES
2800 POWDER MILL ROAD
ADELPHI, MD 20783-1197

BY
HIGH PERFORMANCE MATERIALS INC
500 W, NINTH STREET
HERMANN, MO-65041

FEBRUARY 1997

DTIC QUALITY INSPECTED 4

TABLE OF CONTENTS

FIGURES	ii
TABLES	vi
PREFACE	viii
1. INTRODUCTION	1
2. OBJECTIVES OF II PHASE CONTRACT	2
3. TASKS OF II PHASE CONTRACT	2
4. SUMMARY	2
5. DESCRIPTION OF RESEARCH WORK	6
5.1 Scaling Up Of HPM's Powder Production Facility To 100 Lbs Per Batch	6
5.2 Processing Of Eutectic Lead-Tin, Alloy Lead-Tin Powders And Lead Less Powders	9
5.3 Consolidation and Extrusion of Solder Powders	19
5.4 Microstructures And Mechanical Property Testing Of Eutectic and Alloy Solders	20
5.4.1 Tensile Properties Of Bulk Solder Alloys	23
5.4.2 Tensile /Shear Properties Of Lap-shear Joints	31
5.4.3 Fatigue testing of lap shear joints	39
5.4.4 Fractography Of Lap-Shear Joints Deformed In Low Cycle Fatigue.	40
5.4.5 High Cycle Fatigue Behavior Bulk Solder Alloys	46
5.4.6 Creep Properties Of Lap-Shear Joints	48
5.4.7 Thermomechanical Fatigue Tests Of lap-Shear Joints	55
5.4.8 Metallography Of Lap-Shear Joint Samples Tested For TMF	63
5.5 Straddle Board Tests	73
5.6 Scaling Up Of HPM's Powder Production Facility To 500 Lbs Per Batch	85
5.6.1 Production of eutectic lead-tin and composite lead-tin powders.	90
5.6.2 Production of composite Pb-Sn -1 % WC ₃ , Pb-Sn-1% SiO ₂ , and Pb-Sn-1% Al ₂ O ₃ powders.	91
6. CONCLUSIONS	97
REFERENCES	99

FIGURES

Figure 1.	Schematic diagram of the HPM's 100 lbs per batch powder production equipment.	7
Figure 2.	Schematic diagram of the guide tube assembly.	8
Figure 3.	Effect of exit hole diameter on the mean powder size during atomization process.	10
Figure 4.	Scanning electron micrograph of eutectic solder powder in the size range 25 -44 μm .	11
Figure 5.	Scanning electron micrograph of eutectic solder powder in the size range 25 -44 μm .	11
Figure 6.	Scanning electron micrograph of eutectic solder powder in the size range 25 -44 μm before sieving.	12
Figure 7.	Scanning electron micrograph of Pb-Sn-In solder powder in the size range 25 -44 μm (a) before sieving (b) after ultrasonic sieving.	13
Figure 8.	Scanning electron micrograph of Pb-Sn-Bi solder powder in the size range 25 -44 μm before sieving.	13
Figure 9.	Scanning electron micrograph of Pb-Sn-Ag solder powder in the size range 25 -44 μm before sieving.	14
Figure 10.	Scanning electron micrograph of Pb-Sn-Cu solder powder in the size range 25 -44 μm before sieving.	14
Figure 11.	Scanning electron micrograph of Pb-Sn-Sbsolder powder in the size range 25 -44 μm before sieving.	15
Figure 12.	Scanning electron micrograph of Pb-Sn-2.5%Ni solder powder in the size range 25 -44 μm (a) before sieving and (b) after sieving.	15
Figure 13.	Scanning electron micrograph of Pb-Sn-5%Ni solder powder in the size range 25 -44 μm (a) before sieving and (b) after sieving.	16
Figure 14.	Powder size distribution in the case of Pb-Sn-In powders.	16
Figure 15.	Powder size distribution in the case of Pb-Sn-2.5 %Ni powders.	17
Figure 16.	Powder size distribution in the case of Pb-Sn-5 % Ni powders.	17
Figure 17.	SEM micrograph of the Sn-3.2% Ag-6.8% Bi alloy after ultrasonic sieving.	18
Figure 18.	SEM micrograph of the Sn-3 % Ag-4.2 % Bi-6.8 5 In alloy after ultrasonic sieving.	18

Figure 19.	Extrusion press used for extruding consolidated solder powders into cylindrical rods.	19
Figure 20.	Geometry and dimensions of the tensile specimen.	20
Figure 21.	Geometry of the copper substrate for fabrication of lap-shear joint.	21
Figure 22.	Schematic diagram of the sample holder for fabrication of lap-shear joint.	22
Figure 23	(a) SEM micrograph of the extruded Pb-Sn-5%Ni alloy.	28
	(b) SEM micrograph of the extruded and annealed Pb-Sn-5%Ni alloy.	28
Figure 24.	EDAX of the intermetallic phase in SEM micrograph of the extruded Pb-Sn-5 %Ni alloy.	29
Figure 25.	(a) SEM micrograph of the extruded Pb-Sn-5% Cu alloy.	30
	(b) SEM micrograph of the extruded and annealed Pb-Sn-5%Cu alloy.	30
Figure 26.	Tensile yield strengths of Sn-Ag based solders compared with other solder alloys.	31
Figure 27.	Side view of layers in a solder joint.	32
Figure 28.	A SEM micrograph of the lap shear joint of dispersion strengthened alloy.	33
Figure 29.	(a)SEM micrograph of the eutectic lap shear joint failed in tension at room temperature.	38
	(b)SEM micrograph of the eutectic lap shear joint failed in tension at 125 °C.	39
Figure 30.	Life times for room temperature low cycle fatigue tests.	40
Figure 31.	SEM fractographs of Pb-Sn eutectic failed in low cycle fatigue at displacements of (a) ± 1.0 mil (b) ± 1.5 mil and (c) ± 2 mil.	41

Figure 32.	SEM fractographs of dispersion strengthened solder alloy failed in low cycle fatigue at displacements of (a) ± 1.0 mil (b) ± 1.5 mil and (c) ± 2 mil.	42
Figure 33.	Summary of low cycle fatigue lives of selected lap-shear joint solder alloys as a function of temperature.	44
Figure 34.	Hysteresis curve and maximum load, minimum load and area vs. cycle for low cycle fatigue test of Sn-Pb-2.5 In at 75 ° C.	45
Figure 35.	High cycle fatigue properties of bulk solders.	46
Figure 36.	SEM fractograph of the Pb Sn -5 Ni sample failed in high cycle fatigue test under stress amplitude of ± 4 ksi, at 75 ° C, and at R= -1.	47
Figure 37.	Typical displacement vs. time plots obtained for eutectic Pb-Sn at 75 ° C.	49
Figure 38.	Steady state creep rate vs. applied stress for lap shear joints of selected solder compositions (a) Room temperature (b) 75 ° C and (c) 125 ° C.	50
Figure 39.	Fracture surfaces of Pb-Sn eutectic samples failed in creep at (a) room temperature (b) 75 ° C and (c) 125 ° C.	52
Figure 40.	Fracture surfaces of dispersion strengthened Pb-Sn -5 % Ni samples failed in creep at (a) room temperature (b) 75 ° C and (c) 125 ° C.	53
Figure 41.	SEM micrographs of eutectic Sn-Pb solder joint after 3 hours of creep test at (a) room temperature and (b) 125 ° C.	54
Figure 42.	Flow diagram of computer and its interface with controllers and data acquisition boards.	55

Figure 43.	Schematic diagram of the furnace and attachments used in TMF tests.	56
Figure 44.	Typical temperature and displacement curves for a TMF test.	57
Figure 45.	Hysteresis curves and maximum load, minimum load and area vs cycle for HPM Pb-Sn eutectic alloy during TMF tests.	60
Figure 46.	Hysteresis curves and maximum load, minimum load and area vs cycle for Pb-Sn-5 %Ni alloy during TMF tests.	61
Figure 47.	Comparison of the lifetimes of various solder alloy compositions obtained during TMF testing of lap shear joints.	62
Figure 48.	Schematic diagram of the location of lap-shear joints for metallographic examination.	63
Figure 49.	Sample EDS of the intermetallic layer.	64
Figure 50.	SEM micrograph of eutectic solder alloy after TMF test	65
Figure 51.	SEM micrograph of Sn-Pb-5%Ni alloy after TMF test.	66
Figure 52.	SEM micrograph of Sn-Pb-5%Cu alloy after TMF test.	67
Figure 53.	SEM micrograph of Sn-Pb-2.5%Ag alloy after TMF test.	68
Figure 54.	SEM micrograph of Sn-Sb alloy after TMF test.	69
Figure 55.	Typical reflow profile of low range solder paste.	74
Figure 56.	Typical reflow profile of mid range solder paste.	75
Figure 57.	Typical reflow profile of high range solder paste.	76

Figure 58.	Drawing of the straddle board with various devices.	81
Figure 59.	The test set-up used in thermal cycling of straddle board.	81
Figure 60.	Fracture surfaces of joints made in (a) high vacuum and (b) low vacuum.	84
Figure 61.	Lay out of HPM's 500 lbs per batch powder production equipment.	85
Figure 62.	The schematic diagram of new convergent type atomizer.	86
Figure 63.	Schematic diagram of modified guide tube assembly.	87
Figure 64.	Stairs and landing drawing of the 500 pounds per batch powder production equipment.	88
Figure 65.	Engineering drawing of the 500 pounds per batch powder production equipment (a) top view and (b) side view.	89
Figure 66.	SEM micrograph of sieved eutectic solder powders.	91
Figure 67.	SEM micrograph of the sieved Sn-Pb-1 wt% WC ₃ solder powders.	93
Figure 68.	SEM micrograph of the sieved Sn-Pb-1 wt% SiO ₂ solder powders.	95
Figure 69.	SEM micrograph of the sieved Sn-Pb-1 wt% Al ₂ O ₃ solder powders.	96

TABLES

Table 1.	Tensile properties of dispersion strengthened and tin based solder alloys.	24
Table 2.	Tensile properties of dispersion strengthened and tin based solder alloys.	25
Table 3.	Comparison between the present tensile data and the previous tensile data obtained during SBIR Phase I for dispersion strengthened alloys.	26
Table 4.	Comparison between the present tensile data and the previous tensile data obtained during SBIR Phase I for solid solution strengthened alloys.	27
Table 5.	Analysis of as made lap shear joints.	34

Table 6.	Tensile test results of unaged lap shear joints at a displacement rate of 0.0001 inch sec ⁻¹ .	35
Table 7.	Tensile test results of aged lap shear joints at a displacement rate of 0.0001 inch sec ⁻¹ .	36
Table 8.	Results of the room and elevated temperature tensile testing of lap shear joints at a displacement rate of 1.67×10^{-6} sec ⁻¹	37
Table 9.	Low cycle fatigue data at elevated temperatures.	43
Table 10.	Creep exponents and activation energies.	51
Table 11.	TMF test parameters.	58
Table 12.	Lifetime results of TMF tests.	59
Table 13.	Summary of measurements made for SEM micrographs after TMF tests.	70
Table 14.	Crack propagation sites for samples failed in thermomechanical fatigue.	71
Table 15.	Solder compositions used in the straddle board testing.	73
Table 16.	Results of the thermal cycling tests of the straddle boards.	77
Table 17.	Flux activation and melting temperatures of solder pastes and alloy solders	80
Table 18.	Summary of the results of thermal cycling test.	82
Table 19.	Process parameters used for processing eutectic solder powders.	90
Table 20.	Powder size distribution for eutectic solder powders.	90
Table 21.	Process parameters maintained for production of composite solder powders.	92
Table 22.	Sieve analysis of Pb-Sn-1 wt% WC ₃ powders.	92
Table 23.	Sieve analysis of Pb-Sn-1 wt % SiO ₂ and Pb-Sn-1 wt % Al ₂ O ₃ composite solders.	94

PREFACE

High Performance Materials Inc., submits this final report of the research on "Advanced Composite Solders for Microelectronics" conducted under SBIR phase II contract No. DAAL01-93-C-0056 with Ms. Cynthia Sarafidis, Mr. Tom Gher, Mr. George Lucey as the program Managers. The work was done by High Performance Materials Inc., in collaboration with Washington University St. Louis, MO: Dr. Rao K. Mahidhara and Dr. Hariprasad Sreedharamurthy were the co-principal investigators of High Performance Materials Inc. and Prof. Shankar M.L. Sastry was the principal investigator for Washington University St. Louis. Other co-investigators were Frank Guss of High Performance Materials Inc., and Prof. K.L. Jerina, Dr. Gerald Kuo, Mr. Steven Bayhnam and Mr. Brett Goldstein of Washington University St. Louis.

1. INTRODUCTION

Advanced solder alloys are needed in the electronics industry due to increased use of surface mount technology [1]. In the surface mount technology, the components are directly mounted to the board surface. As a result, the solder joints function as structural members in addition to providing electrical connections. As structural members solders require improved mechanical properties such as high creep resistance, higher fatigue resistance and higher thermo mechanical fatigue resistance [2]. Conventional solders do not possess these attractive mechanical properties. The properties of conventional solders can be improved by adopting a composite strategy i.e., adding fibrous or particulate reinforcement in a solder matrix to increase the overall yield stress, to improve creep resistance, extend fatigue life and increase fracture toughness by terminating or dispersing propagating cracks. The technology gap to be resolved, however is selection of a filler material which is lead-free, has high strength, wets and disperses well in solder joints, and resists degradation in long term aging. Several approaches are being pursued such as mechanical alloying, powder blending in solid or molten state and placing fiber cloth over the solder melt. Mechanical alloying produces significant oxygen contamination and is not a viable approach for solders. Powder blending introduces reinforcements which are coarse resulting in degradation of mechanical properties. The fiber composite would be unsuitable for penetrating crevice areas of solder joints and the concept is not practical for mass production applications.

High Performance Materials Inc. (HPM, Hermann, MO) has developed a method to produce in-situ composite solders employing rapid solidification process and has successfully demonstrated under an Army SBIR Phase I program on Advanced Composite Solder for Microelectronics (Contract No. DAAL02-92-C-0012), the feasibility of developing, by induction melting and inert gas atomization, in-situ composite solders with a good balance of strength, ductility, creep resistance and high cycle fatigue resistance. In the Phase II of this program, HPM developed a low cost commercial method for producing in-situ composite solders as well as lead-free solder for use as solder paste and bulk solder applications. In this report, the results of the work carried out in II phase program are discussed.

2. OBJECTIVES OF THE PHASE II CONTRACT

The objectives of the Phase II work were

- 1) Increase solder powder production capacity of the HPM production facility from 10 lb/batch to 500 lbs/batch for the production of conventional 63 Sn-37 Pb solder powders, ternary and quaternary 63Sn-37 Pb-X(X=Ni,Cu,Ag,Sb,In or Bi) solder powders, and lead free Sn-based solder powders.
- 2) Perform a comprehensive study of the physical, mechanical and solderability/wettability properties of the solder powders.

3. TASKS OF PHASE II CONTRACT

The four main tasks of the phase II contract were

i) Optimization of the 100 lb/batch powder production unit

- Evaluate melt-flow control by melting-plug/melt-freezing (MPMF) approach
- Evaluate gas atomization by nitrogen at cryogenic, room, and elevated temperatures
- Determine best conditions for melt-flow and atomization stability,
- Produce 100 lb solder alloy powders of each composition,
- Determine chemical composition, size distribution, and morphology of powders, and powder yield in the 25-75 μm size range.

ii) Consolidation, Extrusion, Microstructural evaluation and Mechanical property testing of Solders

- Consolidate solder powders by cold pressing at room temperature and extruding at 100 ° C into 0.25 in. diameter rods with an extrusion ratio of 16:1.
- Prepare 0.25in. diameter 3.0 in long reflowed specimens from extruded samples.
- Determine microstructures of powders, and extruded and reflowed samples.
- Perform tensile tests at 25, 75 , and 125 ° C, isothermal fatigue tests at 25 and 75 °C, constant stress tests at 25-125°C on extruded and selected reflowed samples.

iii) Optimization of the 500 lb/batch commercial powder production unit

Design, fabricate, and install a 500 lbs 63/37 Sn-Pb solder crucible unit.

Rearrange and modify the melt and powder unit into the powder production facility.

Incorporate nitrogen recirculation unit into the powder production facility.

Evaluate the feasibility and cost effectiveness of using cryogenic or heating unit for atomization gas (nitrogen)

Test the performance of the 500 lb solder crucible units. The objective is to establish a reliable operation within a definable variation in powder size range, yield, and quality.

Determine the feasibility of recycling of residual charge material, and minimizing turnaround time between production runs.

Establish methodology and necessary facilities for powder sieving in quantities of upto 500 lbs , and at the same time, safeguards for removing fine and extrafine powders from polluting the environment and for protecting workers from health hazard by dust pollution.

iv) Tensile, creep, isothermal and thermomechanical fatigue testing of bulk solder specimens and solder-joints

Consolidate the solder powders by cold pressing at 25°C and extruding at 100 ° C into 0.25 in diameter rods with an extrusion ratio of 16:1.

Prepare 0.25 in. diameter 3.0 in long reflowed specimens.

Perform tensile tests at 25, 75, and 125 ° C , isothermal fatigue tests at 25 and 75 ° C, constant stress creep tests at 25-125 ° C on extruded and selected reflowed samples.

Develop experimental procedures for thermomechanical fatigue testing of solder alloys and perform in-phase and out-of-phase TMF tests on selected solder compositions.

Develop experimental techniques for the preparation and testing of double shear solder joint specimens and perform joint tests on selected specimens.

4. SUMMARY

During the period from July 15, 1994 to December 31, 1996 the following results were accomplished.

- The powder production facility at HPM was scaled up from 10 lbs per batch to 100 lbs per batch successfully and design modifications were completed for capacity. This involved redesigning, fabrication and assembly of the melt, atomization and powder collection chambers, induction furnace, and cyclone system. Several new features such as, stainless steel control rod for control of flow of molten metal, guide tube heater assembly, modified ceramic bracket to position the graphite crucible, water cooled top plate, and energy efficient gas atomizer were introduced.
- Eutectic solder powders and alloy solder powders containing alloying elements such as Ag, Bi, Cu, In, Ni and Sb were successfully produced. The quality of the sieved powders was excellent and the percentage yield of 25 -44 μm range powders was 70 %.
- Physical characterization of sieved powders was done using Scanning electron Microscopy (SEM) and the chemical composition of the powders was analyzed. The powders were smooth and spherical in nature without occurrence of satellites and the powders conformed to the desired chemical composition. The sieved powders were consolidated and extruded to make bulk specimens and powders were used to make solder paste. The melting points for the eutectic and alloy solders were determined.
- The lap shear joints were prepared using solder paste on copper substrates. Single lap-shear specimens and an auxiliary jig were used to insure reproducible joint thickness and alignment during fabrication. Bulk samples were machined from the extruded cylindrical bars.
- Microstructures of extruded, reflowed and lap shear joints were determined. Mechanical properties such as tensile strengths, creep properties and fatigue properties at room and elevated temperatures, were carried out for extruded bulk samples and for lap shear joints.

- Experimental procedures for thermomechanical fatigue testing of solder alloys for performing in-phase and out-of-phase were developed. Thermomechanical fatigue testing of selected alloy compositions was carried out for lap shear joints. The dispersion strengthened solder alloy compositions exhibited the best tensile strengths, creep resistance and high cycle fatigue behavior at room and elevated temperatures among lead containing alloys. The dispersion strengthened solder alloy and lead free alloys had the longest life times in the thermomechanical fatigue tests. In the thermomechanical tests, the solid solution strengthened alloys had the lowest life times while the eutectic alloys exhibited life times which were in-between. Creep results of the lap-shear joints showed that solid solution strengthened and eutectic alloys deformed by dislocation climb. The presence of large threshold stress was observed for dispersion strengthened solder alloys indicative of dispersion strengthening remaining effective at higher temperatures.
- Printed wire assemblies on a straddle board using different types of components were assembled at Electronics Manufacturing Productivity facility (EMPF) using solder pastes of HPM solders. Thermal cycling tests were carried out at EMPF and at Trace Laboratories, Chicago, for 1000 hours. The eutectic and solid solution strengthened solder alloys showed higher lifetimes than dispersion strengthened and lead free alloys. These results do not agree with those obtained in the thermomechanical tests. The poor performance of the dispersion strengthened and lead free alloys in the straddle board tests may be attributed to (i) unsatisfactory wetting properties of the alloy solder compositions during mounting of components, (ii) absence of good vacuum during reflowing and (iii) use of an unsuitable flux during paste making of these alloy solders.
- The 100 lbs per batch powder production equipment was scaled up to 500 lbs per batch. Several design modifications were implemented and a few test runs were conducted to optimize the powder production. The 500 lbs powder production equipment was successfully used to produce the eutectic solder powders and composite solder powders containing 1wt% Al_2O_3 , 1wt% SiO_2 and 1wt% WC_3 . The powder size distribution of the powders is narrow and the percentage yield of 25-44 μm is about 65 %.

5. DESCRIPTION OF RESEARCH WORK

5.1 Scaling Up Of HPM's Powder Production Facility To 100 Lbs Per Batch

In the phase I of this SBIR program, a 10 pounds per batch powder production equipment was fabricated [3]. The HPM's free fall powder production equipment essentially consists of (1) A melting chamber, (2) A furnace and a crucible, (3) Induction power supply, (4) An atomizer, (5) An atomization chamber, (6) Inert gas supply and gas lines, (7) A vacuum pump, (8) A powder collection chamber, and (9) A cyclone. Figure 1 shows a schematic diagram of the powder production equipment. In the phase II of the SBIR program, the existing powder production equipment was scaled up to a capacity of 500 pounds per batch in two stages.

In the first stage, the capacity of the powder production equipment was increased to 100 pounds per batch. This involved redesign, assembly and fabrication of melt chamber. The height of the furnace was increased to 17 inches with an internal diameter of 8.5 inches and a wall thickness of 3 inches. The heating elements consisted of 34 turns of copper tubing which had an outer diameter of 0.375 inch and wall thickness of 0.062 inch. The 17 inches tall graphite crucible with an internal diameter of 7.75 inches is housed inside the furnace. The graphite crucible is tapered at the bottom with a 0.25 inch in exit hole. A conical shaped nozzle with a centered through hole of variable diameter was snugged into the exit hole at the crucible bottom. The molten metal flow, through the crucible exit hole is controlled by a 2 inch diameter stainless steel stopper. The stopper is called control rod and its vertical motion is controlled by a piston in an air cylinder operable at 90 lbs pressure.

A ceramic bracket positions the graphite crucible. A stainless steel plate (B100-1) supports the ceramic bracket and the crucible. The rocking of this steel plate is avoided by bolting it to another 35 inch diameter base plate of stainless steel using 8, 4.25 inches long threaded steel rods of 0.25 inch diameter. The base plate separates the melt section from the atomization section. Between the base plate and plate (B100-1) is another circular plate designated (C100-1). This plate snugs into the groove of a hollow circular plate (A1) which serves as an inlet and outlet for the flowing atomizing gas. The circular plate A1 snugs into another plate called A2 which houses the atomizer.

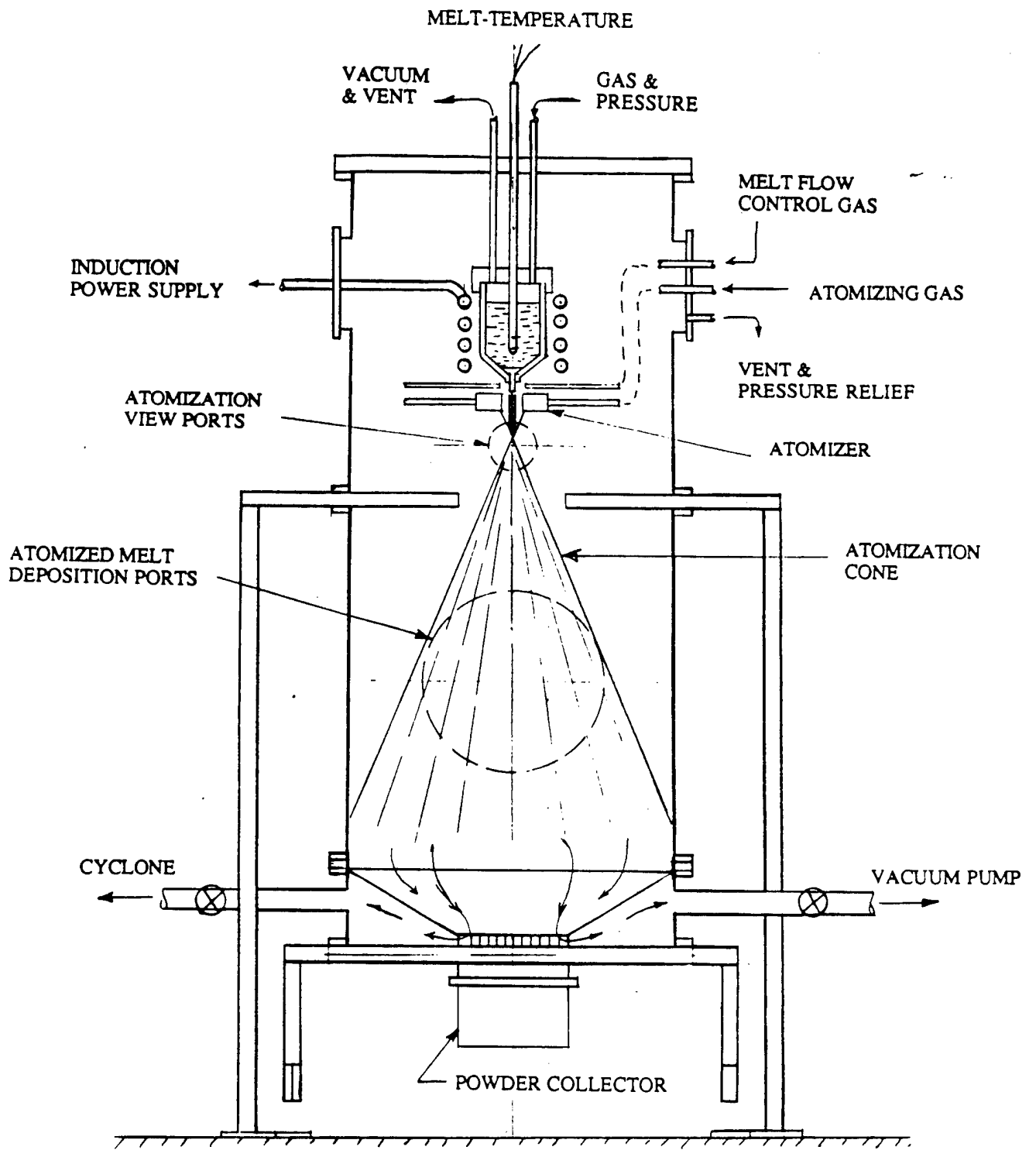


Figure 1. Schematic diagram of the HPM's 100 lbs per batch powder production equipment.

A guide tube was introduced in the new design, to avoid metal freeze up during atomization. The guide tube was modified several times before the final design shown in Figure 2 was adopted. The initial design of the guide tube did not have heater and was in intimate contact with plates A1 and A2. The guide tube was later machined to avoid contact with plates A1 and A2. The guide tube shown in Figure 2 consists of 4.5 inch long concentric stainless steel tubes of diameter 1 and 1/4 respectively. A removable tip of stainless steel with a centered through hole is threaded into the plate C100-1. The guide tube is maintained at high temperature by means of resistance heater which surrounds it, to provide a steady stream of molten metal. The heater can achieve as high a temperature as 820° C. The process of atomization occurs [4,5] below the guide tube and the guide tube is isolated from the plates A1 and A2 to avoid cooling of the guide tube.

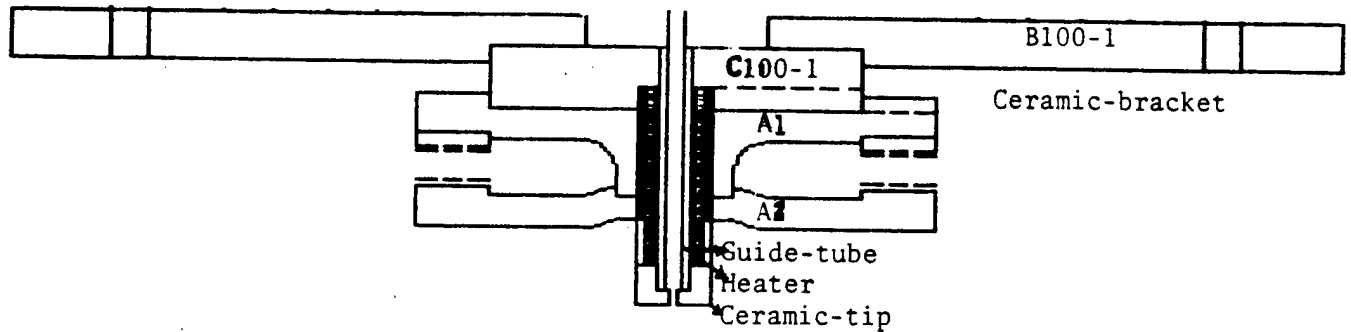


Figure 2. Schematic diagram of the guide tube assembly.

In the atomization chamber, an atomizer is used for atomization of molten metal stream. Atomizer is made out of stainless steel and has 12 holes placed equidistantly in a 12 inch diameter base circle. The holes have a half apex angle of 19.5° . The inert gas exits through these holes at any given pressure and the gas jets from these 12 holes meet at one point on the metal stream leading to atomization. Stainless steel tubing was used to carry high pressure gas and replaced copper tubing in the existing set up.

The atomization chamber has a powder collection chamber attached to it to collect powders. This also was redesigned and fabricated to avoid the problem of caking. It consists of a rectangular stainless steel box of 3 feet by 3 feet with a height of 1 foot. The box has a centered 12 inches diameter circular throat. With a rubber O-ring the box is air-tight fixed to the bottom of the atomization chamber. The large area of the bottom surface of the box will allow the powders to spread more and not to accumulate within a small area thus avoiding caking.

The melt chamber was also designed for a high temperature melting application by incorporating a 1/2 inch thick ceramic plate between the crucible and stainless steel plates B100-1/C 100-1 to prevent dissipation of heat into the stainless steel plates. In addition, the aluminum top plate was water cooled to prevent over heating by radiation from the crucible. The coupling connecting the cylinder (for control rod) and the control rod was changed to a heat insulating ceramic from stainless steel. The control rod was changed from stainless steel to high quality graphite. A half inch thick insulating board was also incorporated between crucible and the top aluminum plate.

5.2 Processing Of Eutectic Lead-Tin, Alloy Lead-Tin Powders And Lead Less Powders

Using 100 lbs powder maker, eutectic lead-tin powders, alloy lead-tin powders and lead less powders were produced. Several powder runs were made by varying process parameters, such as metal stream diameter, gas pressure and super heat to optimize the gas atomization process and obtain maximum yield of powders in the 25 to 44 μm range. Nitrogen was used as atomizing gas at a pressure varying from 300 to 600 psi. Fine powders are produced when the gas flow rate to metal flow rate is higher [6]. The crucible exit hole diameters were varied as 4/64", 5/64 "and 3/32 " and pressure was varied from 150 to 450 psi. The melt temperature was maintained at 500°C .

The yields of 25 to 44 μm size powders were strong functions of gas pressure and the exit hole diameter. A lower exit hole diameter and a higher gas pressure yielded a higher percentage of fine size powders. Figure 3 shows the effect of exit hole diameter on the mean powder size at a gas pressure of 300 psi.

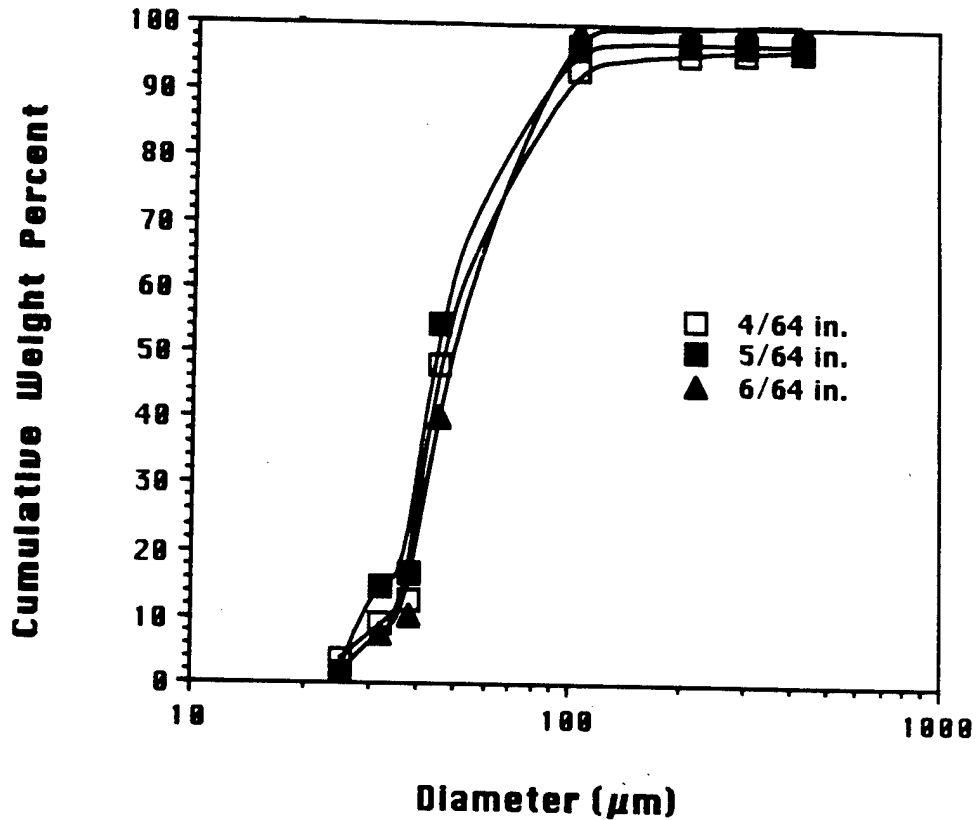


Figure 3. Effect of exit hole diameter on the mean powder size during atomization process.

Figures 4 to 5 show typical Scanning electron micrographs (SEM) of lead-tin eutectic powders in 25-44 μm size range after sieving for 2 hours. The powders are spherical in shape and satelliting of small particles with larger particles is minimal. Since the powders were mechanically sieved for 2 hours, mechanical erosion of powder particles has taken place.

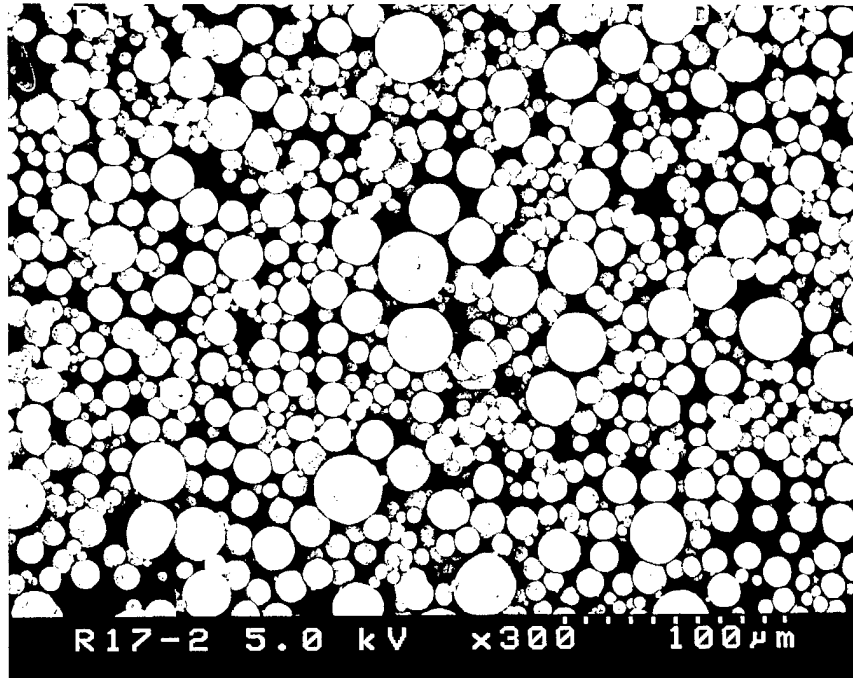


Figure 4. Scanning electron micrograph of eutectic solder powder in the size range 25 -44 μm .

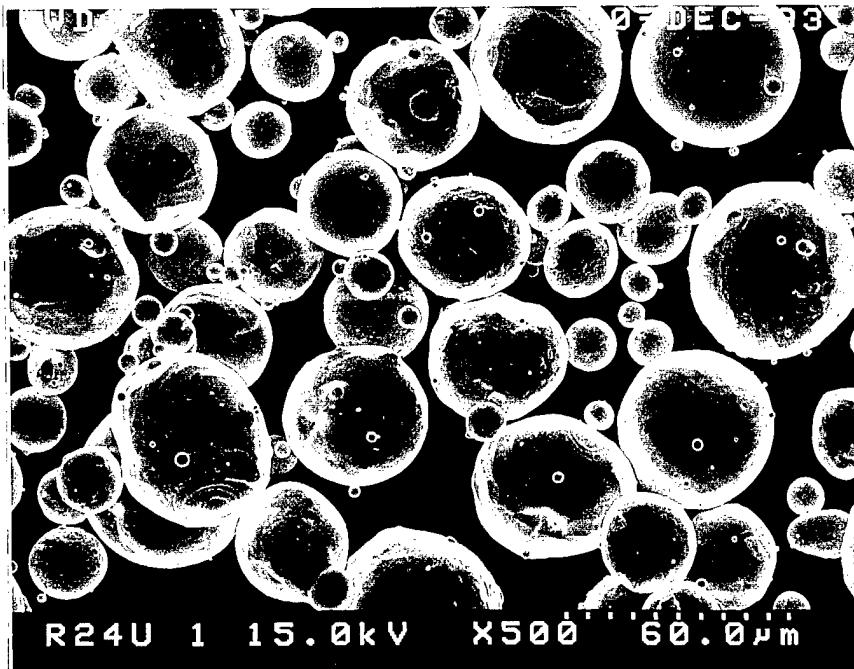


Figure 5. Scanning electron micrograph of eutectic solder powder in the size range 25 -44 μm .

Figure 6 shows SEM micrograph of powders before sieving and it can be seen that presieved powders are spherical and have smooth surface. Therefore an alternate method of sifting powders namely ultrasonic sieving was tried. The ultrasonic sieving was done at Connecticut Engineering Associates Inc.

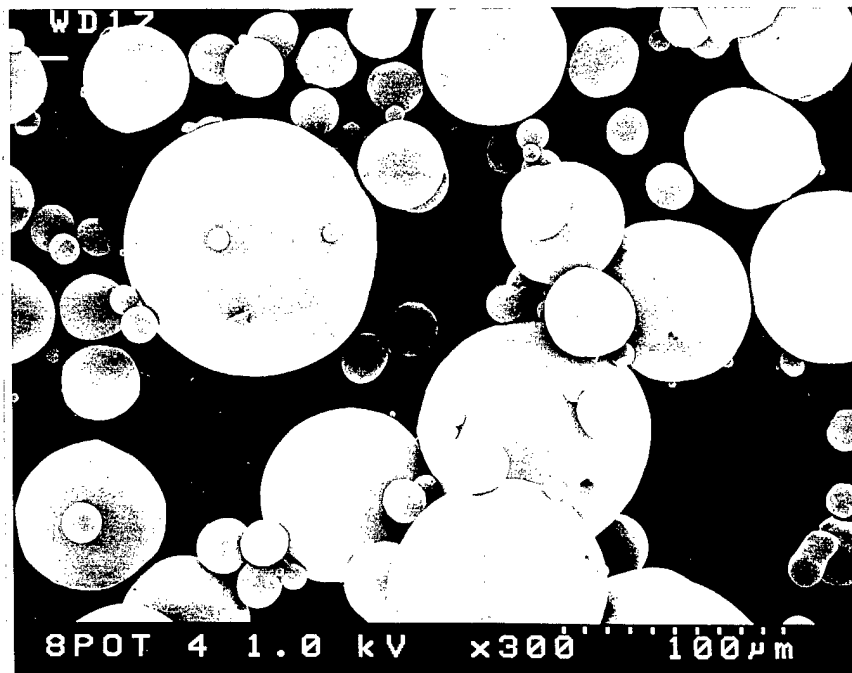
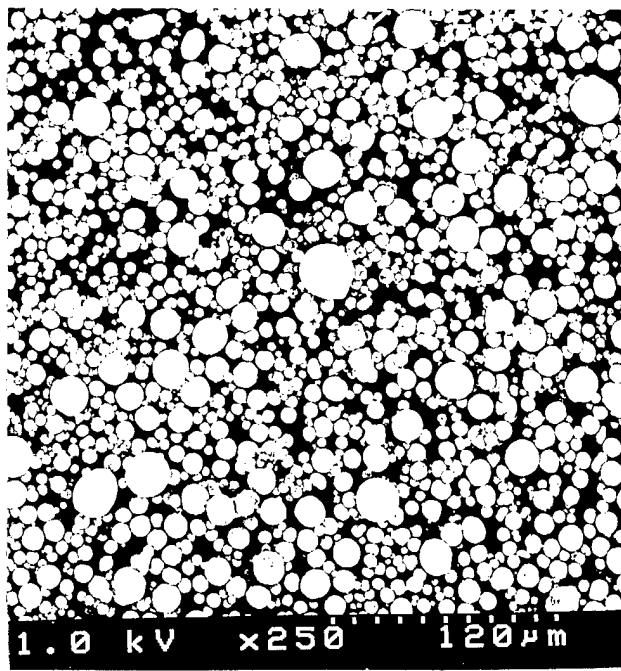
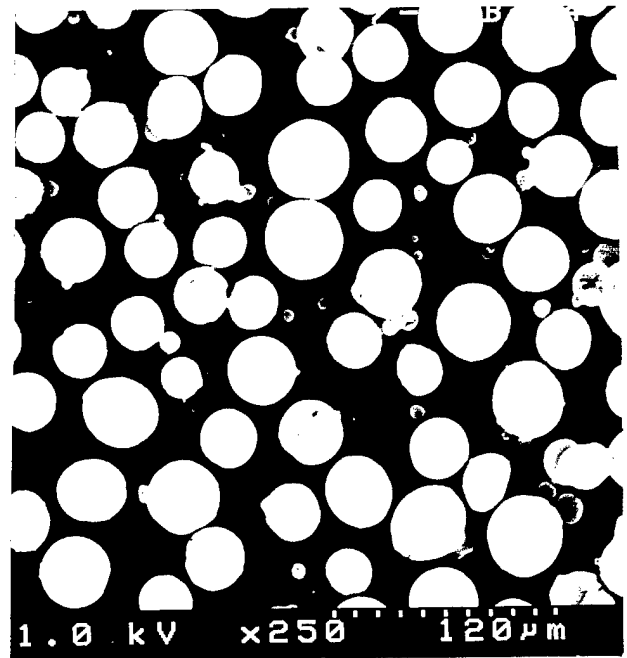


Figure 6. Scanning electron micrograph of eutectic solder powder in the size range 25 -44 μm before sieving.

Alloy eutectic powders such as Pb-Sn-2.5%In, Pb-Sn-2.5%Bi, Pb-Sn-2.5%Ag, Pb-Sn-5%Cu, Pb-Sn-2.5% Ni, Pb-Sn-5% Ni and Pb-Sn-2.5%Sb were produced. For alloy solder powders with alloying elements such as nickel and copper, a higher melt temperature was maintained. For copper, the melt temperature was 1150 ° C to 1200 ° C while melt temperature for nickel was 1450 ° C to 1500 ° C. The operating gas pressure in these runs was 500 psi and the guide tube was maintained at 820 ° C. Figure 7 SEM micrograph of Pb-Sn-In solder powder in the size range 25 -44 μm before and after ultrasonic sieving. Figures 8 to 11 show the SEM micrographs of other solder alloy powders in the pre-sieved condition. Figures 12 to 13 show the Pb-Sn-Ni alloy powders in the pre sieved and after ultrasonic sieving.



(a)



(b)

Figure 7. Scanning electron micrograph of Pb-Sn-In solder powder in the size range 25 -44 μm (a) before sieving (b) after ultrasonic sieving.

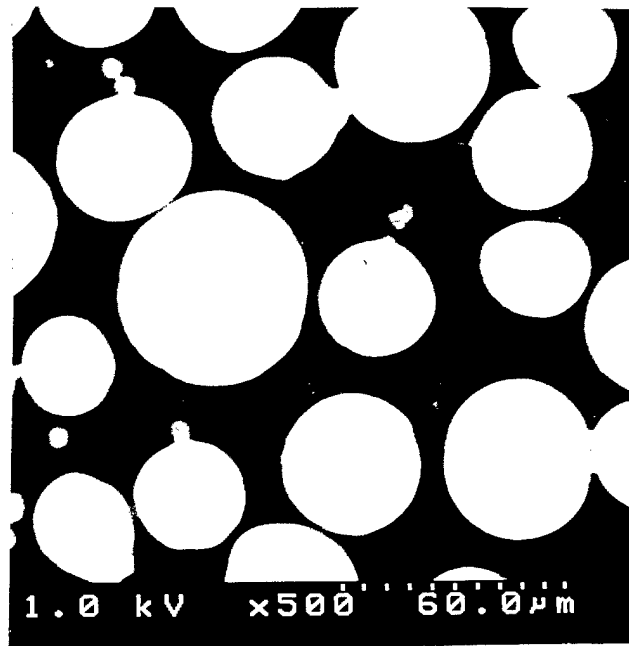


Figure 8. Scanning electron micrograph of Pb-Sn-Bi solder powder in the size range 25 -44 μm before sieving.

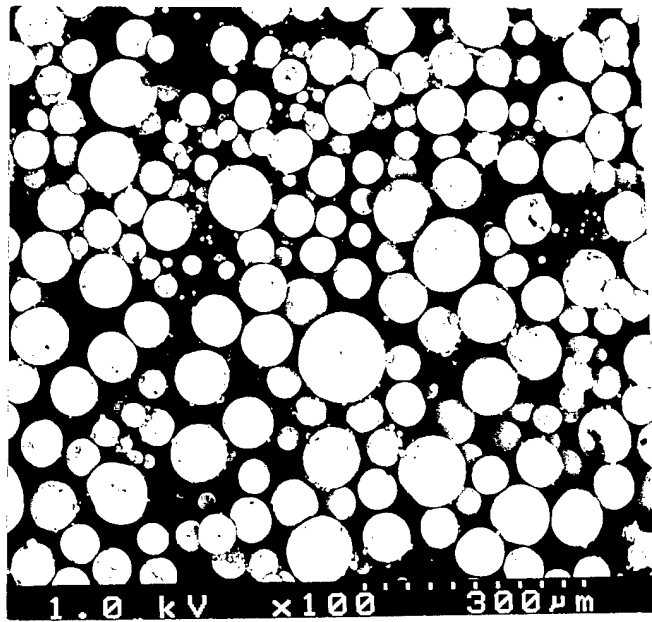


Figure 9. Scanning electron micrograph of Pb-Sn-Ag solder powder in the size range 25 -44 μm before sieving.

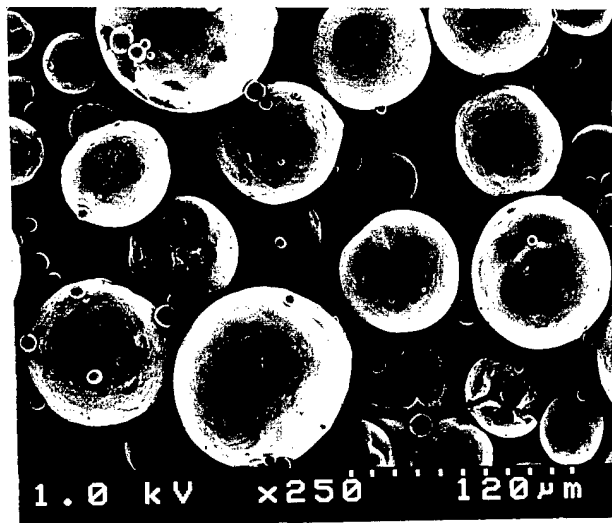


Figure 10. Scanning electron micrograph of Pb-Sn-Cu solder powder in the size range 25 -44 μm before sieving.

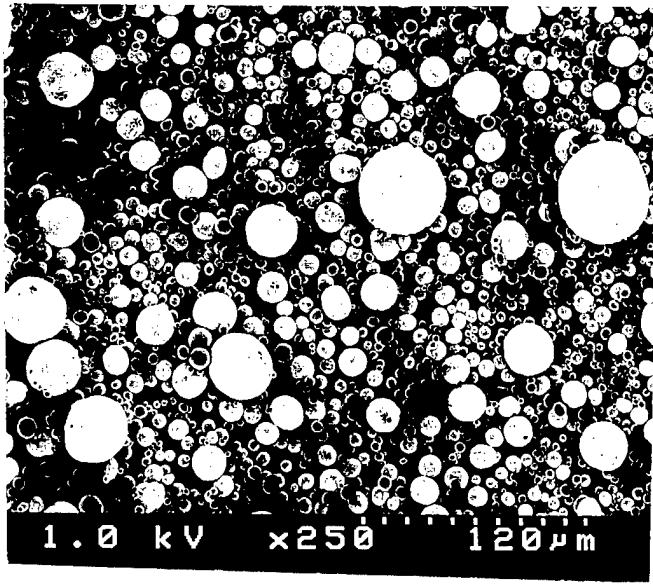
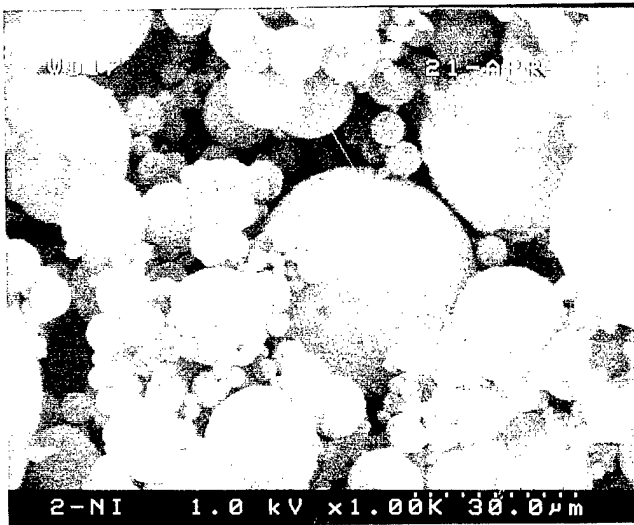
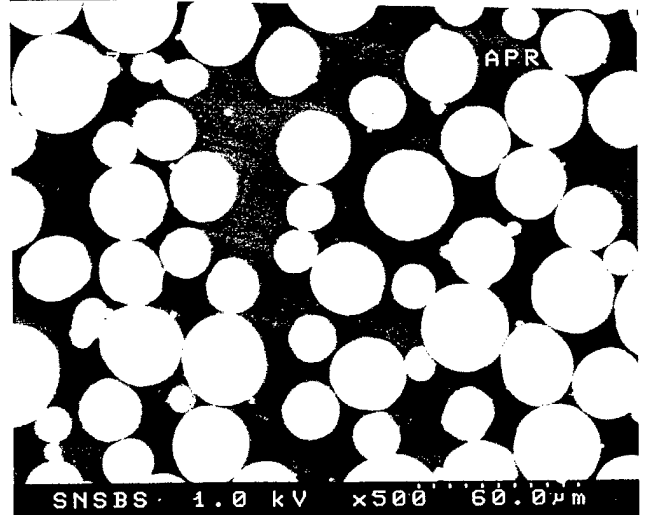


Figure 11. Scanning electron micrograph of Pb-Sn-Sb solder powder in the size range 25 -44 μm before sieving.

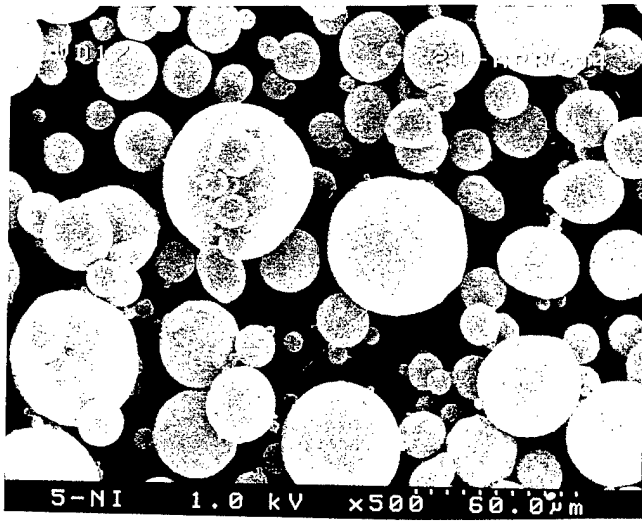


(a)

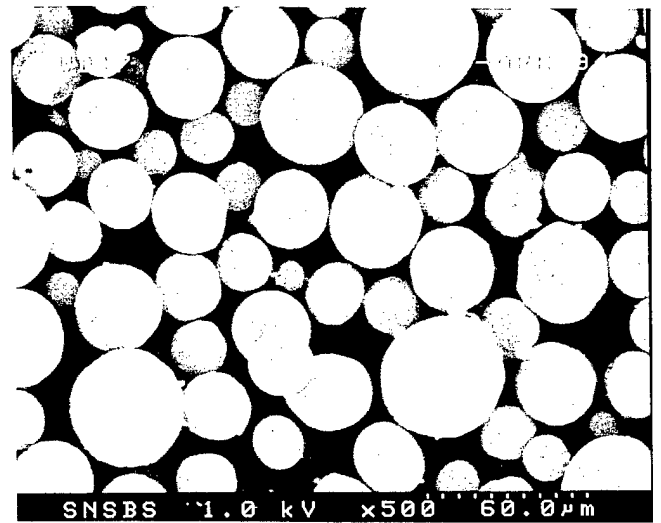


(b)

Figure 12. Scanning electron micrograph of Pb-Sn-2.5%Ni solder powder in the size range 25 -44 μm (a) before sieving and (b) after sieving.



(a)



(b)

Figure 13. Scanning electron micrograph of Pb-Sn-5%Ni solder powder in the size range 25 -44 μm (a) before sieving and (b) after sieving.

The particle size distribution of the powders after sieving is narrow and more than 70 % are in the 25-44 μm size range as shown in Figure 14 for Pb-Sn-In alloy.

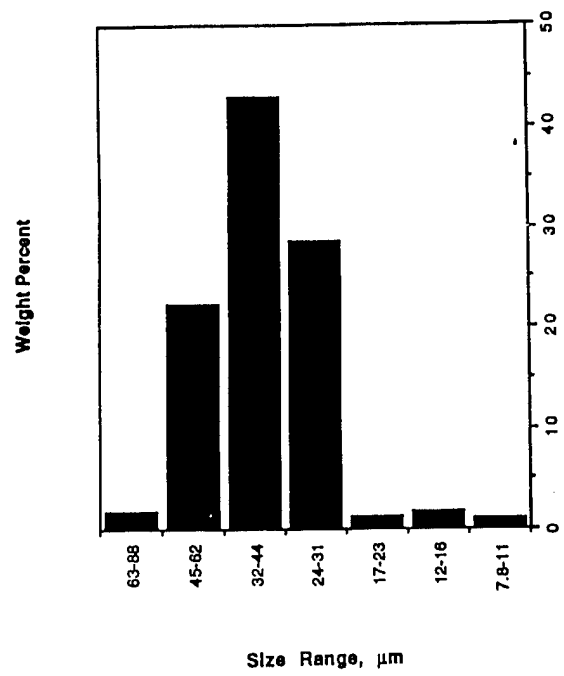


Figure 14. Powder size distribution in the case of Pb-Sn-In powders.

Figures 15 and 16 show the narrow powder size distribution in the case of Pb-Sn-Ni alloys.

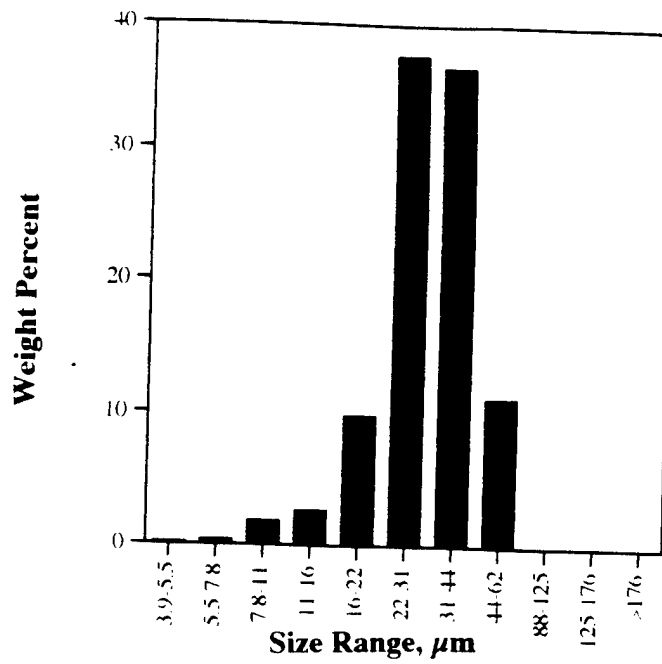


Figure 15. Powder size distribution in the case of Pb-Sn-2.5 % powders.

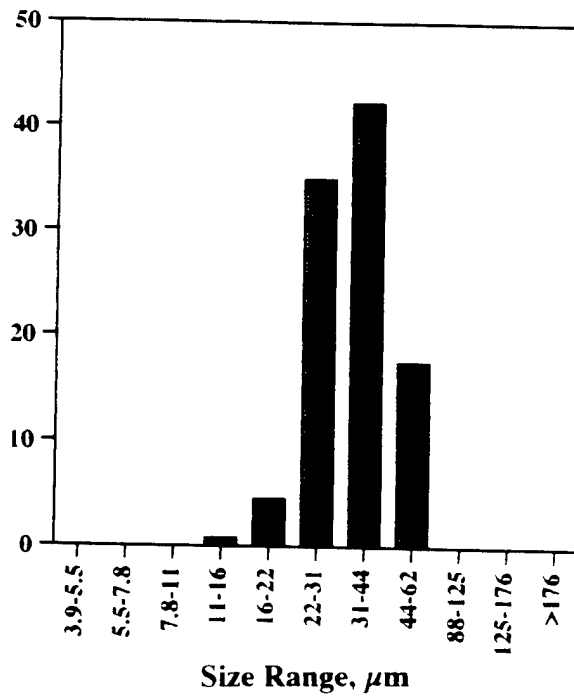


Figure 16. Powder size distribution in the case of Pb-Sn-5 % Ni powders.

Two solder alloy compositions without lead were also produced using 100 lbs powder maker. These alloys included Sn-3.2%Ag-6.8%Bi and Sn-3% Ag-4.2% Bi-6.8 %In. Figures 17 and 18 show the SEM micrograph of the post sieved Sn-Ag based alloy powders. The powders are spherical in shape and have no surface roughness.

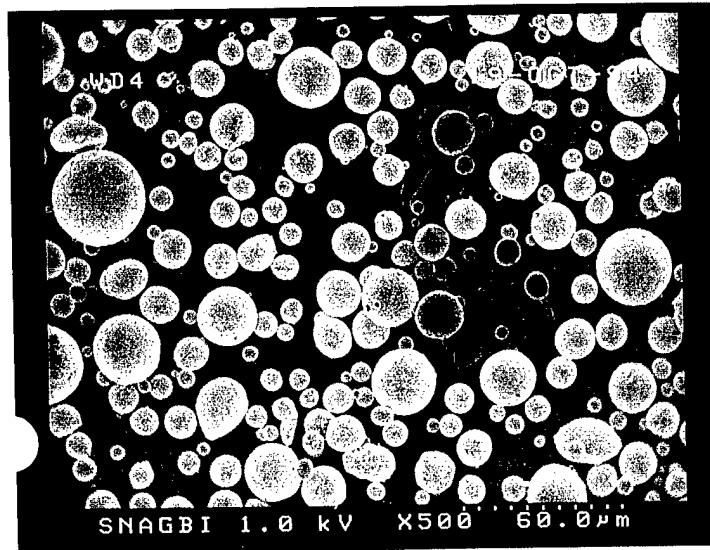


Figure 17. SEM micrograph of the Sn-3.2% Ag-6.8% Bi alloy after ultrasonic sieving.

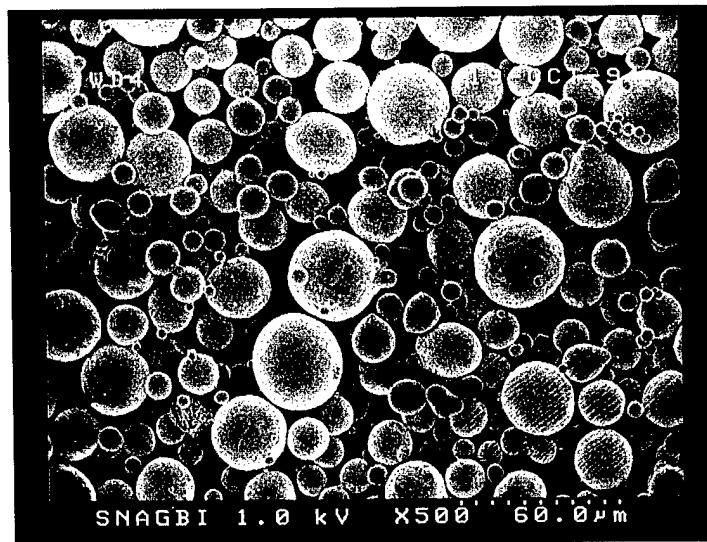


Figure 18. SEM micrograph of the Sn-3 % Ag-4.2 % Bi-6.8 5 In alloy after ultrasonic sieving.

5.3 Consolidation and Extrusion of Solder Powders

Solder powders of different compositions were sieved and powders in the size range $<25 \mu\text{m}$ and 45 to $74 \mu\text{m}$ were chosen for further consolidation and extrusion of solder powders to bulk form. The powders were first consolidated at room temperature by applying 9000 Newtons of force [7]. The consolidated samples were then extruded into 6 mm rods at 120°C with extrusion ratio of $16 : 1$. The extrusion press used for extruding solder rods is shown in Figure 19. Because the extrusion is done at 100°C any residual stress due to extrusion is annealed during cooling down to room temperature.

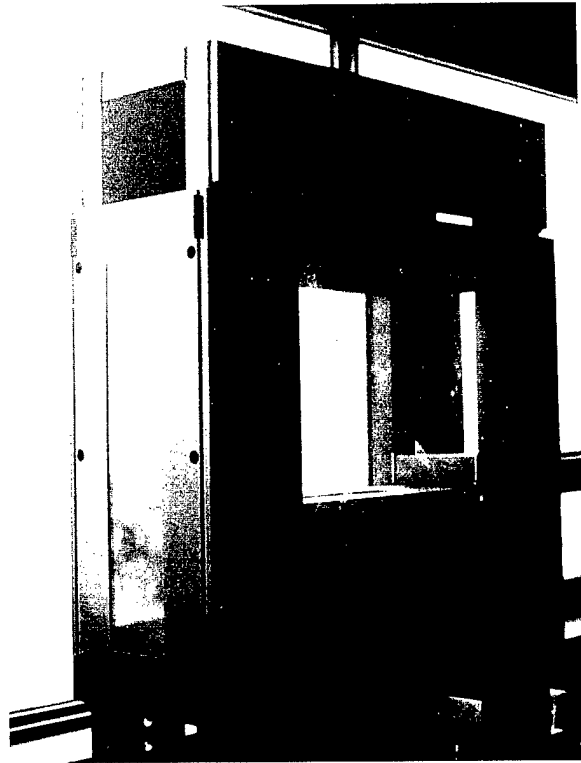


Figure 19. Extrusion press used for extruding consolidated solder powders into cylindrical rods.

5.4 Microstructures And Mechanical Property Testing Of Eutectic and Alloy Solders

Mechanical characterization of eutectic and solder alloys were carried out using i) Bulk samples and ii) Lap-shear joint testing. For mechanical property testing of bulk samples tensile specimens were machined from the extruded cylindrical rods [7]. The geometry and dimensions of the specimens are shown in Figure 20. The reduced section was finished by polishing after turning with a final surface roughness of $0.2 \mu\text{m}$. No circumferential machining marks were evident at a magnification 20 X. The specimens were handled with care to insure no bending or prestressing occurred before testing.

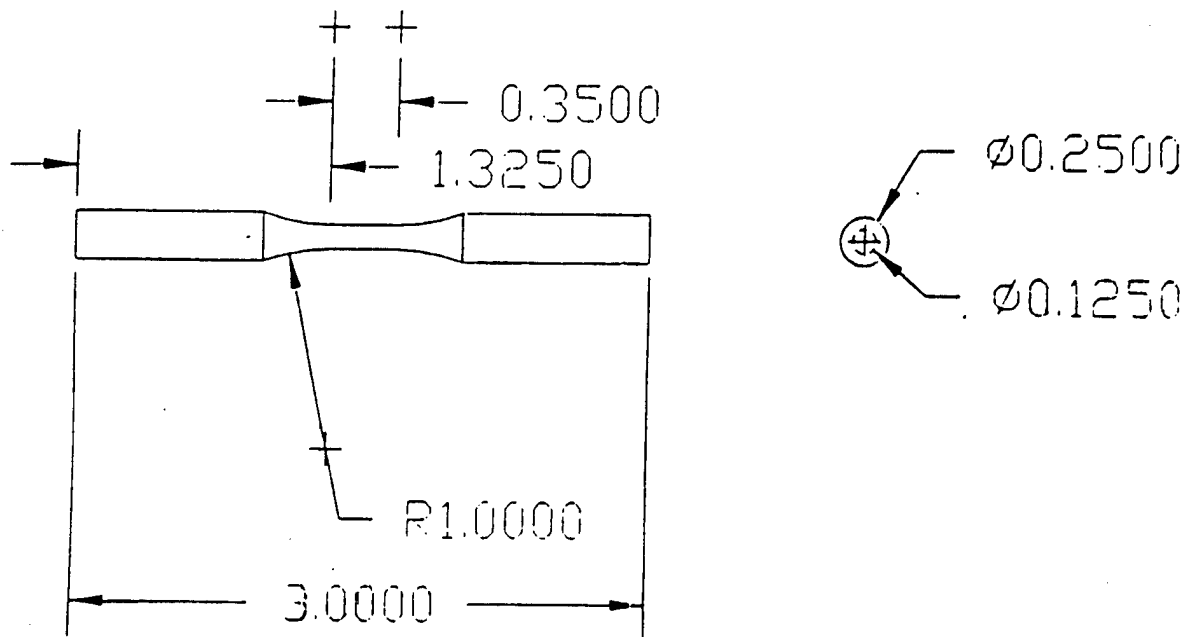


Figure 20. Geometry and dimensions of the tensile specimen.

A miniature single-lap-shear specimen and a jig, an auxiliary equipment to insure reproducible joint thickness and alignment during fabrication were designed for testing solder joints [8]. To prepare lap shear joints substrate blanks were machined from OFHC copper rod to the dimensions shown in Figure 21. These were soaked in 50 % sulfuric acid for 5 minutes to remove surface oxides and rinsed in water and acetone.

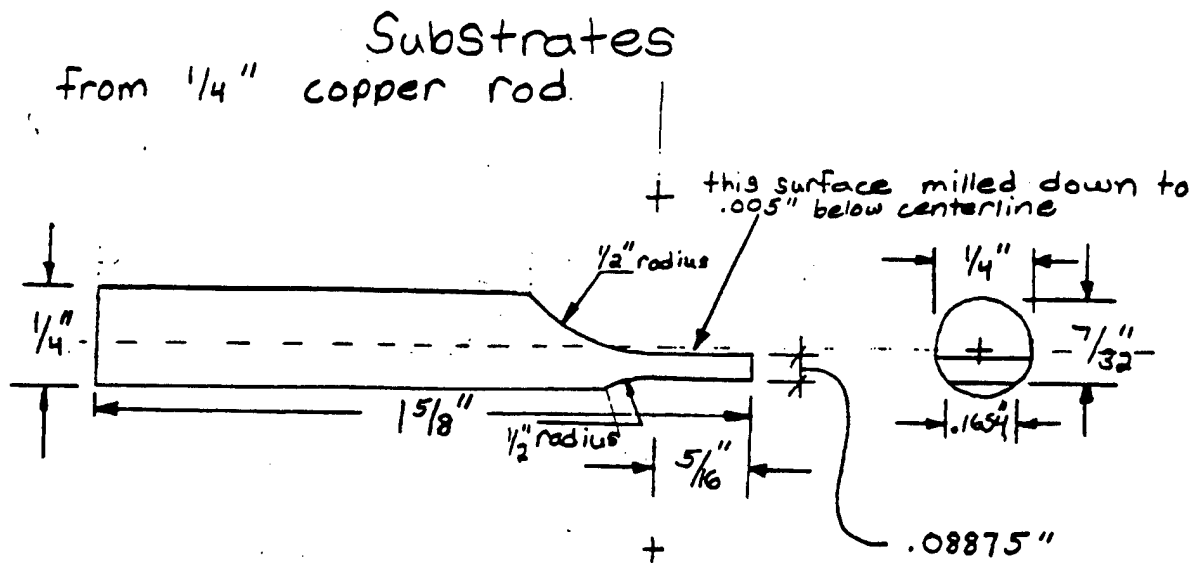


Figure 21. Geometry of the copper substrate for fabrication of lap-shear joint.

Figure 22 shows the schematic of jig. This method of lap shear joint preparation resulted in a typical joint thickness of 508 μm and a solder joint area of 7.93 x 6.35 square mm. Each of the copper blank halves were initially pretinned with a particular solder paste prepared by mixing 89 % of solder powder with 11 % of flux. Three types of lead free, mildly acidic and tinning fluxes manufactured by Kester Company were tried. These were (i) SP-244 (rosin based, no clean flux), (ii) SP371 (activated rosin) and (iii) SP-593 (organic water soluble). SP-244 was found to be optimum in terms of oxidation control and hence was used in joint making.

Bottom Half

Fine tolerances on these dimensions are not necessary

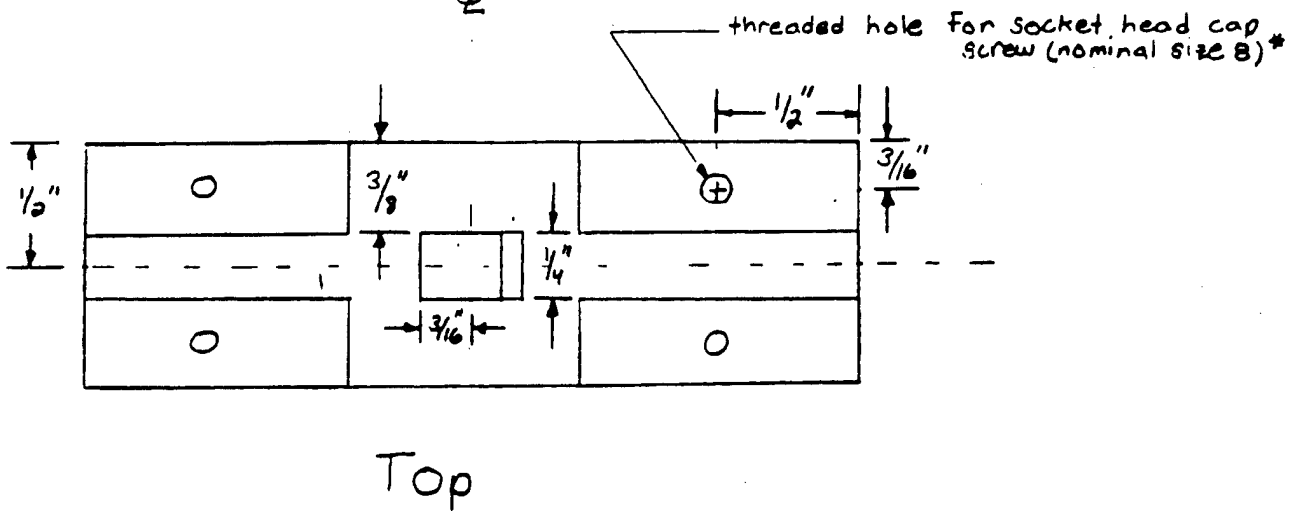
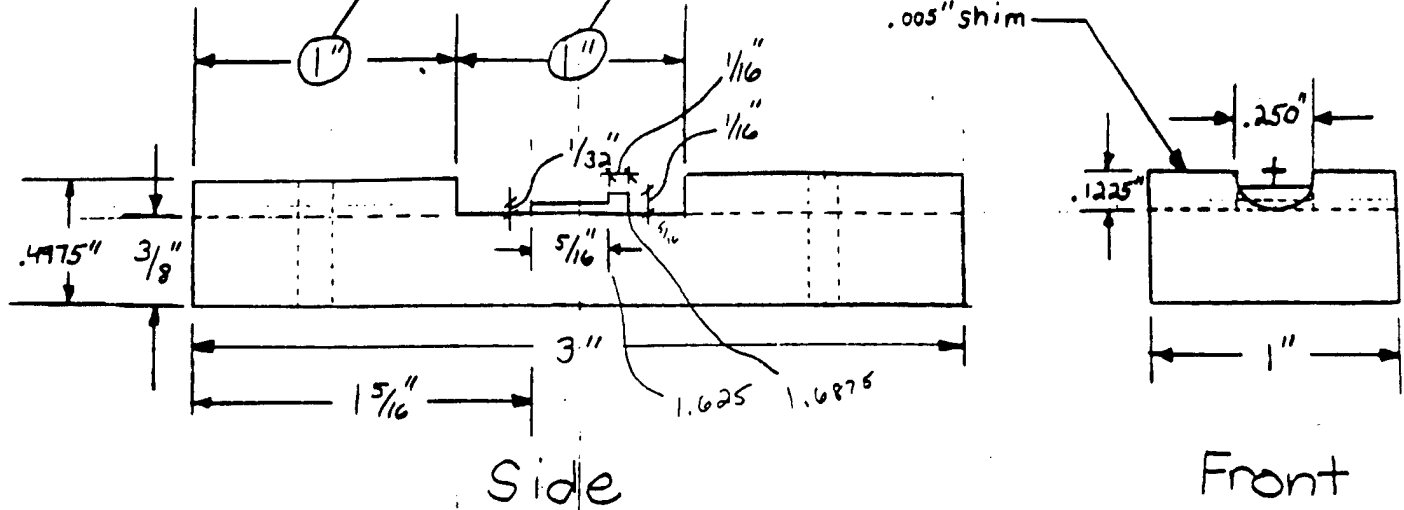


Figure 22. Schematic diagram of the sample holder for fabrication of lap-shear joint.

The procedure of joint making involved heating the copper blank halves to 300 ° C on a hot plate to melt the solder. The copper blanks were then ultrasonically cleaned in acetone. The paste was then applied to one half of the copper blank and the other half was placed on top of it. The copper blank halves were then aligned in the jig. The jig assembly and the copper halves were then heated in a vacuum chamber maintained at < 1 mm torr to a temperature of $T_m + 30$ ° C where T_m is the melting point the solder alloy. The solder was then reflowed at the same temperature for one minute. After reflowing, the chamber was back filled with air to cool the assembly at a rate of 1.5 ° C /second to a temperature of 60 ° C. The specimens were then removed from the chamber and cooled in the ambient conditions to room temperature.

5.4.1 Tensile Properties Of Bulk Solder Alloys

Tensile properties of bulk solder samples were determined in the as extruded condition and after aging. The aging of the extruded specimens were done at 100 ° C for 1 week. Room temperature tensile properties at a strain rate of $2 \times 10^{-3} \text{ s}^{-1}$ were evaluated using an Instron machine. The alloying elements Ni and Cu with high melting points strengthen the Pb-Sn solders by dispersion strengthening. The intermetallic dispersoids resist the dislocation motion and hence strengthen these solder alloys at room and elevated temperatures. Alloying elements such as Ag, In, Bi, and Sb strengthen the solder alloys by mechanism of solid solution strengthening.

Tables 1 and 2 summarize the tensile properties of the dispersion strengthened solder alloys, tin based solder alloys and solid solution strengthened solder alloys. Dispersion strengthened alloys show strengths higher than that of solid solution strengthened alloys. The comprehensive data shown in these tables give tensile properties of the bulk specimens prepared from starting powders of size < 25 μm and of size 45-74 μm and in the as extruded condition and after aging. These results show that the tensile properties of the solder alloys are not strongly dependent on the starting powder size for the range of powder size considered in this study. Similarly aging at 100 ° C for 1 week does not deteriorate the tensile properties of these solder alloys. The effect of aging on the strength of dispersion strengthened alloys is minimum because of the presence of stable ternary intermetallic dispersoids in the microstructure. The lead less solder alloys with higher melting points show higher strengths than the lead containing solder alloys.

Table 1. Tensile properties of dispersion strengthened and tin based solder alloys.

Cross-head speed = 0.06 in./min.

Engineering strain rate = $2 \times 10^{-3} \text{ s}^{-1}$

Composition	Condition	Powder Size μm	Young's Modulus ksi	0.2% Yield Strength ksi	UTS ksi	RA %
63Sn 32Pb 5Ni	E	< 25	3488	9.5	11.3	34
			3460	10.0	12.0	32
			3495	10.2	12.5	35
	A	< 25	3420	6.8	7.8	36
			3450	8.8	8.5	38
63Sn 32Pb 5Ni	E	45-74	3472	9.7	11.9	32
			3480	10.9	11.9	30
			3506	10.8	12.1	33
	A	45-74	3420	7.8	10.4	30
			3462	8.9	10.6	33
63Sn 34.5Pb 2.5Ni	E	< 25	3245	8.3	9.2	35
			3290	8.9	9.8	37
	A	< 25	3210	7.9	8.8	39
63Sn 34.5Pb 2.5Ni	E	45-74	3188	8.5	9.0	36
	A	45-74	3155	7.8	8.5	39
63Sn 32Pb 5Cu	E	< 25	3158	8.2	10.8	33
			3166	10.8	11.0	34
			3169	10.6	11.5	34
	A	< 25	3158	8.9	9.8	37
63Sn 32Pb 5Cu	E	45-74	3166	10.5	11.5	32
			3176	11.5	10.8	35
			3156	10.8	10.9	34
	A	45-74	3168	9.5	10.5	38
95Sn 5Sb	E	< 25	3480	8.6	9.3	38
			3490	8.9	9.8	38
	A	< 25	3444	8.5	9.0	36
			3460	8.6	9.5	38
95Sn 5Sb	E	45-74	3466	8.8	10.5	36
			3476	9.5	10.2	38
	A	45-74	3385	8.6	9.5	38
			3410	8.8	9.8	36
95Sn 5Sb	E	25-44	3466	8.8	10.5	36
			3466	9.5	10.9	37

E-extruded only; A-extruded and aged at 100 °C for 1 week; Δ y-change in 0.2% yield strength;

Δ U-change in Ultimate Tensile Strength; RA-reduction of cross-sectional area; Δ A-change in RA

Table 2. Tensile properties of solid solution strengthened solder alloys

Cross-head speed = 0.06 in./min.
Engineering strain rate = $2 \times 10^{-3} \text{ s}^{-1}$

E-extruded only; A-extruded and aged at 100 °C for 1 week; Δ y-change in 0.2% yield strength;
 Δ U-change in Ultimate Tensile Strength; RA-reduction of cross-sectional area; Δ A-change in RA

Composition	Condition	Powder Size μm	Young's Modulus ksi	0.2% Yield Strength ksi	UTS ksi	RA %
6337	E	< 25	2113	3.5	4.6	56
	A	< 25	2065	5.2	5.6	43
6337	E	45-74	2166	3.0	3.7	59
	A	45-74	2123	4.3	4.2	46
63Sn 34.5Pb 2.5In	E	< 25	1760 1790	4.0 4.2	5.0 5.3	54 56
	A	< 25	1742	5.4	6.0	45
63Sn 34.5Pb 2.5In	E	45-74	1777	3.8	4.6	50
	A	45-74	---	---	---	---
63Sn 34.5Pb 2.5Bi	E	< 25	1748 1760	5.2 4.8	5.7 5.3	52 56
	A	< 25	1725	5.8	6.2	45
63Sn 34.5Pb 2.5Bi	E	45-74	---	---	---	---
	A	45-74	---	---	---	---
63Sn 34.5Pb 2.5Ag	E	< 25	1890	4.9	5.8	52
	A	< 25	1842	6.4	6.9	46
63Sn 34.5Pb 2.5Ag	E	45-74	1863	5.2	5.9	54
	A	45-74	---	---	---	---
63Sn 34.5Pb 2.5Sb	E	< 25	2465	6.0	7.8	35
	A	< 25	3410	6.6	7.7	32
63Sn 34.5Pb 2.5Sb	E	45-74	2438	5.9	7.5	38
	A	45-74	---	---	---	---

The tensile data obtained for eutectic and alloy solders were compared with the previous tensile data obtained for these alloys during SBIR Phase I. The comparison is shown in Tables 3 and 4. As seen from these tables, the tensile properties do not vary indicating that the consistency of powder production and the quality of the powders are maintained during scaling up of powder production equipment from 10 lbs per batch to 100 lbs per batch.

Table 3. Comparison between the present tensile data and the previous tensile data obtained during SBIR Phase I for dispersion strengthened alloys.

Composition	Condition	Powder Size μm	Average				% Change				Previous Results			
			ksi			%	0.2% YS	UTS	E	RA	ksi			%
			0.2% YS	UTS	E	RA					0.2% YS	UTS	E	RA
63Sn 32Pb 5Ni	E	< 25	9.9	11.9	3481	34.0					9.1	10.5	3480	---
	A	< 25	7.8	9.5	3435	37.0	-20	-20	-1	+9				
63Sn 32Pb 5Ni	E	45-74	10.4	11.9	3486	31.0								
	A	45-74	9.9	10.5	3441	32.0	-14	-12	-1	+4				
63Sn 34.5Pb 2.5Ni	E	< 25	8.6	9.5	3267	36.0					7.39	7.8	3045	---
	A	< 25	7.9	8.8	3210	39.0	-8	-7	-1	+8				
63Sn 34.5Pb 2.5Ni	E	45-74	8.5	9.0	3218	36.0								
	A	45-74	7.8	8.5	3155	39.0	-8	-6	-1	+8				
63Sn 32Pb 5Cu	E	< 25	9.8	11.1	3164	33.5					7.54	8.7	3054	---
	A	< 25	8.9	9.8	3158	37.0	-9	-9	-1	+10				
63Sn 32Pb 5Cu	E	45-74	10.9	11.1	3166	33.5								
	A	45-74	9.5	10.5	3168	37.5	-11	-10	-1	12				
95Sn 5Sb	E	< 25	8.75	9.55	3485	36.5								
	A	< 25	8.55	9.25	3452	39.0	-2	-3	-1	+7				
95Sn 5Sb	E	45-74	9.15	10.35	3471	37.0								
	A	45-74	8.7	9.65	3397	39.0	-2	-3	-1	+7				
95Sn 5Sb	E	25-44	9.2	10.7	3466	36.5								

Table 4. Comparison between the present tensile data and the previous tensile data obtained during SBIR Phase I for solid solution strengthened alloys.

Composition	Condition	Powder Size μm	Average				% Change				Previous Results			
			ksi			% RA	0.2% YS	UTS	E	RA	ksi			% RA
			0.2% YS	UTS	E						0.2% YS	UTS	E	
6337	E	< 25	3.5	4.6	2113	56					4.2	4.6	2030	---
	A	< 25	5.2	5.6	2065	43	+48	+22	-2.0	-20				
6337	E	45-74	3.0	3.7	2116	59								
	A	45-74	4.3	4.2	2123	46	+54	+35	-2.0	-20				
63Sn 34.5Pb 2.5In	E	< 25	4.1	5.1	1775	55					3.6	4.2	1740	---
	A	< 25	5.4	6.0	1742	45	+35	+20	-18	-16				
63Sn 34.5Pb 2.5In	E	45-74	3.8	4.6	1777	50								
	A	45-74												
63Sn 34.5Pb 2.5SbI	E	< 25	5.0	5.5	1754	54					3.9	4.3	1740	---
	A	< 25	5.8	6.2	1725	45	+4	+13	-1.0	-16				
63Sn 34.5Pb 2.5SbI	E	45-74	5.2	5.5	1750	53								
	A	45-74												
63Sn 34.5Pb 2.5Ag	E	< 25	4.9	5.8	1890	52					5.2	6.0	1885	---
	A	< 25	6.4	6.9	1842	46	+30	+19	-2.0	-12				
63Sn 34.5Pb 2.5Ag	E	45-74	5.2	5.9	1863	54								
	A	45-74												
63Sn 34.5Pb 2.5Sb	E	< 25	6.0	7.8	2465	35					4.4	5.0	2465	---
	A	< 25	6.5	7.7	2410	32	+8	+2	-2.0	-9				
63Sn 34.5Pb 2.5Sb	E	45-74	5.9	7.5	2438	38								
	A	45-74												

Optical micrographs of the as extruded Pb-Sn-5% Ni alloy are shown in Figures 23 (a) and (b). The dark areas are lead rich while the gray areas are tin rich. Figure 24 shows the Energy Dispersive X-ray analysis (EDAX) done for the intermetallic phase in Pb-Sn-5Ni alloy.

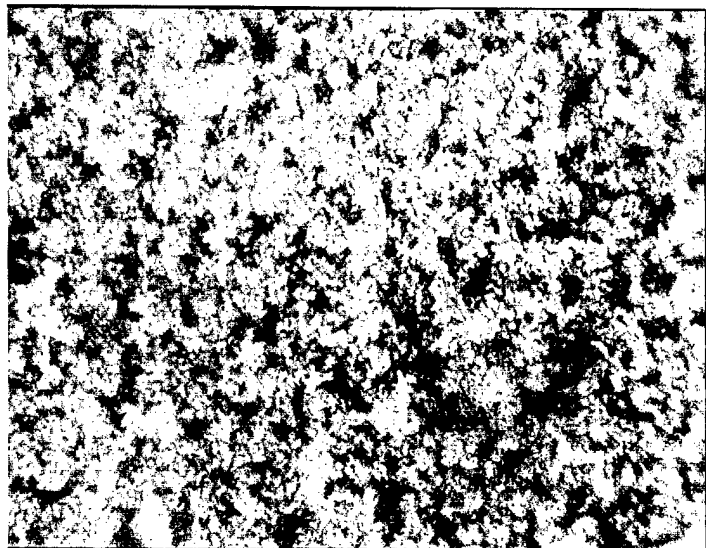


Figure 23. (a) SEM micrograph of the extruded Pb-Sn-5%Ni alloy.

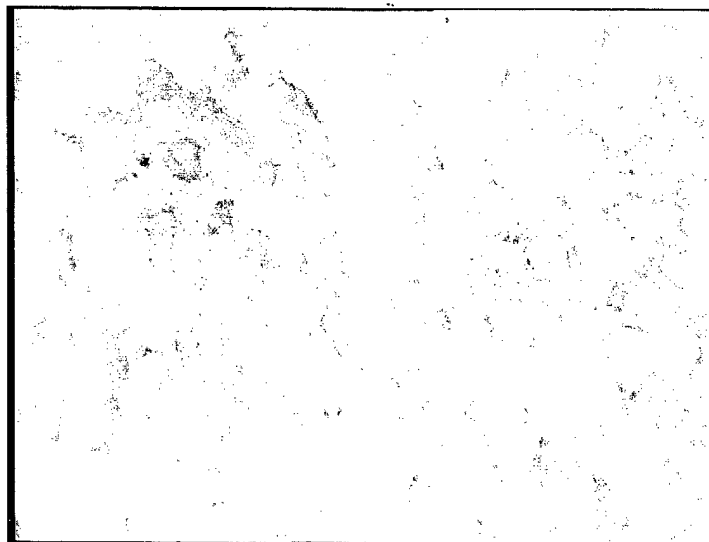
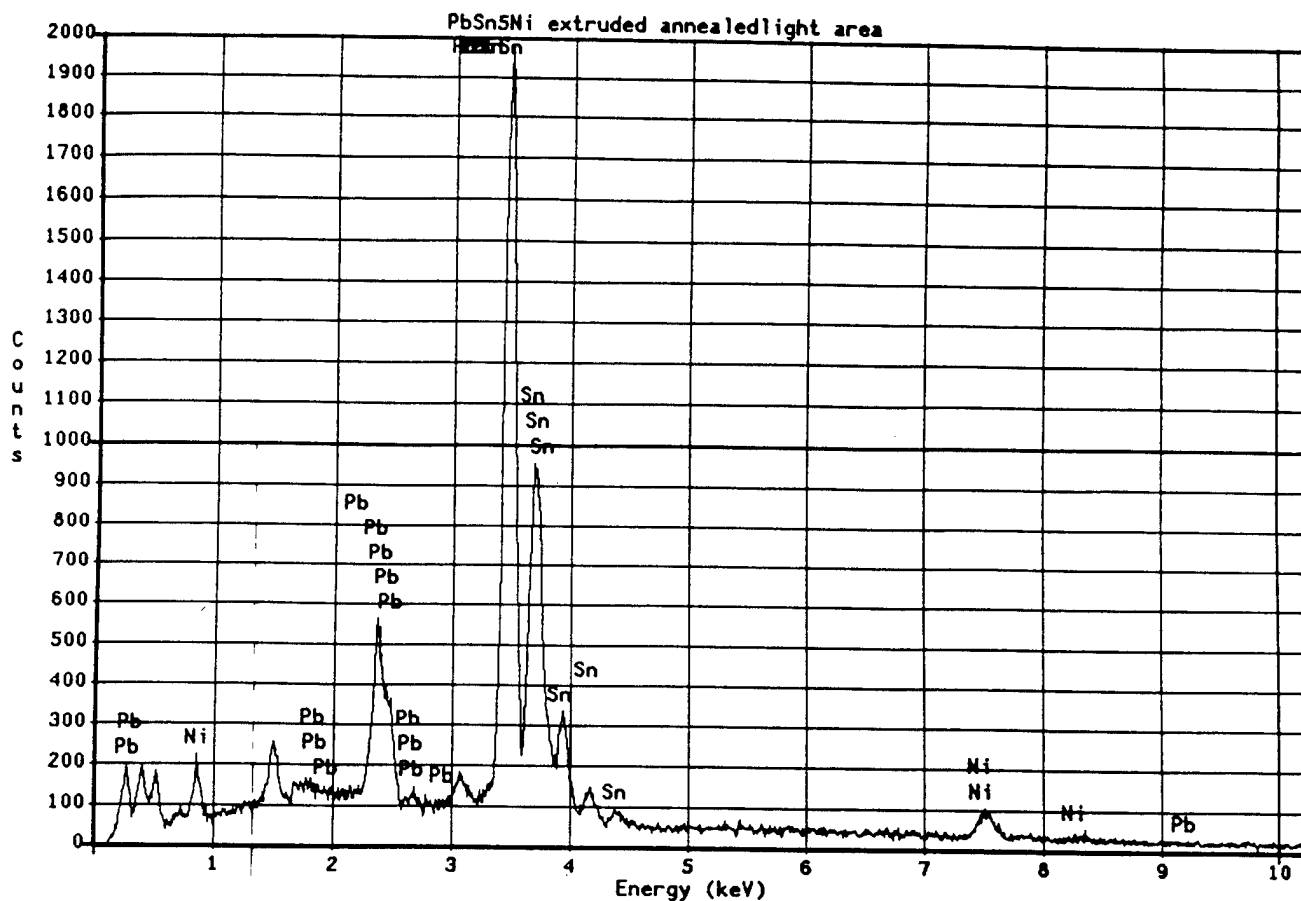


Figure 23 (b). SEM micrograph of the extruded and annealed Pb-Sn-5%Ni alloy.



PROZA Correction 15.00 kV 30.03 deg
 No. of Iterations = 2

Element	k-ratio	Z	A	F	Atom %	Wt %
Ni-L	0.03718	0.835	2.799	1.000	17.14	8.69
Sn-L	0.71227	1.005	1.067	1.000	74.47	76.30
Pb-M	0.13075	1.107	1.048	0.989	8.39	15.01
Total						100.00 %

Figure 24. EDAX of the intermetallic phase in SEM micrograph of the extruded Pb-Sn-5 %Ni alloy.

Optical micrographs of the as extruded Pb-Sn- 5% Cu alloy are shown in Figures 25 (a) and (b). After aging, there is coarsening of dispersoids which decrease the yield strength marginally and increase the percentage ductility.

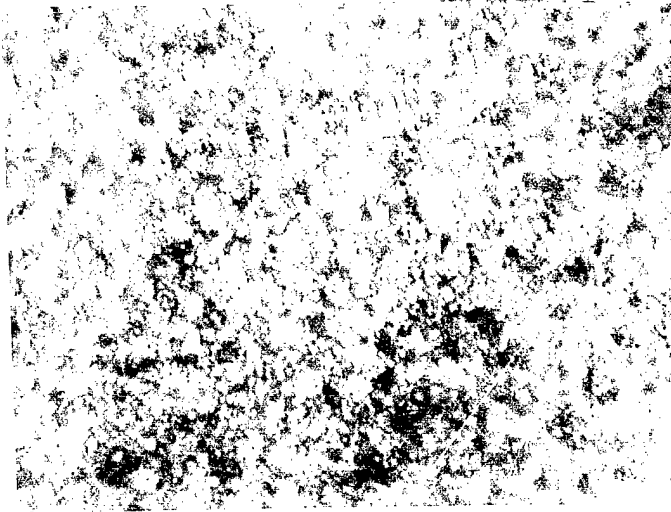


Figure 25. (a) SEM micrograph of the extruded Pb-Sn-5% Cu alloy.

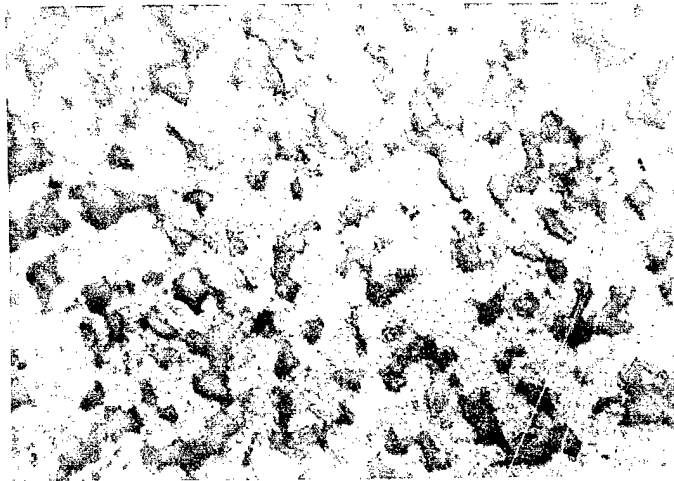


Figure 25. (b) SEM micrograph of the extruded and annealed Pb-Sn-5%Cu alloy.

The tensile yield strengths of the Sn-Ag solders made by HPM are shown in Figure 26 and compared with other solder alloys. These compositions of Sn-Ag solder alloys were made by HPM for IEM Fusion incorporated.

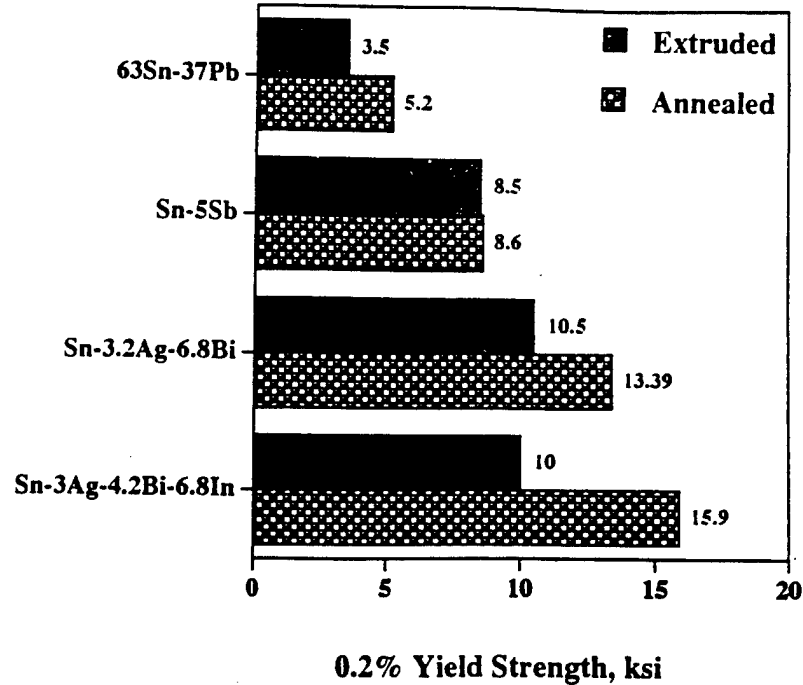


Figure 26. Tensile yield strengths of Sn-Ag based solders compared with other solder alloys.

5.4.2 Tensile /Shear Properties Of Lap-shear Joints

Tensile testing of lap shear joints was conducted using an Instron load frame with a 30,000 lbs (133 kN) load cell and at a cross head displacement rate of $0.0001 \text{ inch sec}^{-1}$. The uniaxial tensile load applied to lap shear joints gives rise to a shear type of load and hence the tensile tests for lap-shear joints are actually shear tests [9]. An extensometer was used to measure the displacement and Load v/s displacement was recorded. Stress and extension at maximum load were determined. The stress is defined as the load divided by the cross sectional area which is taken as $0.05875 \text{ square inch (} 0.380 \text{ cm}^2)$ and the strain is the actual displacement as measured by the extensometer divided by the joint thickness (20 mils) [10]. The solder joints in these tests were prepared using Kester SP 244 flux and the solder paste was prepared manually at Washington university in St. Louis. The manual paste making was not a very well controlled process.

The different configurations in bulk and joint solder samples may lead to significantly different results for similar tests. In addition, the solder joints contain a layer of intermetallics which is absent in bulk samples. Figure 26 shows a schematic of the formation of intermetallic layer between the copper and eutectic solder when the solder is allowed to reflow on copper substrate. Initially the Cu is coated by a thin layer of the Cu_3Sn (ϵ) phase. Next a layer of the Cu_6Sn_5 (η) grows in between the ϵ phase and the eutectic solder. Both these intermetallic phases can grow considerably with time, even at room temperature [11]. The solder intermetallics are extremely brittle in comparison to eutectic solder. A large difference in the elastic moduli exists between the solder and the intermetallic layers which can cause stress concentrations to form at the solder intermetallic interface. The solder in joints is also constrained at the substrate which is not the case in bulk samples. In the solder joints unlike bulk samples the stress and strain distributions are not uniform due to stress concentrations and variations of the cross sectional area, due to fillets and imperfections. Therefore, it is difficult to compare directly the results from bulk tests to joint tests [9].

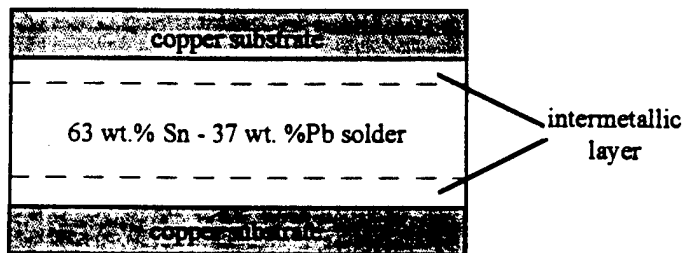
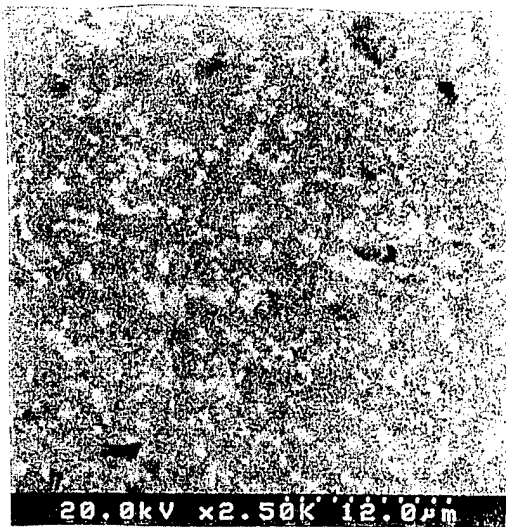


Figure 27. Side view of layers in a solder joint.

Figure 28 shows a typical SEM micrograph of the lap shear joint for Pb-Sn-5 Ni and Pb-Sn-5Cu solder alloys. Unetched polished samples were used in back scattered mode in SEM to obtain the micrographs. Percentage volume of different phases were analyzed using NIH software package. Table 5 shows the analysis of the as made joints for several solder alloys. The eutectic alloy has the largest average grain size for lead. The Ni containing solder alloy showed significantly thicker intermetallic layers and lower volume percentage of Pb rich phases. This suggests that the addition of ternary particles to eutectic solder impedes the grain growth during solidification and reflow.



63Sn-32Pb-5Ni



63Sn-32Pb-5Cu

Figure 28. A SEM micrograph of the lap shear joint of dispersion strengthened alloy.

Table 5. Analysis of as made lap shear joints.

composition	element X	Pb-rich phase			Sn-rich phase		
		wt.% Sn	wt.% Pb	wt.% X	wt.% Sn	wt.% Pb	wt.% X
AMT 6337	-	42.8 %	56.8 %	-	85.3 %	14.6 %	-
IEM 6337	-	34.4 %	65.7 %	-	85.9 %	13.7 %	-
AMT FRS	-	40.8 %	57.5 %	-	96.2 %	35.1 %	-
Sn-Pb-2.5Ni	Ni	44.0 %	54.3 %	0.9 %	91.1 %	6.1 %	1.9 %
Sn-Pb-5Ni	Ni	26.6 %	71.7 %	1.3 %	91.4 %	0.0 %	6.5 %
Sn-Pb-5Cu	Cu	48.4 %	51.4 %	0.3 %	98.2 %	1.6 %	0.2 %
Sn-Pb-2.5Ag	Ag	54.4 %	42.4 %	2.9 %	84.4 %	14.6 %	0.4 %
Sn-Pb-2.5In	In	26.3 %	72.1 %	0.0 %	80.8 %	18.7 %	0.2 %

Tables 6 and 7 show the results of the tensile tests conducted on lap shear joints for several of the solder alloy compositions in unaged and aged conditions. Dispersion strengthened solder alloys have higher strengths than solid solution strengthened alloys and the trends are similar to what was observed in bulk tensile testing.

Table 6. Tensile test results of unaged lap shear joints at a displacement rate of 0.0001 inch sec⁻¹.

Composition	Number of Joint Tested	Average Maximum Load lbs. (Stress ksi & MPa)	Standard Deviation Load lbs. (Stress psi & MPa)
63Sn-34.5Pb-2.5Bi	3	334 (5.7) & (39)	15 (250) & (1.7)
95Sn-5Sb	3	323 (5.5) & (38)	26 (450) & (3.1)
63Sn-34.5Pb-2.5Sb	3	318 (5.4) & (37)	7.0 (110) & (.76)
63Sn-32Pb-5Ni	1	313 (5.3) & (37)	19 (320) & (2.2)
63Sn-32Pb-5Cu	3	300 (5.1) & (35)	16 (270) & (1.7)
63Sn-34.5Pb-2.5Ag	3	294 (5.0) & (34)	7.7 (130) & (.90)
63Sn-34.5Pb-2.5In	3	287 (4.8) & (33)	1.7 (30) & (2.1)
AMT 63Sn-37Pb	3	280 (4.7) & (32)	4.7 (79) & (.54)
Kester 63Sn-37Pb	3	272 (4.6) & (32)	13 (220) & (1.5)
43Sn-57Bi	3	270 (4.5) & (31)	17 (290) & (2.0)
AMT-FRS	3	267 (4.5) & (31)	23 (400) & (2.8)
HPM 63Sn-37Pb	3	244 (4.1) & (28)	28 (481) & (3.3)

Table 7. Tensile test results of aged lap shear joints at a displacement rate of 0.0001 inch sec⁻¹.

Composition	Maximum Load lbs (kN)	Apparent Ultimate Shear Stress ksi (MPa)	Change in Strength	Apparent Shear Strain at Maximum Load (in/in)
95Sn-5Sb	325 (1.4)	5.5 (38)	1%	0.39
43Sn-57Bi	288 (1.3)	4.9 (34)	7%	0.23
AMT FRS	276 (1.2)	4.7 (32)	4%	0.22
63Sn-34.5Pb-2.5Sb	274 (1.2)	4.6 (32)	-14%	0.25
63Sn-32Pb-5Cu	251 (1.1)	4.2 (29)	-16%	0.26
63Sn-34.5Pb-2.5Ag	246 (1.1)	4.2 (29)	-16%	0.30
HPM 63Sn-37Pb	246 (1.1)	4.1 (28)	1%	0.29
AMT 63Sn-37Pb	242 (1.1)	4.1 (28)	-14%	0.25
63Sn-34.5Pb-2.5In	231 (1.0)	3.9 (27)	-20%	0.30

The tensile tests at 25 ° C, 75 ° C and 125 ° C were also carried out using a servo hydraulic MTS machine at a displacement rates of $1.67 \times 10^{-6} \text{ sec}^{-1}$. The purpose of these tensile tests were to provide some background information to analyze the thermo mechanical fatigue (TMF) tests which is carried out at a strain rates closer to $1.67 \times 10^{-6} \text{ sec}^{-1}$. The three temperatures, 25 ° C, 75 ° C and 125 ° C were chosen for the tensile tests because they were closer to minimum, median and maximum temperatures respectively for TMF tests. Table 8 summarizes the results of these tensile tests.

Table 8. Results of the room and elevated temperature tensile testing of lap shear joints at a displacement rate of $1.67 \times 10^{-6} \text{ sec}^{-1}$

Composition	25 °C		75 °C		125 °C	
	Max load (lbs)	Extension at Max load (mils)	Max load (lbs)	Extension at Max load (mils)	Max load (lbs)	Extension at max load (mils)
AMT 6337	155	2.4	76	1.5	49	1.0
AMT-FRS	165	2.0	96	1.3	40	0.9
HPM 6337	135	2.0	119	1.9	33	0.7
Sn-Pb-5Ni	221	3.1	108	1.6	44	0.7
Sn-Pb-2.5Ni	138	2.5	110	1.7	67	1.0
Sn-Pb-5Cu	172	2.7	120	1.9	43	1.0
Sn-Pb-2.5In	156	2.5	100	1.3	34	0.6
Sn-Pb-2.5Ag	167	2.8	140	1.7	45	0.6
Sn-Pb-2.5Bi	142	2.1	103	1.6	39	0.8
Sn-Pb-2.5Sb	154	2.1	101	1.5	43	0.6
Sn-5Sb	169	5.0	126	3.3	66	1.1
Sn-Ag-Bi	292	4.9	244	2.8	52	0.9
Sn-Ag-Bi-In	332	5.1	203	2.9	66	1.4
42Sn-58Bi	121	17.9	122	1.7	27	0.7

As can be seen from Table 8, the ultimate strengths of the lap shear joints decrease with increase in temperature. The Sn-Ag-Bi and Sn-Ag-Bi-In compositions had significantly larger ultimate strengths and larger extensions at maximum load at all three temperatures. The maximum loads at room temperature and ultimate strengths for solder alloys are lower in Table 8 than that observed in Table 6 because of the lower displacement rates employed in tensile test results of Table 8.

To understand the mechanism of failure in the tensile tests, two eutectic solder joints were tested under tension at 25 ° C and 125 ° C, until the load dropped to 50 % of the maximum value. The tests were then stopped and each of these joints was polished for SEM examination. SEM micrographs of these samples shown in Figures 29 (a) and (b) indicate that the joint fails by inter linkage of small voids. EDAX done near the crack shows a copper percentage of 28.8 wt % while the region below the crack has a copper content of about 7 wt %. This suggests that the crack propagates in the interface between the solder and intermetallic layer. At elevated temperatures the difference in elastic moduli between the Sn-Pb solder and the intermetallic would cause the solder -intermetallic interface to be a favored site for initiation of cracks.

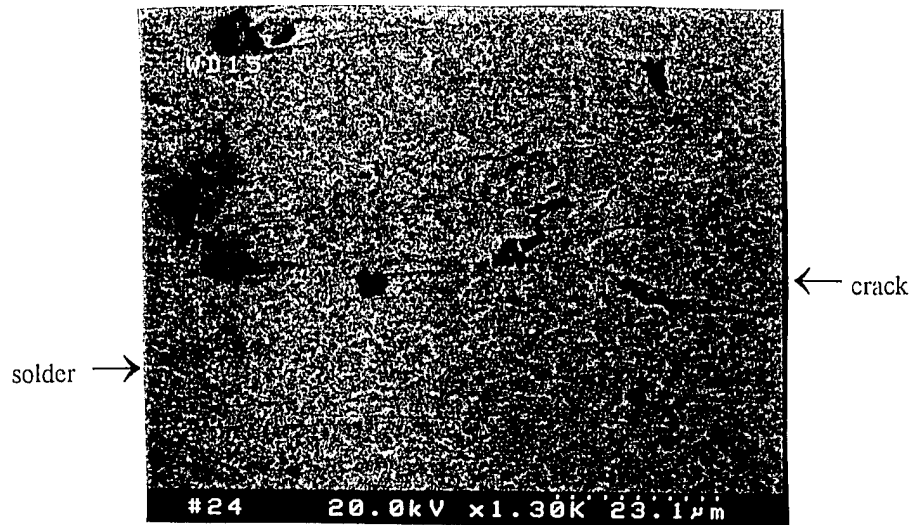


Figure 29. (a)SEM micrograph of the eutectic lap shear joint failed in tension at room temperature.

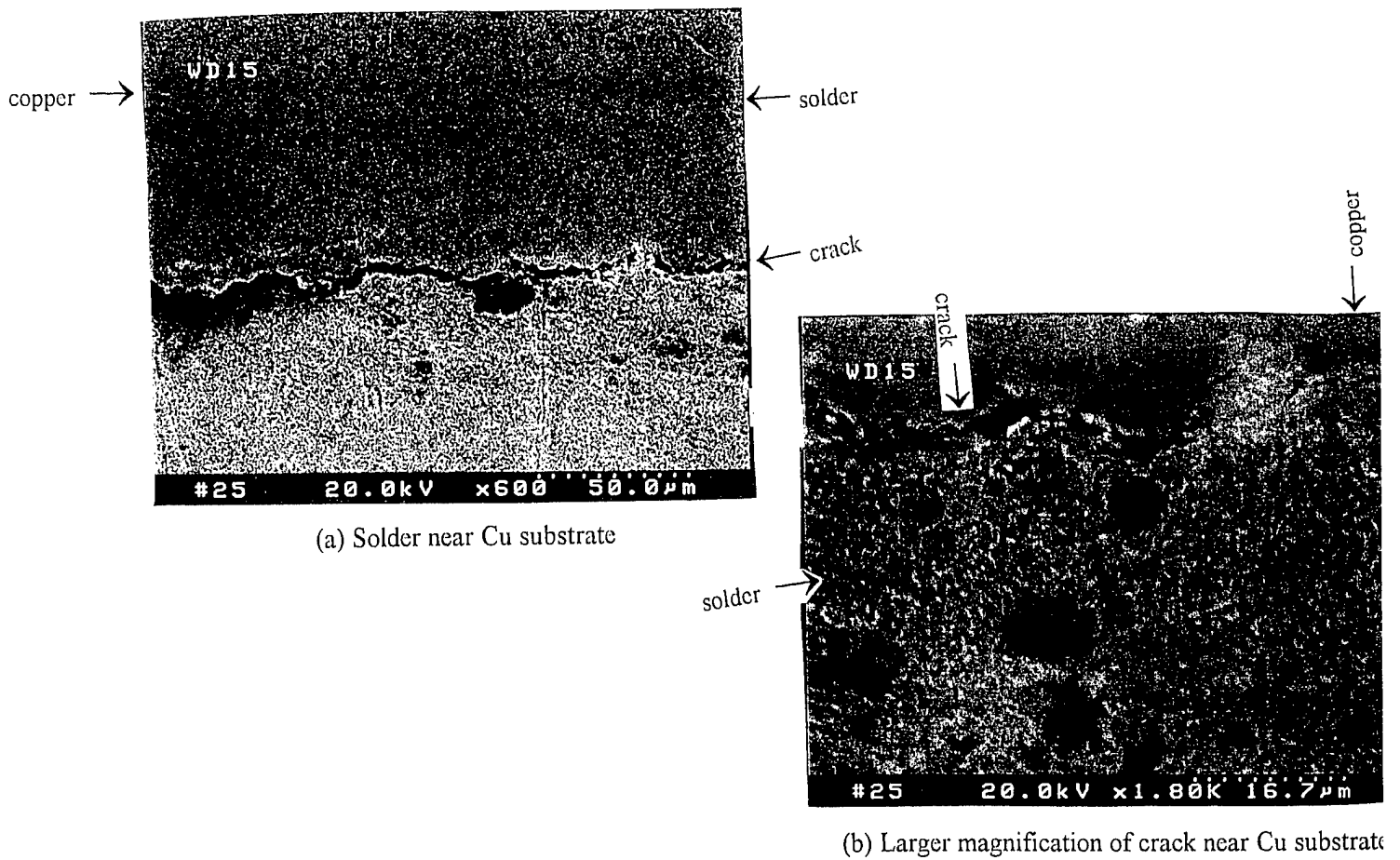


Figure 29. (b) SEM micrograph of the eutectic lap shear joint failed in tension at 125 ° C.

5.4.3 Fatigue testing of lap shear joints

Low cycle fatigue tests were conducted at room temperature on a MTS servo hydraulic load frame at displacement amplitudes of ± 2 mils, ± 1.5 mils and ± 1 mil. The displacement rate was kept constant at 1×10^{-3} in s^{-1} for all of the tests. Figure 30 shows the resulting life times for various solder compositions. Number of cycles to failure corresponds to that for 50 % load drop.

At a displacement amplitude of ± 1 mil, Pb-Sn-5 Ni alloy had the longest life time followed by Pb-Sn2.5Sb and Sn-5Sb and then remaining solid solution and dispersion strengthened alloys. The eutectic and Sn-Bi alloy gave the lowest life times at this amplitude. Eutectic alloy displayed longest life time at greater displacements. Sn-5Sb alloy exhibited some of the longest lifetimes at each displacement amplitude.

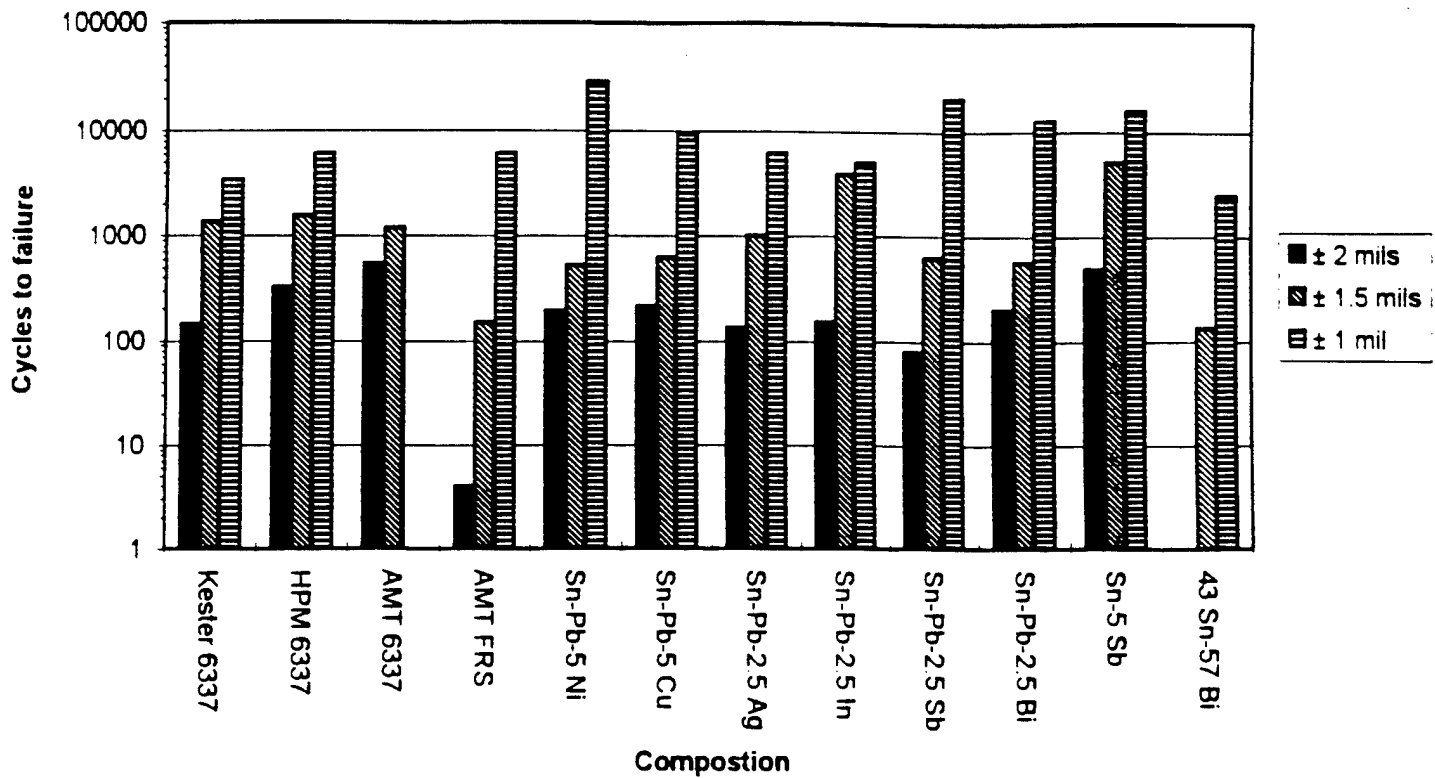
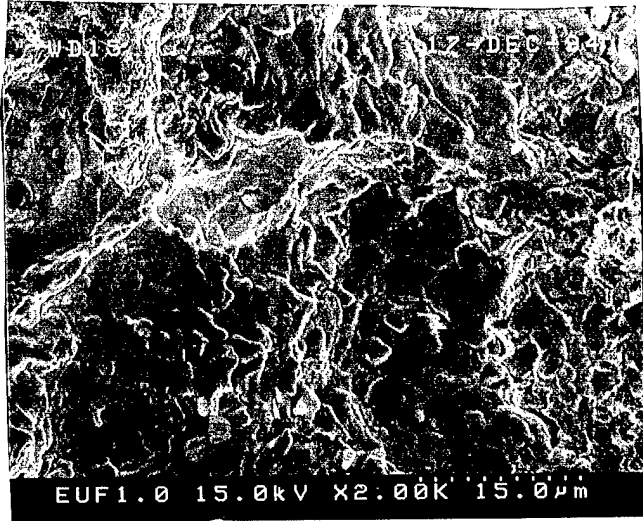


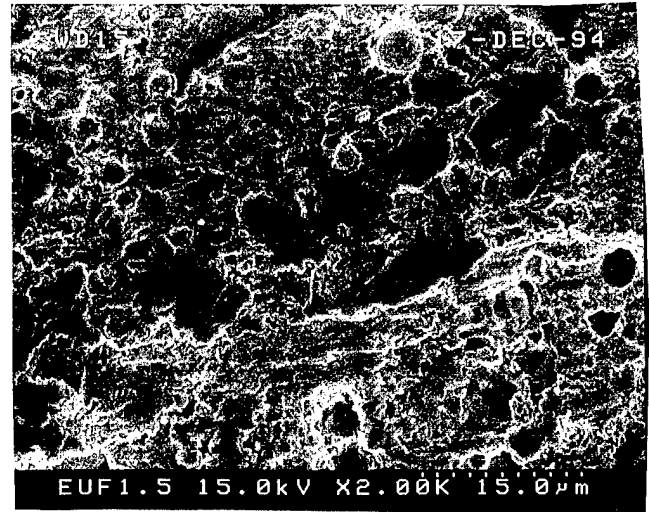
Figure 30. Life times for room temperature low cycle fatigue tests.

5.4.4 Fractography Of Lap-Shear Joints Deformed In Low Cycle Fatigue

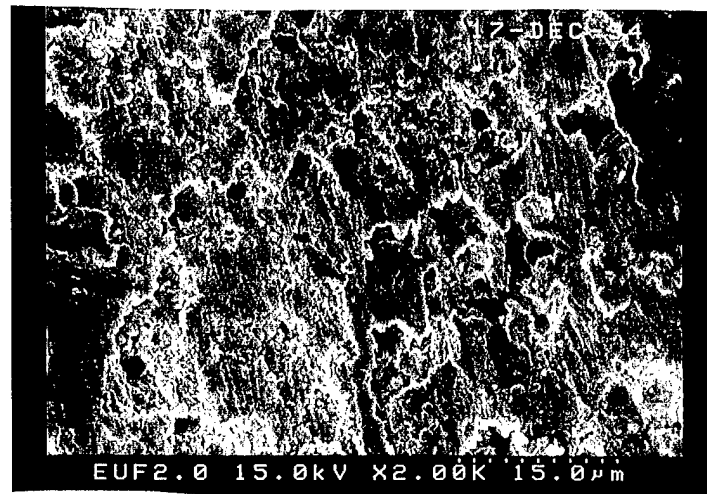
The lap-shear joints after fatigue failure were examined under SEM. Since room temperature corresponds to $0.69 T_m$ homologous temperature, there are considerable chances for cross slipping of lattice dislocations and hence a less chance for striations which are commonly observed for aluminum alloys and steels. Striations were seen randomly in all the solder alloy compositions. Figures 31 (a) to (c) show the SEM fractographs of Pb-Sn eutectic subjected to displacements of ± 2 mils, ± 1.5 mils and ± 1 mil. Failure in lap-shear joints is associated with cavity nucleation and growth. Figures 32 (a) to (c) show representative fractograph of a dispersion strengthened solder alloy.



(a)

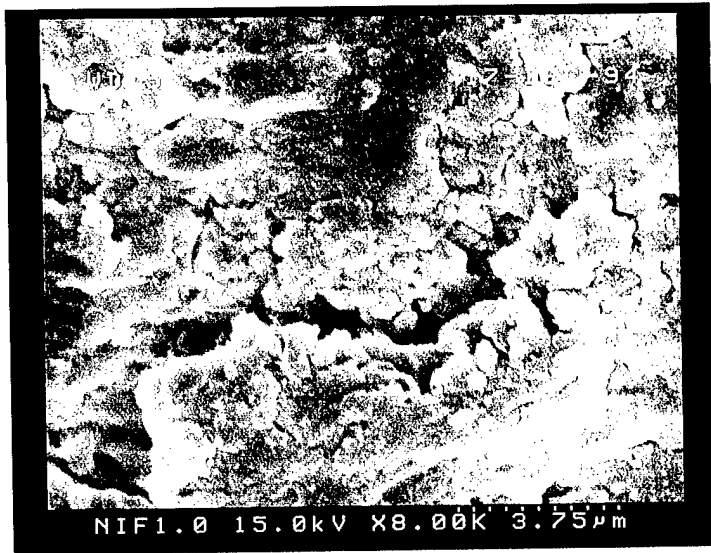


(b)

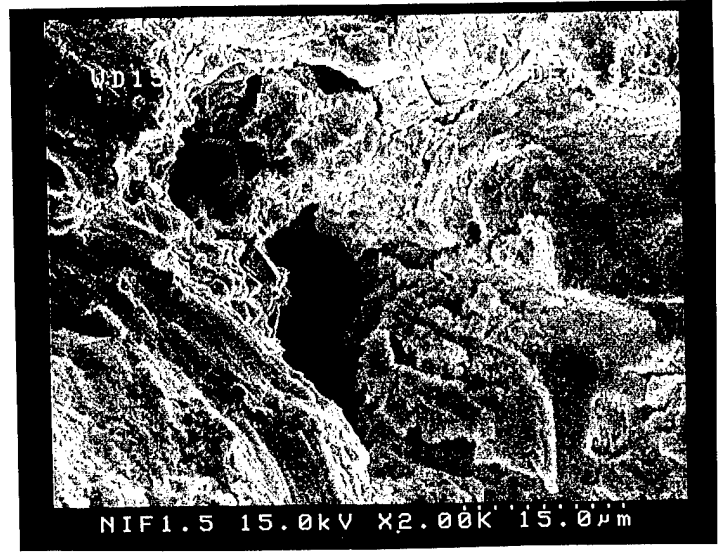


(c)

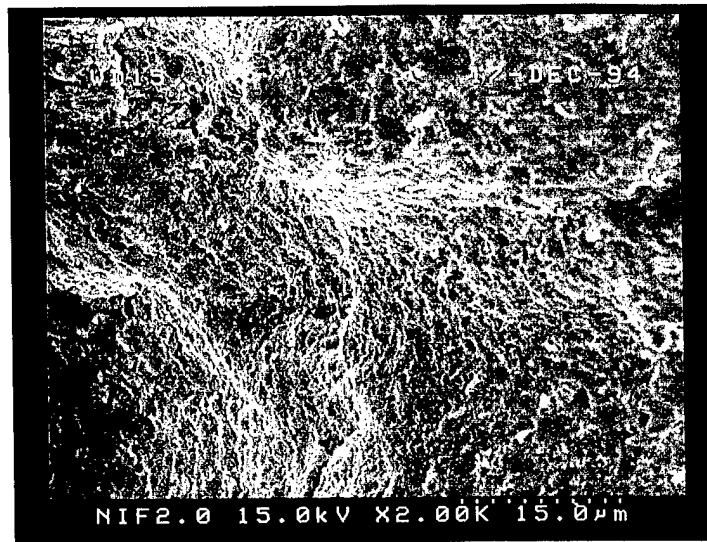
Figure 31. SEM fractographs of Pb-Sn eutectic failed in low cycle fatigue at displacements of (a) ± 1.0 mil (b) ± 1.5 mil and (c) ± 2 mil.



(a)



(b)



(c)

Figure 32 SEM fractographs of dispersion strengthened solder alloy failed in low cycle fatigue at displacements of (a) ± 1.0 mil (b) ± 1.5 mil and (c) ± 2 mil

Low cycle fatigue (displacement controlled) fatigue tests were conducted at a frequency of 0.25 Hz and a displacement amplitude of ± 1.0 mils for selected solder alloy lap-shear joints at 75 ° C and 125 ° C. The results are tabulated in Table 9. Figure 33 summarizes the life times at a displacement of ± 1.0 mils as a function of temperature. A representative hysteresis curve and maximum load vs. cycle plots are shown in Figures 34 (a) and (b).

Sn-Pb-5Ni displayed the greatest fatigue resistance at all three temperatures. This is indicative of the high temperature strengths of the dispersion strengthened alloy. HPM eutectic alloy showed greater fatigue resistance than the AMT eutectic alloy.

Table 9. Low cycle fatigue data at elevated temperatures.

composition	temperature	maximum load, initial cycle (lbs)	cycles to failure
AMT 63Sn-37Pb	75 °C	116.0	1038
HPM 63Sn-37Pb	75 °C	108.9	3878
Sn-Pb-5 Ni	75 °C	125.8	3684
Sn-Pb-2.5 In	75 °C	108.9	464
AMT 63Sn-37Pb	125 °C	113.1	38
HPM 63Sn-37Pb	125 °C	79.8	578
Sn-Pb-5 Ni	125 °C	113.3	1116
Sn-Pb-2.5 In	125 °C	148.7	32

Low cycle fatigue results, ± 1.0 mils displacement

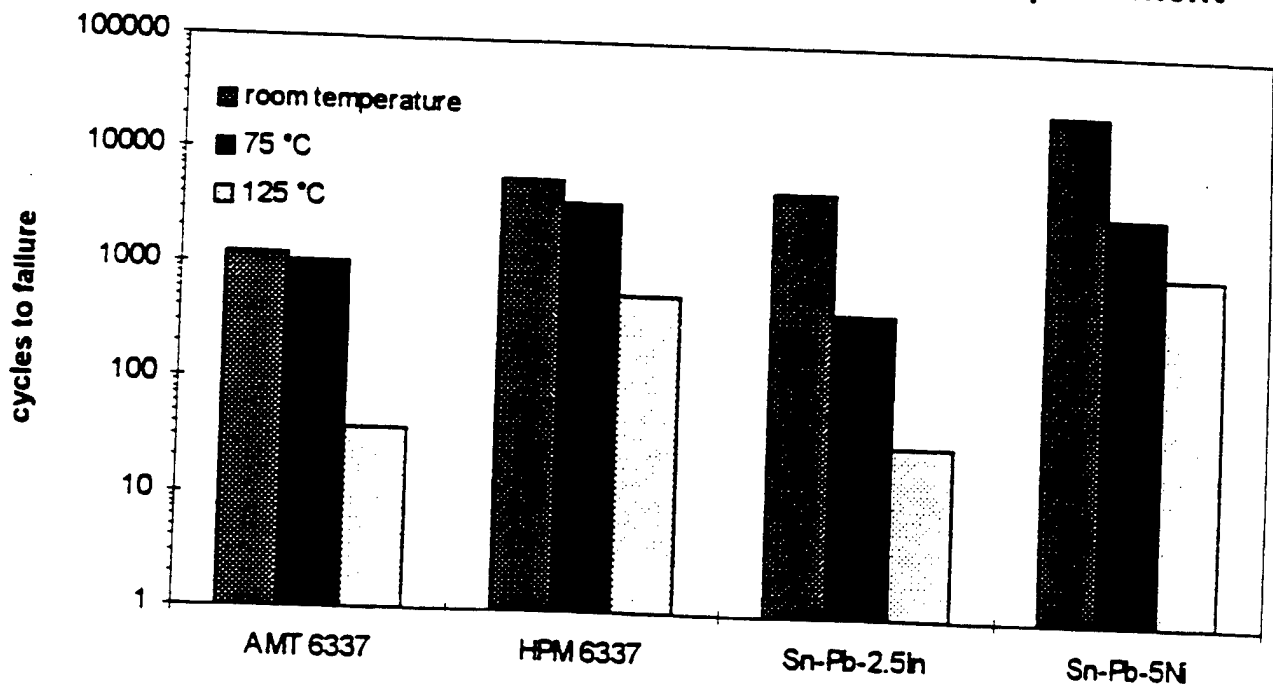
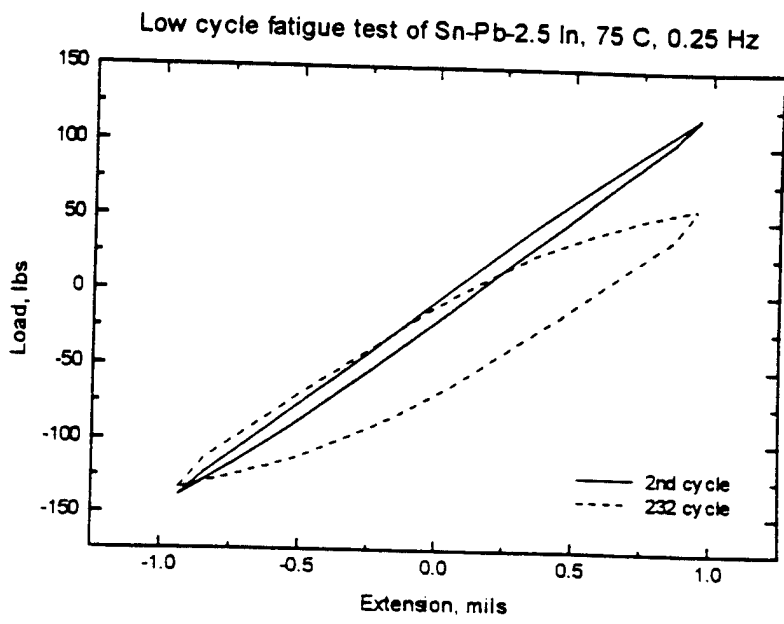
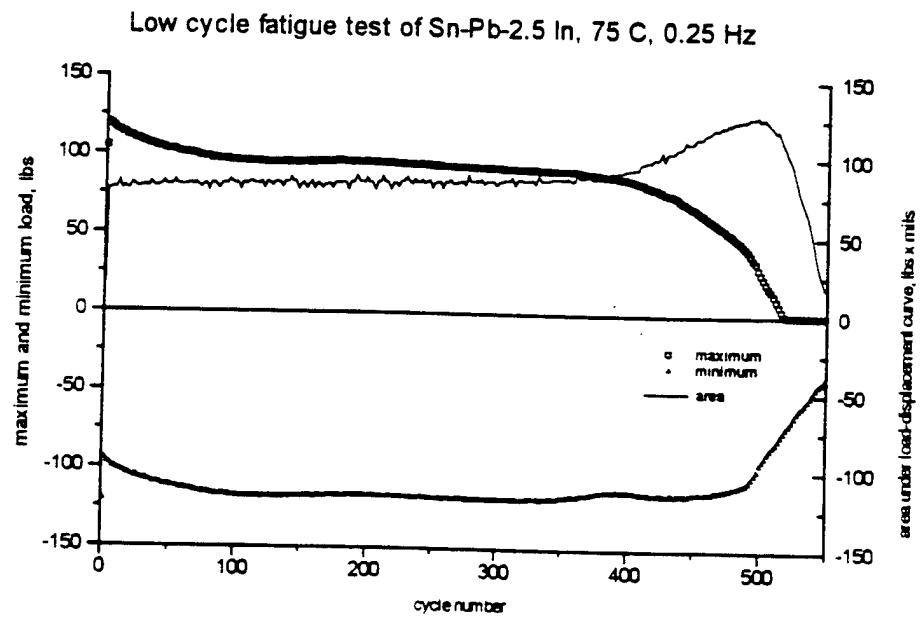


Figure 33. Summary of low cycle fatigue lives of selected lap-shear joint solder alloys as a function of temperature.



(a) Load vs. extension curves for Sn-Pb-2.5 In at 75 °C



(b) Maximum load, minimum load, and area vs. cycle number for Sn-Pb-2.5 In at 75 °C

Figure 34. Hysteresis curve and maximum load, minimum load and area vs. cycle for low cycle fatigue test of Sn-Pb-2.5 In at 75 °C.

5.4.5 High Cycle Fatigue Behavior Bulk Solder Alloys

Some of the solder alloy compositions were tested for high cycle fatigue behavior using bulk samples at room temperature and at 75 ° C. The results are summarized in Figure 35. The high cycle fatigue life of Pb-Sn-5%Cu and Pb-Sn-5%Ni were better than lead less solders such as Sn-5%Sb. At 75 ° C, the high cycle fatigue behavior of dispersion strengthened alloys were much superior to that of Sn-Sb alloys because of presence of thermally stable intermetallic dispersoids in the microstructure.

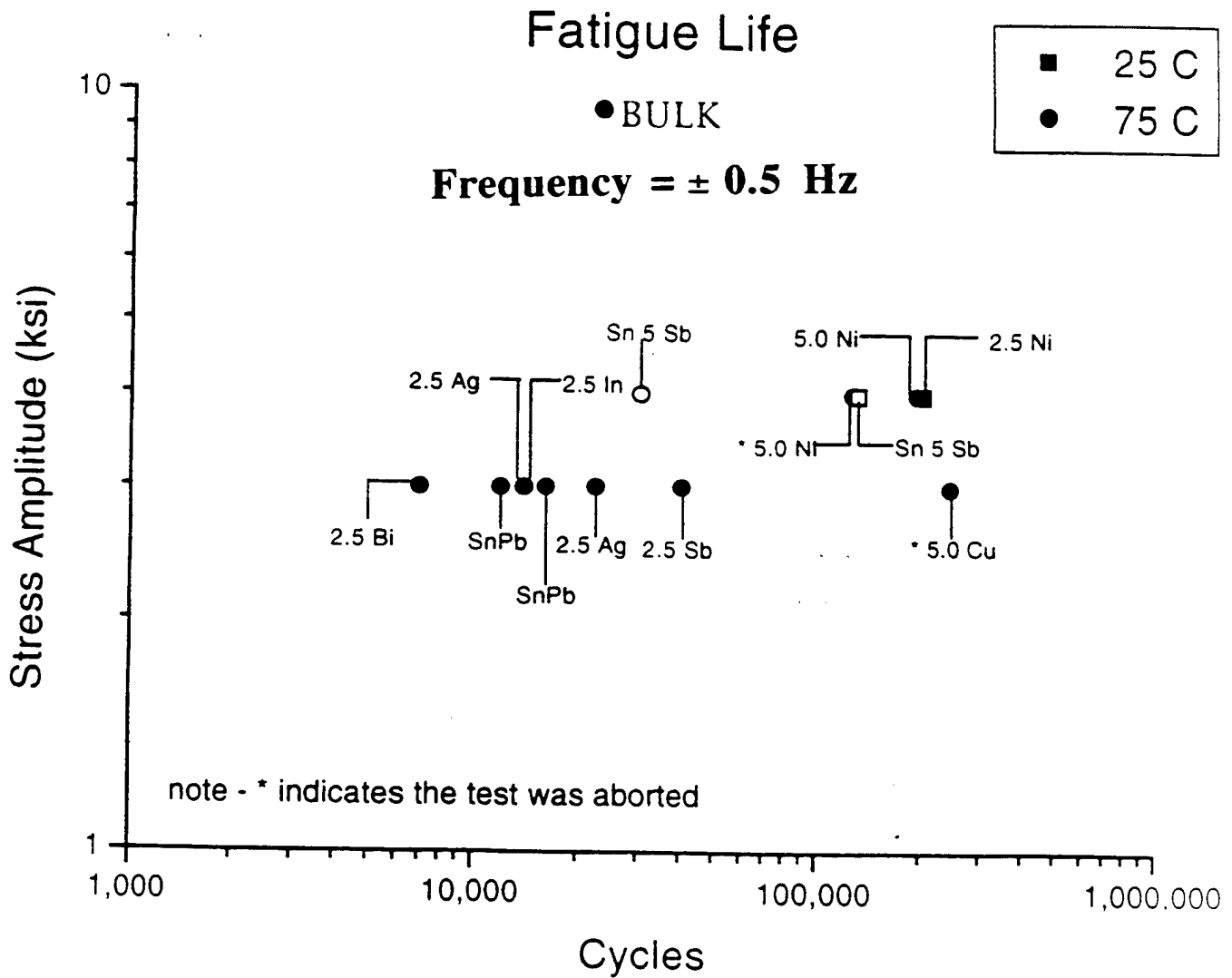
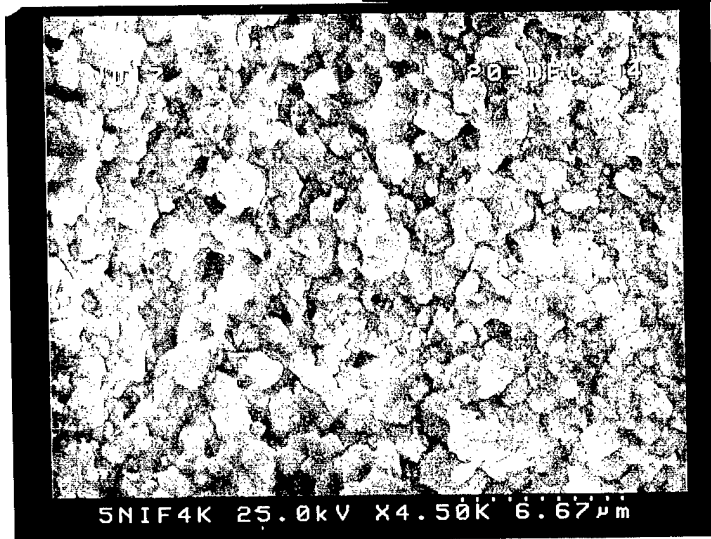
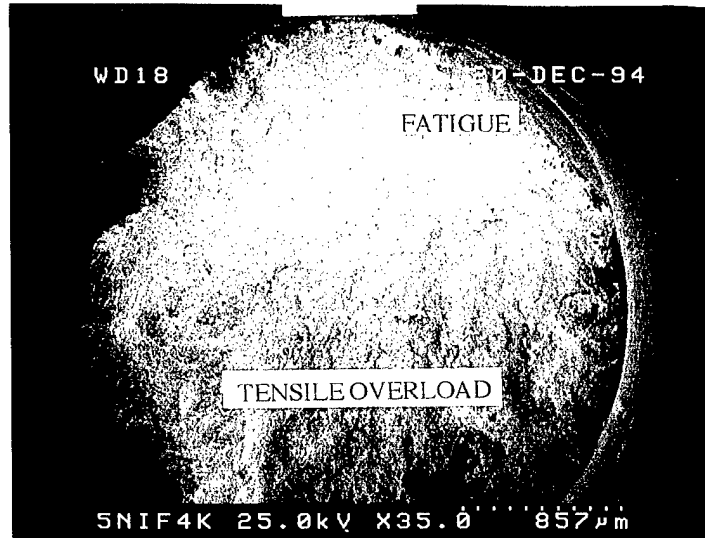


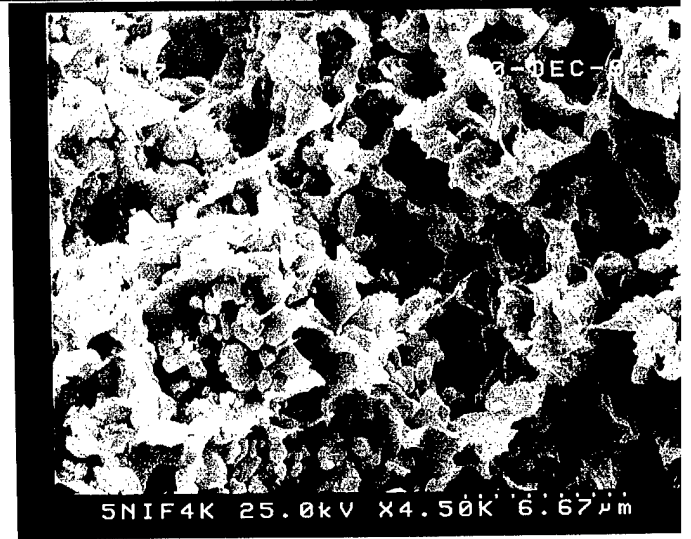
Figure 35. High cycle fatigue properties of bulk solders.

Figures 36 (a) to (c) show the SEM fractograph of the Pb-Sn-5%Ni sample. This specimen survived 120,000 cycles and was interrupted due to power failure and finally failed due to a tensile overload. The fracture mode was intergranular in the fatigued region and ductile in the tensile overload region.

$R = -1$



Fatigued Region (intergranular) mode at higher magnification



Tensile overload Region (ductile) at higher magnification

Figure 36. SEM fractograph of the Pb Sn -5% Ni sample failed in high cycle fatigue test under stress amplitude of ± 4 ksi, at 75°C , and at $R = -1$

5.4.6 Creep Properties Of Lap-Shear Joints

An ATS creep frame with a furnace was used to carry out the creep tests of lap-shear joints. An LVC (Linear variable Capacitance) transducer connected to an IBM-compatible PC was used to measure and record displacement during creep tests at a resolution of 12 bits. Jump creep tests were conducted at room temperature, 75 ° C and 125 ° C. Displacement vs. time was plotted as shown in Figure 37 in order to determine the steady state creep rate $\dot{\epsilon}$. Using a log-log plot of the steady state creep rate and the applied stress, creep exponents were calculated. Figures 38 (a) to (c) show the creep rate vs. applied stress for selected five alloys at room temperature, 75 ° C and 125 ° C. Table 10 gives the creep exponents and activation energies of these solder alloys.

The dispersion strengthened Sn-Pb-5% Ni has a threshold stress below which the solder joint can not creep. The presence of threshold stress makes it difficult, to accurately get the creep exponent. For calculating the creep exponents, threshold stresses have to be subtracted from the applied stresses. The dispersion strengthened Sn-Pb-5Ni and Sn-Sb alloy displayed higher creep exponent than the solid solution strengthened and eutectic alloys. The activation energies calculated for Sn-Pb eutectic and solid solution strengthened Sn-Pb-In are close to the activation energy in Sn and Pb for lattice self diffusion.

The failure mechanism is by cavity nucleation and growth. In the case of eutectic solders this is due to grain boundary cavitation. In the case of solid solution alloys, cavity formation may be due to cavitation from strain mismatches at triple junctions. In the case of dispersion strengthened alloys, cavities are nucleated at dispersoids. Representative solder samples failed under creep are shown in Figures 39 and 40. The activation energies were calculated for these solder compositions and the values are in the range of dislocation climb. Since creep exponents varied widely over the temperature range, activation energy was not determined for Sn-Sb alloy. Creep tests of eutectic alloy at room temperature and at 125 ° C were conducted for three hours. The tests were then stopped and the samples were then polished for SEM examination. This SEM micrograph is shown in Figure 41. There are no traces of cracks near Cu-solder interface. There is some evidence that these joints deformed by the interlinkage of voids by cracks throughout solder joint. The deformed sample at 125 ° C contained cracks parallel to the Cu substrate possibly at the interface between the intermetallic layer and the solder or in the solder near the interface.

The damage mechanisms at room temperature and at elevated temperature are thus different as supported by the difference in creep exponents and the crack propagation sites.

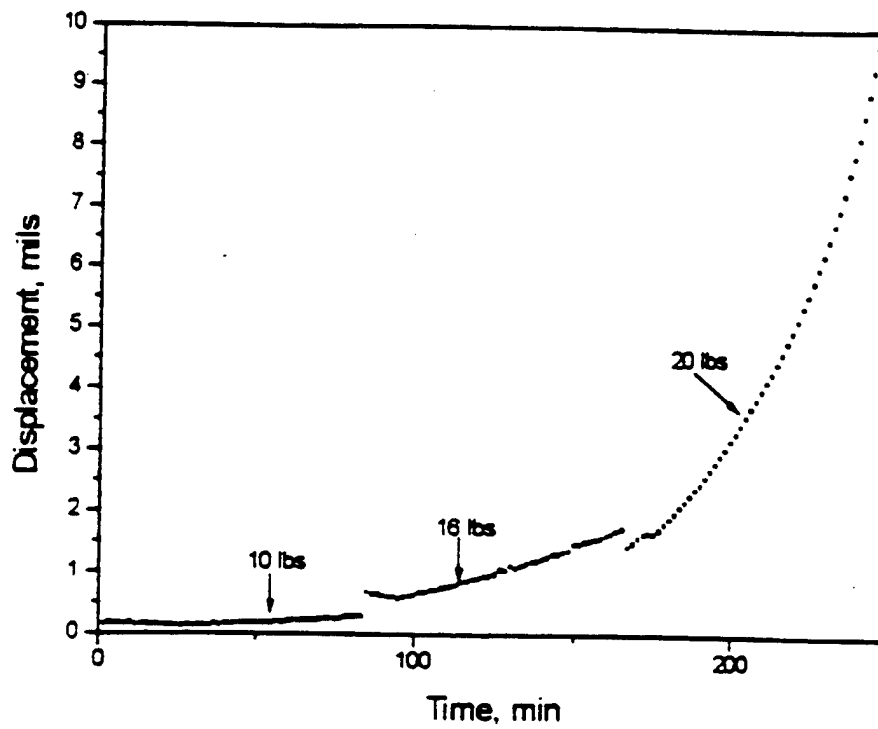


Figure 37. Typical displacement vs. time plots obtained for eutectic Pb-Sn at 75 ° C.

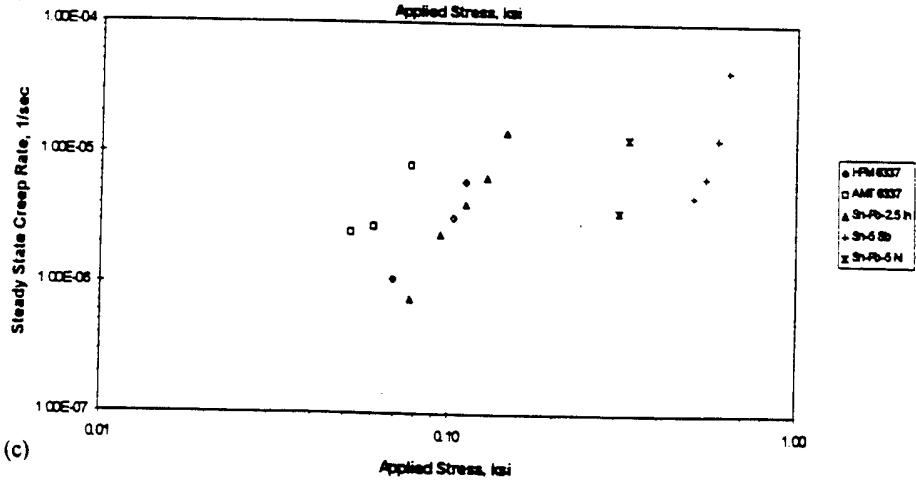
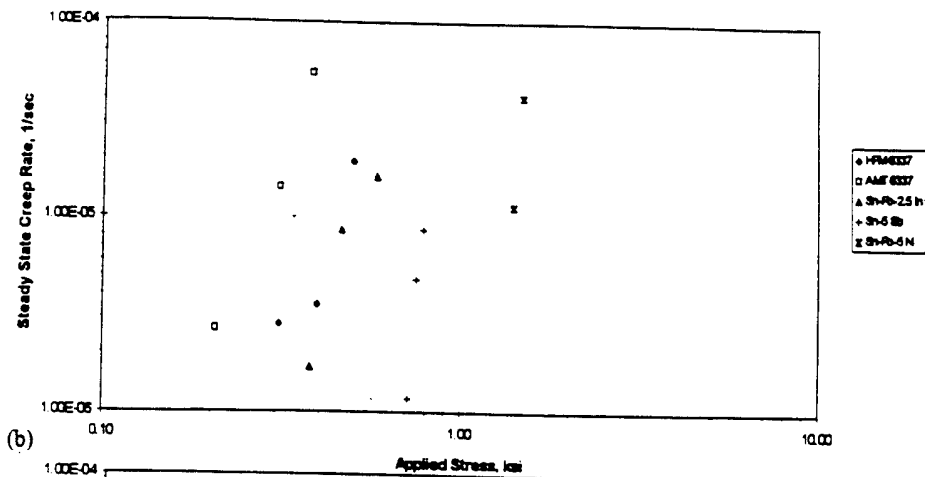
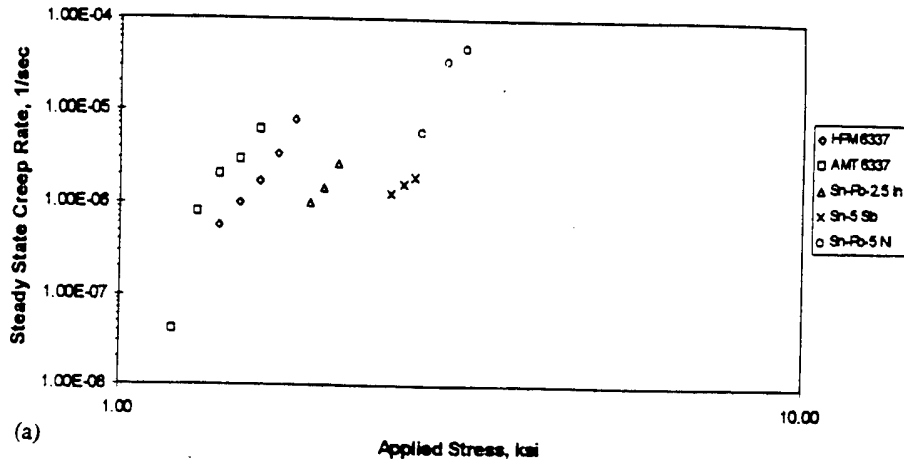


Figure 38. Steady state creep rate vs. applied stress for lap shear joints of selected solder compositions (a) Room temperature (b) 75 ° C and (c) 125 ° C.

Table 10. Creep exponents and activation energies.

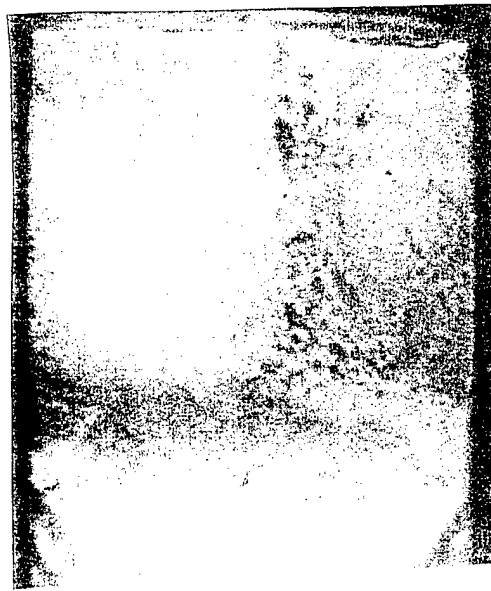
composition	creep exponent			activation energy (Kcal/mol)
	room temperature	75 °C	125 °C	
HPM 63Sn-37Pb	10.0	3.98	3.33	30.8
AMT 63Sn-37Pb	9.3	4.88	3.07	30.4
Sn-Pb-2.5In	10.5	5.12	4.41	34.2
Sn-5Sb	5.12	33.8	9.48	
Sn-Pb-5Ni	14.7	21.8	21.8	177.3
Sn-Pb-5Ni (threshold stress subtracted)		2.41	4.19	11.3



(a) HPM 63Sn-37Pb, room temperature

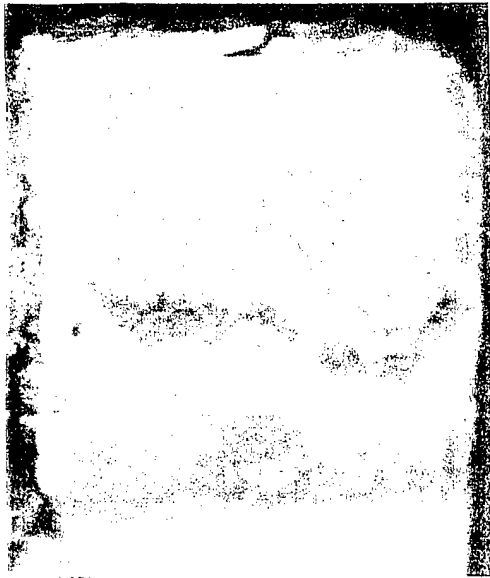


(b) HPM 63Sn-37Pb, 75 °C



(c) HPM 63Sn-37Pb, 125 °C

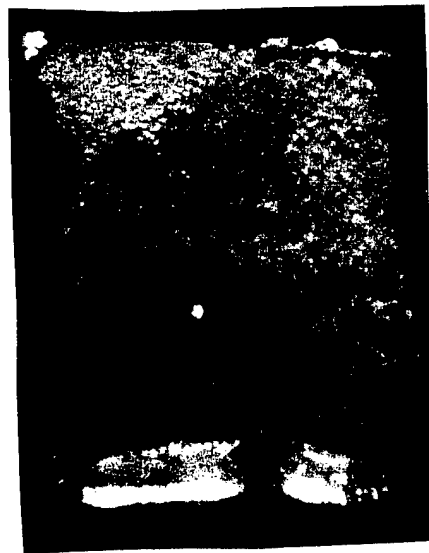
Figure 39. Fracture surfaces of Pb-Sn eutectic samples failed in creep at (a) room temperature (b) 75 ° C and (c) 125 ° C.



(g) Sn-Pb-5Ni, room temperature

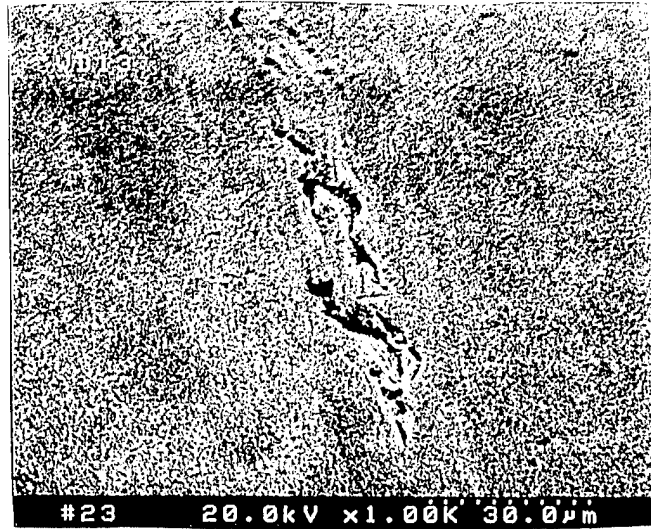


(h) Sn-Pb-5Ni, 75 °C

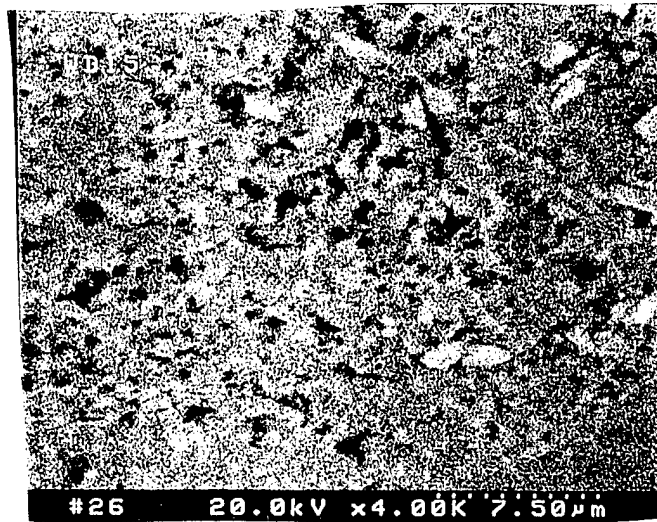


(i) Sn-Pb-5Ni, 125 °C

Figure 40. Fracture surfaces of dispersion strengthened Pb-Sn -5 % Ni samples failed in creep at (a) room temperature (b) 75 ° C and (c) 125 ° C.



(a) HPM 63Sn-37Pb tested at room temperature



(b) AMT 63Sn-37Pb tested at room temperature

Figure 41. SEM micrographs of eutectic Sn-Pb solder joint after 3 hours of creep test at (a) room temperature and (b) 125 ° C.

5.4.7 Thermomechanical Fatigue Tests Of lap-Shear Joints

Thermomechanical fatigue (TMF) tests were conducted by applying in phase, triangular temperature (25 ° C to 100 ° C) and extension (± 0.7 mils) waveforms. Hysteresis plots of load vs. extension were recorded for every cycle. These plots were analyzed to measure the number of cycles to failure (defined as 50 % load drop from the maximum load in the initial cycle). In addition, plots were made for each test of the area under each hysteresis curve and the maximum cyclic load vs. the number of cycles.

A TMF test setup was designed to allow displacement waveforms to be applied to a solder joint, while simultaneously cycling the temperature in a test furnace. An IBM compatible PC is used to control the tests as well to record and analyze the data. The computer has Keithley DAS-HRES data acquisition board, a Keithley DAS-TC thermocouple board and a Keithley anti-aliasing filter (AAF). Labtech Notebook Pro Software is used to control the fatigue tests. Figure 42 shows a flow diagram of the computer interfaced with controllers and data acquisition boards.

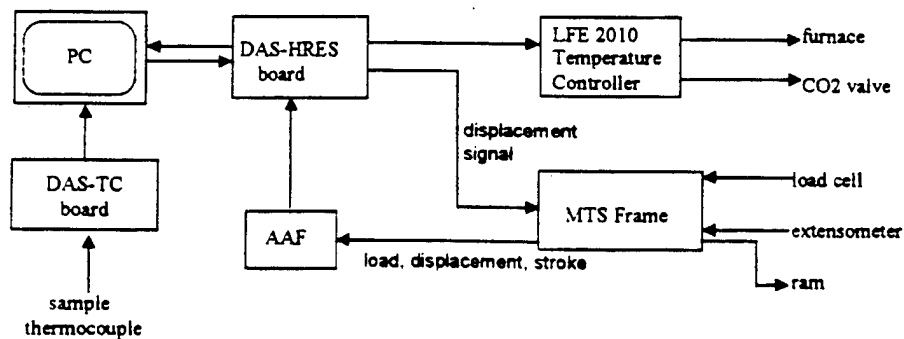


Figure 42. Flow diagram of computer and its interface with controllers and data acquisition boards.

The computer is connected via the DAS-HRES board to a servo-hydraulic MTS test frame. An extensometer is attached to the sample and is used to measure displacement. The TMF tests are conducted under displacement control. The DAS-HRES board is also used to interface the computer to a LFE Model 2010 temperature controller. The temperature controller is connected to a furnace on MTS frame which is capable of achieving temperatures of around 200 ° C, with maximum heating rates of approx. 7.5 ° C per minute. The controller is also connected to a solenoid valve, which when open allows liquid CO₂ to enter the furnace and rapidly cool the chamber as the gas expands. The CO₂ allows the furnace to be cooled to a temperature of 0 ° C with rates of around 15 ° C per minute. Figure 43 shows the schematic diagram of the furnace and attachments used in TMF tests.

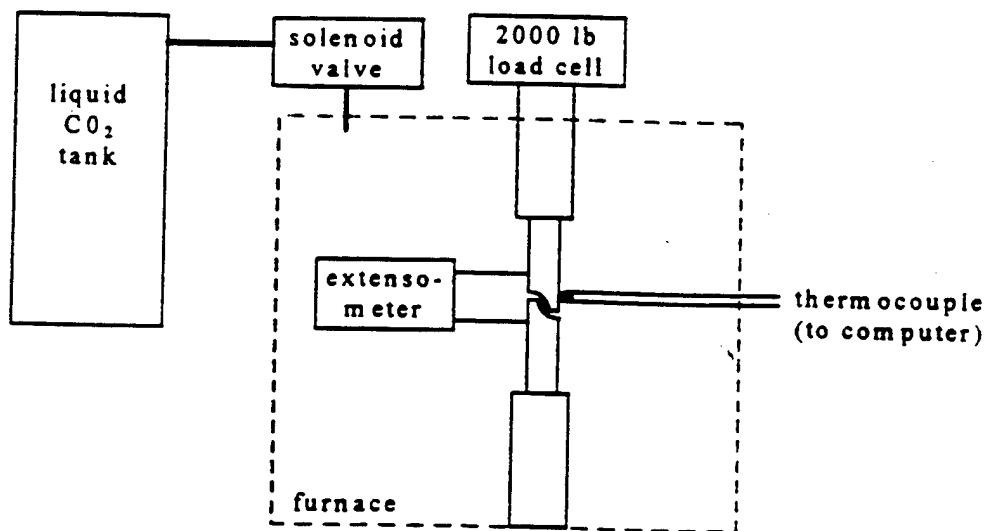


Figure 43. Schematic diagram of the furnace and attachments used in TMF tests.

Figure 44 shows typical temperature and displacement curves for a TMF test [9]. As shown in this figure, the temperature and displacement are cycled in phase to attempt to simulate the conditions experienced by an actual solder joint. Table 11 summarizes the TMF test parameters.

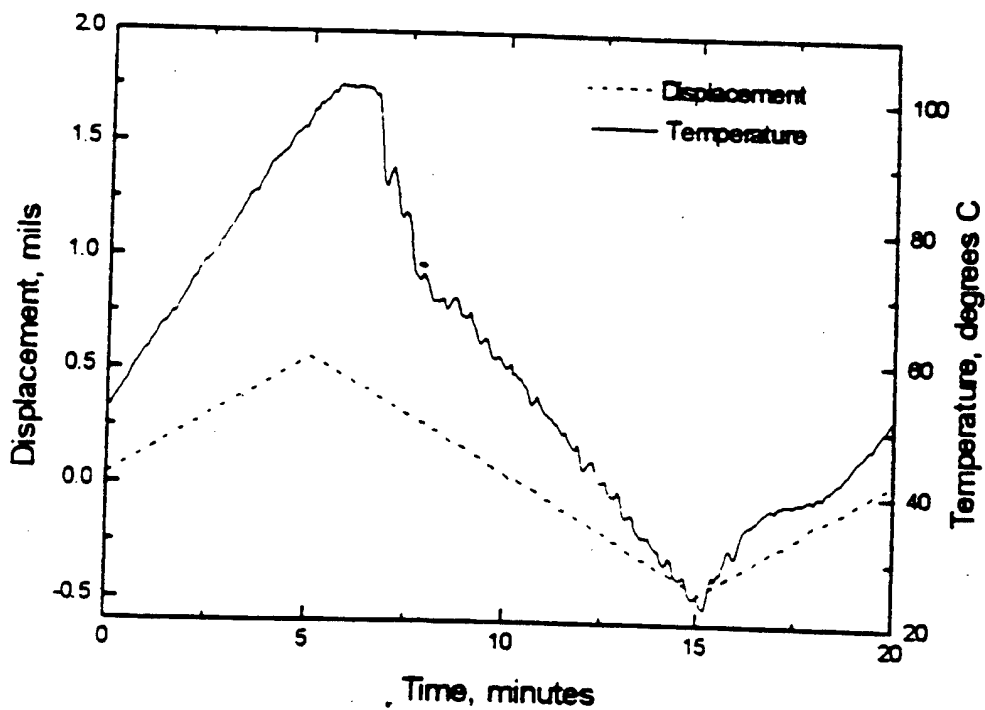


Figure 44. Typical temperature and displacement curves for a TMF test.

Table 11. TMF test parameters.

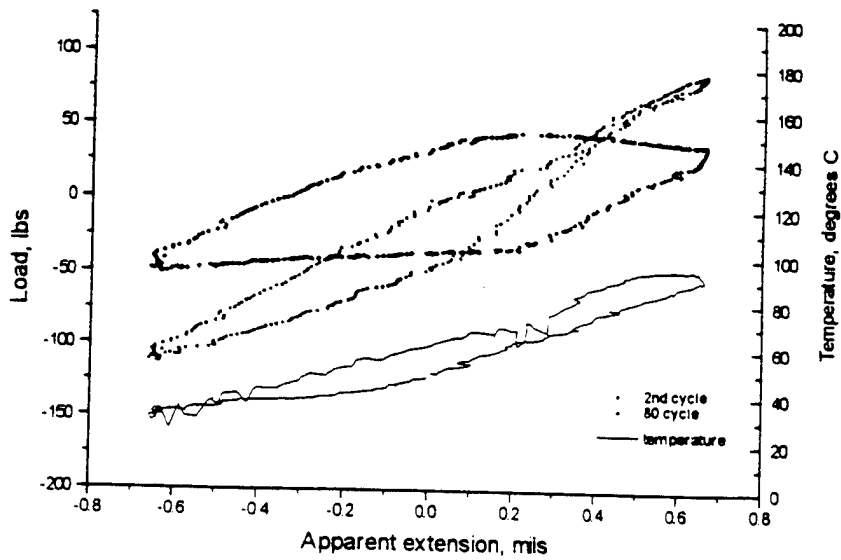
maximum temperature	100 °C
minimum temperature	25 °C
positive (heating) ramp time	10 minutes
positive displacement rate	1.167×10^{-6} in/sec
negative (cooling) ramp time	10 minutes
negative displacement rate	$- 1.167 \times 10^{-6}$ in/sec
cycle time	20 minutes
apparent displacement range	± 0.7 mils
phase difference between temperature and displacement curves	0°
failure definition	maximum load decreased 50% from the initial cycle
data acquisition	load, displacement, stroke, and temperature recorded 15 times per minute

TMF tests were conducted for 12 solder alloy compositions using in-phase, triangular waveforms for temperature and displacement with ranges of 25 ° C to 100 ° C and -0.7 mils to +0.7 mils, respectively [12,13]. Life times which were defined as the cycle in which the maximum cyclic load had dropped by 50 % from the initial cycle are listed in the Table 12 . Figures 45 and 46 show representative hysteresis curves for an eutectic and dispersion strengthened alloy. These figures also contain a plot of the variation of temperature with extension during each cycle.

Table 12. Lifetime results of TMF tests.

composition	cycles to failure	average cycles to failure	maximum load during initial cycle (lbs)	average maximum load in initial cycle (lbs)
AMT 63Sn-37Pb	100	94.4	71.7	82.6
	62		86.9	
	96		91.1	
	146		77.6	
	68		85.5	
HPM 63Sn-37Pb	80	116.0	90.5	93.1
	152		95.6	
IEM 63Sn-37Pb	106	106	116.5	116.5
AMT FRS	73	73	78.0	78.0
63Sn-34.5Pb-2.5Ni	146	173.0	88.1	80.4
	200		72.7	
63Sn-32Pb-5Ni	372	265 +	89.3	89.7
	160 +		90.1	
63Sn-32Pb-5Cu	114	124.0	115.8	105.2
	134		94.6	
63Sn-34.5Pb-2.5In	72	68.0	71.6	89.4
	64		85.9	
63Sn-34.5Pb-2.5Ag	50	53.0	85.2	85.1
	56		85.0	
95Sn-5Sb	282 +	280 +	88.9	92.3
	278 +		95.7	
90Sn-3.2Ag-6.8Bi	164	164	84.0	84.0
86Sn-3Ag-4.2Bi-6.8In	108	108	94.2	94.2
* note: a "+" indicates that the test was a run-on				

TMF test of HPM 6337



(c) Load and temperature vs. extension curves for HPM 63Sn-37Pb

TMF test of HPM 6337

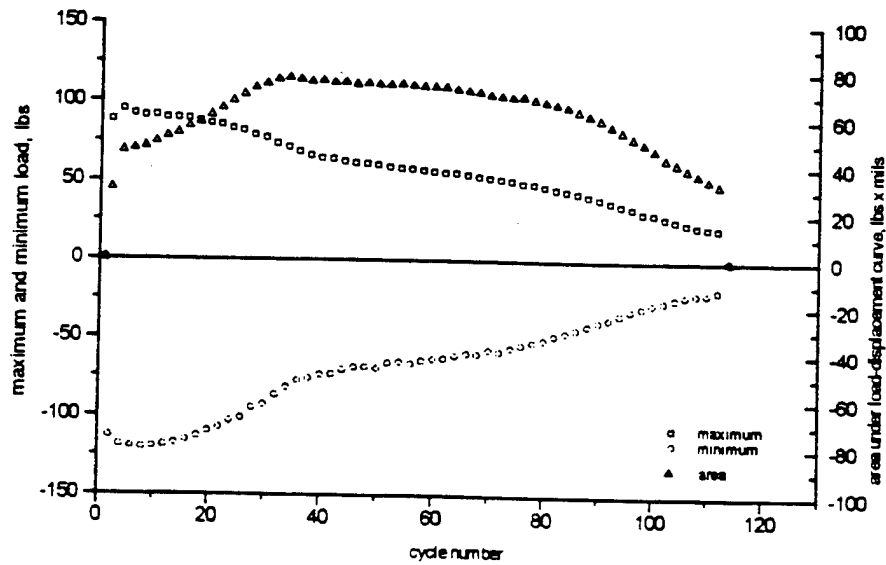
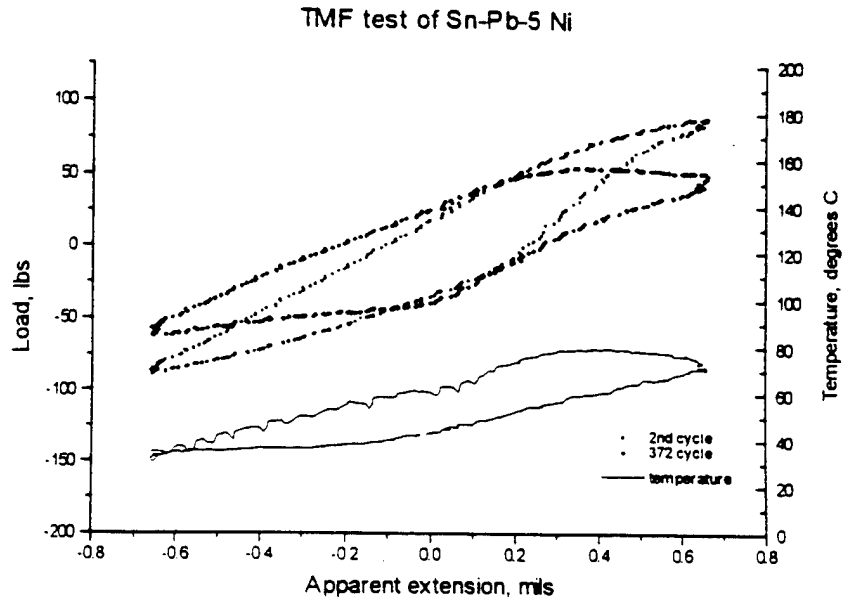


Figure 45. Hysteresis curves and maximum load, minimum load and area vs cycle for HPM Pb-Sn eutectic alloy during TMF tests.



(k) Load and temperature vs. extension curves for Sn-Pb-5Ni

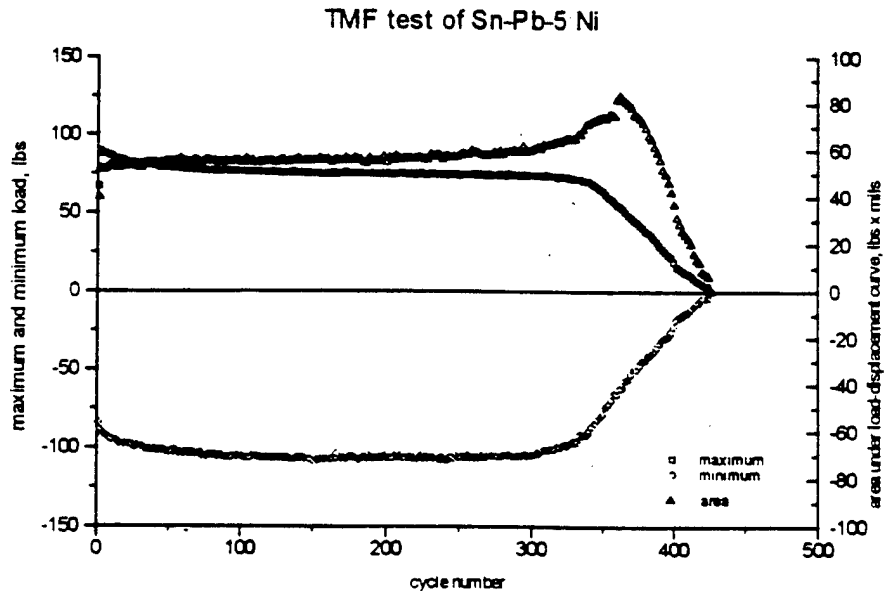


Figure 46. Hysteresis curves and maximum load, minimum load and area vs cycle for Pb-Sn-5 %Ni alloy during TMF tests.

Figure 47 compares the lifetimes of lap-shear joints of various solder alloy compositions during TMF testing.

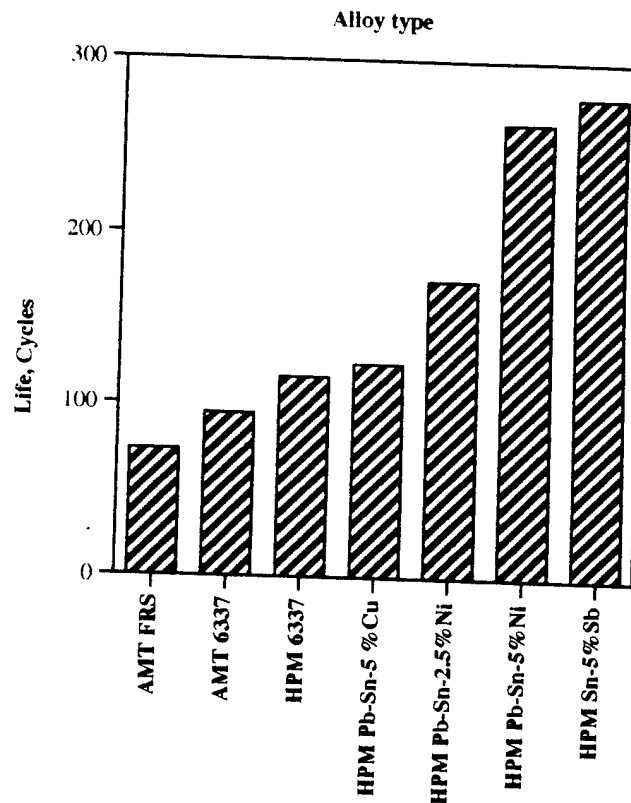


Figure 47. Comparison of the lifetimes of various solder alloy compositions obtained during TMF testing of lap shear joints.

The 95Sn-5Sb alloy, with highest melting point (240° C) showed the longest TMF lifetimes. The Sn-Pb-5%Ni, a dispersion strengthened alloy with a melting point of 184 ° C, had the second longest life time followed by other two dispersion strengthened alloys namely Sn-Pb-2.5%Ni and Sn-Pb-5%Cu and the other high melting point, lead less compositions Sn-Ag-Bi and Sn-Ag-Bi-In. The eutectic alloys performed better than the two solid solution strengthened alloys.

The majority of the alloys tested displayed a steady, almost linear decrease in maximum cyclic load with the number of cycles. The exceptions to this were Sn-Ag-Bi, Sn-5Sb and Sn-Pb-5% Ni. These three solders had maximum cyclic loads which changed very little with the number of cycles. The area in each hysteresis curve remained almost constant with time for the high melting temperature alloys (Sn-Ag-Bi, Sn-Ag-Bi-In and Sn-Sb) as well as for Sn-Pb-5Ni. The areas under the hysteresis curve represent the amount of plastic work deforming the sample.

The Sn-Pb-5%Ni had the best fatigue resistance at room and elevated temperatures. The creep strengths and microhardness values of Sn-Pb-5%Ni and Sn-5Sb were also the best. The TMF life times were also the best for Sn-Pb-5%Ni and Sn-5%Sb alloys. Therefore, there may be a relationship between fatigue strengths, creep strengths, microhardness and the thermomechanical fatigue resistance of alloys.

5.4.8 Metallography Of Lap-Shear Joint Samples Tested For TMF

TMF tests were stopped after the load had dropped by more than 50% from the maximum value on the initial cycle , which resulted in all of the samples remaining intact. One sample of each composition was prepared on one side , as shown by section AA in Figure 48, for optical metallography and SEM studies. A back scattered mode in SEM was used for phase contrast in conjunction with EDS for elemental analysis.

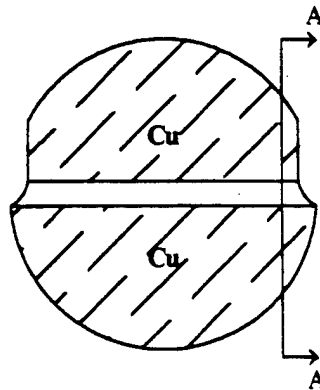


Figure 48. Schematic diagram of the location of lap-shear joints for metallographic examination.

With the help of EDS, intermetallic layer in the solder was examined by taking a series of measurements starting in Cu substrate to inside the solder joint. Figure 49 shows a typical plot obtained from such measurement. The thickness of the intermetallic layer was defined as the position at which the weight percentage of copper dropped below 5%. In the Figure 49, the intermetallic layer is equal to 3.7 μm .

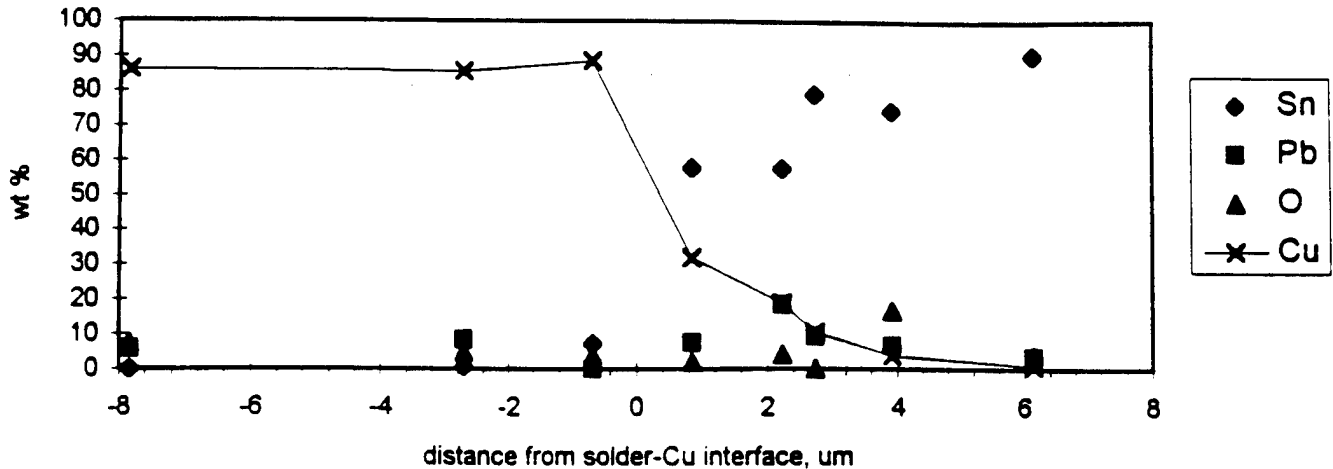
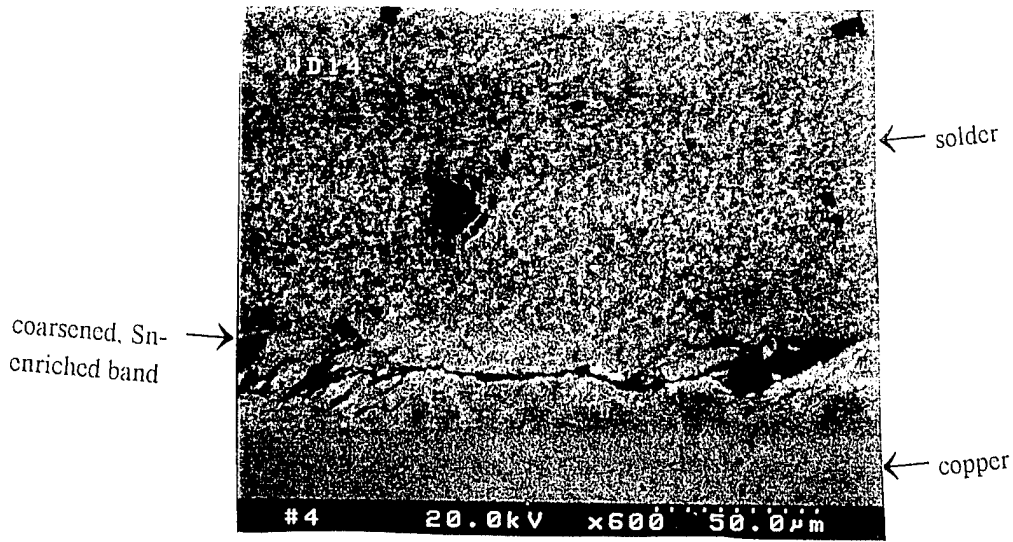
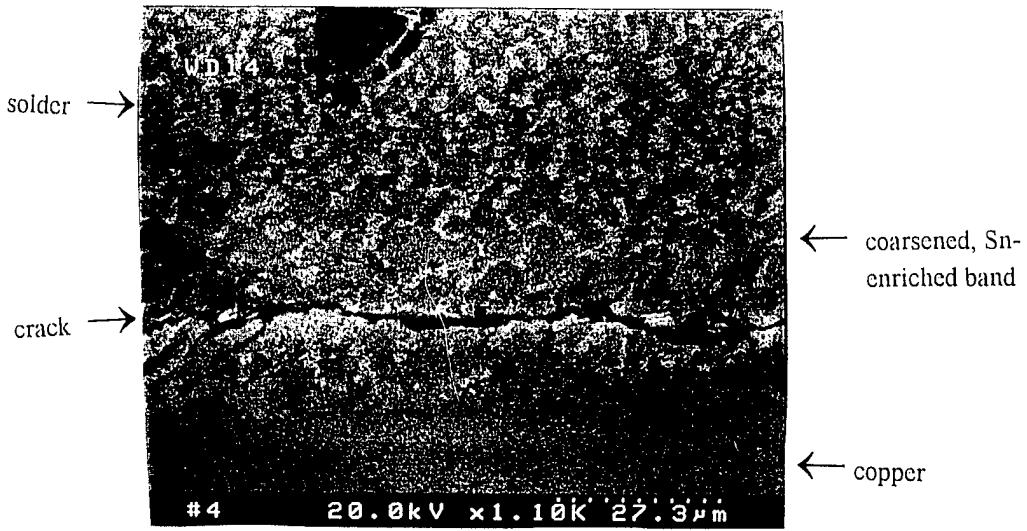


Figure 49. Sample EDS of the intermetallic layer.

Figures 50 to 54 show typical SEM micrographs of lap-shear joint samples failed in thermomechanical fatigue tests. The eutectic samples and solid solution strengthened alloys contained cracks which seemed to propagate through a coarsened band. The dispersion strengthened Sn-Pb-5%Ni and Sn-Pb-5%Cu contained no evidence of a heterogeneously coarsened area possibly due to the dispersoids restricting the heterogeneous growth of grains[14]. This may have led to the longer lifetimes of the dispersion strengthened alloys. Moreover, dispersion strengthened alloys retain their strengths at elevated temperatures leading to a smaller differences in the strengths at intermetallic-solder interface[15].

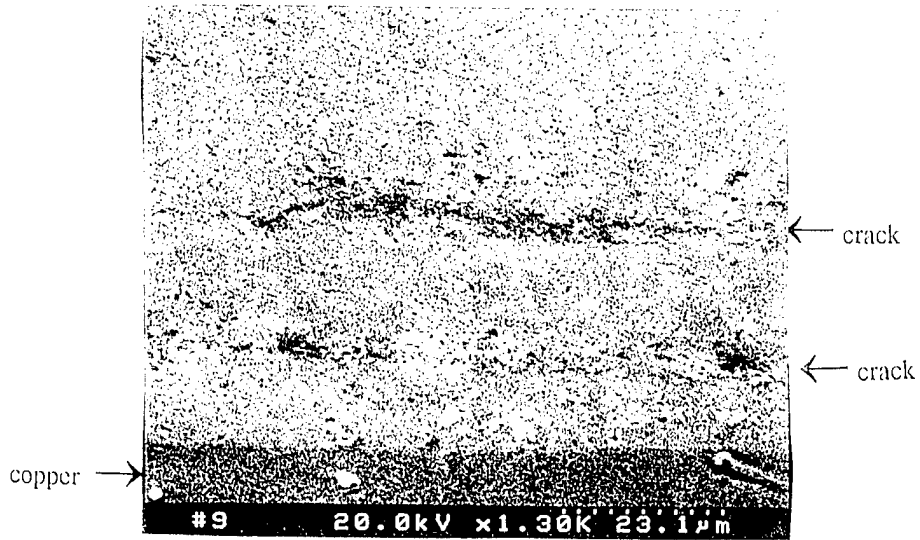


AMT 63Sn-37Pb, near Cu substrate, crack in coarsened area, back-scattered mode

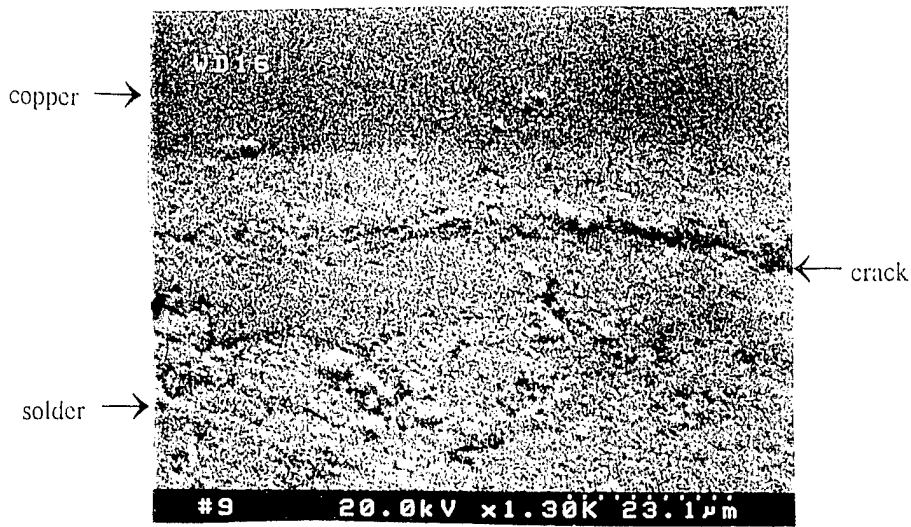


AMT 6337, higher magnification of (a), back-scattered mode

Figure 50. SEM micrograph of eutectic solder alloy after TMF test.

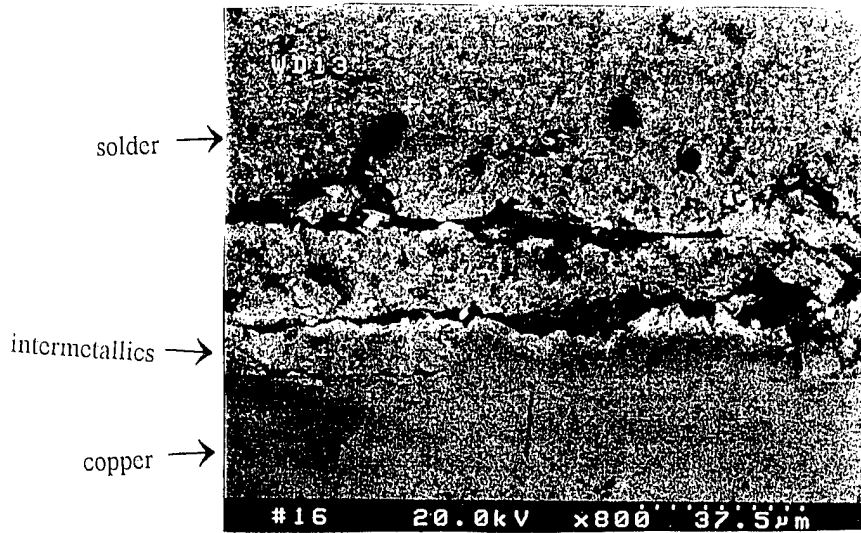


Sn-Pb-5Ni, 2 parallel cracks propagating parallel to Cu substrate, one crack in intermetallic layer, other in solder

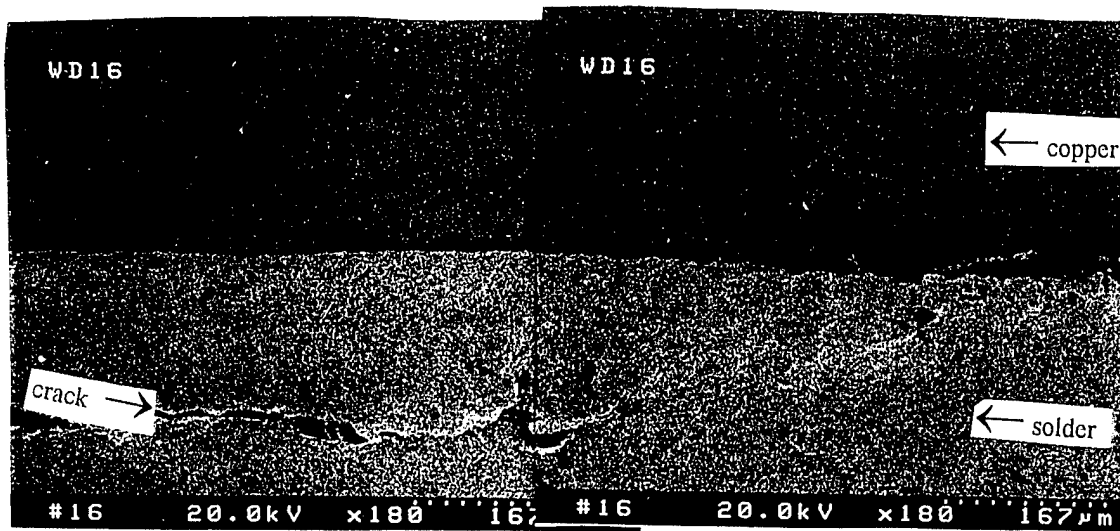


Sn-Pb-5Ni, crack in intermetallic layer

Figure 51. SEM micrograph of Sn-Pb-5%Ni alloy after TMF test.

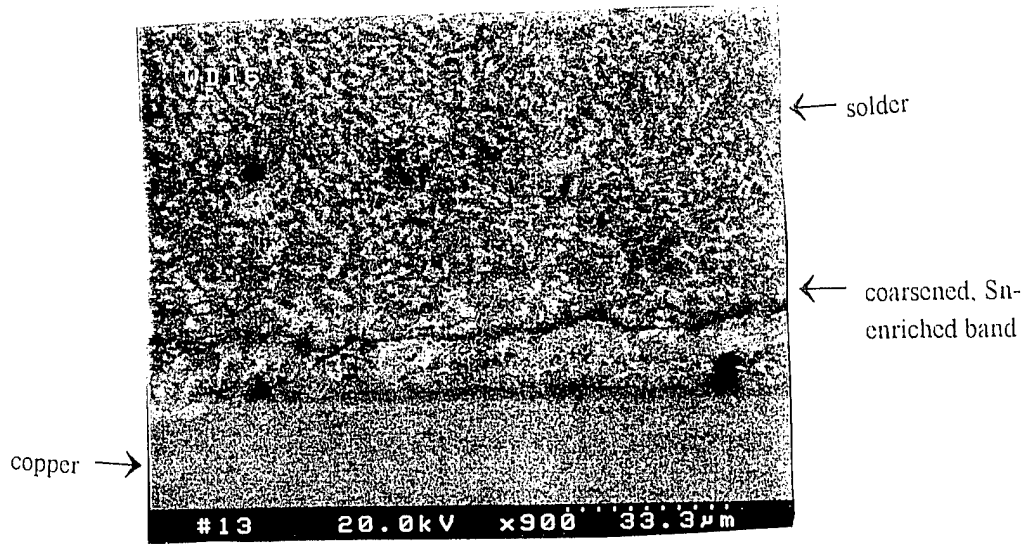


Sn-Pb-5Cu, 2 cracks parallel to Cu substrate, one crack in intermetallic layer, other crack in solder, back-scattered mode

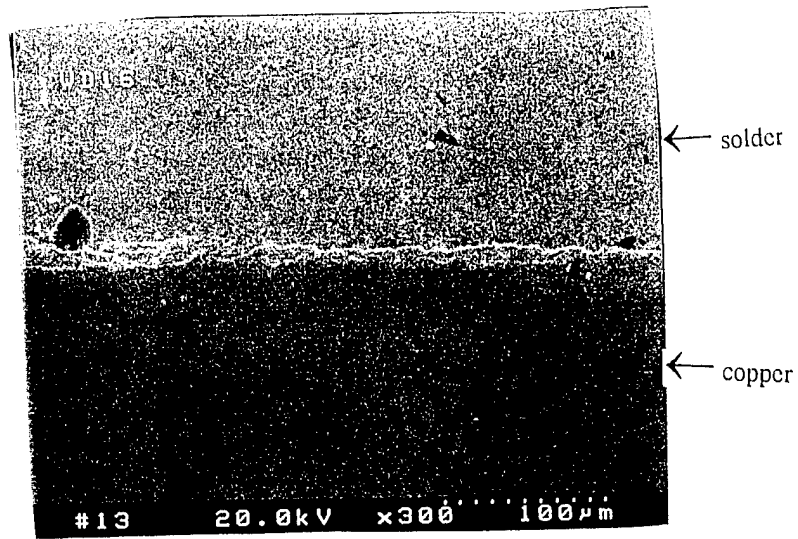


Sn-Pb-5Cu, crack initially near Cu, propagates into the middle of the solder joint

Figure 52. SEM micrograph of Sn-Pb-5%Cu alloy after TMF test.

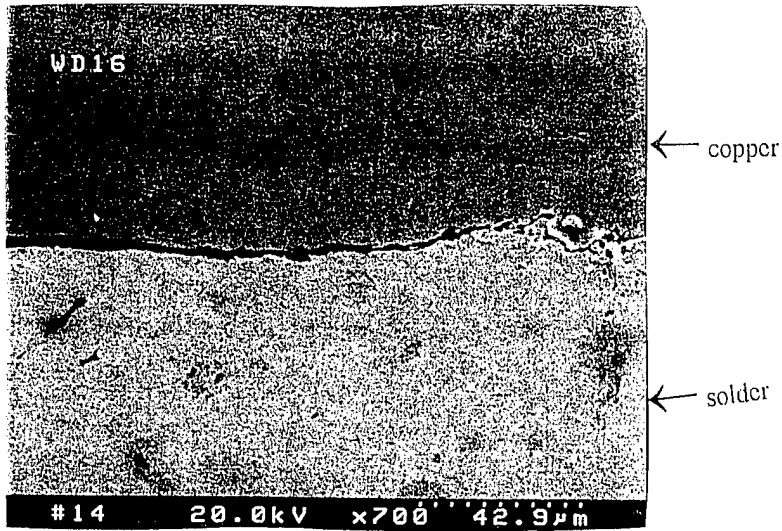


Sn-Pb-2.5Ag, crack in coarsened band near Cu, back-scattered mode

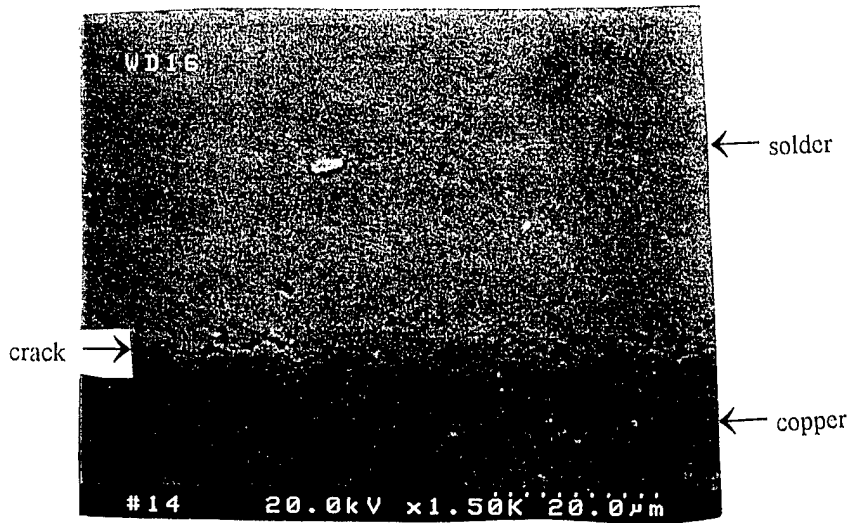


Sn-Pb-2.5Ag, crack runs parallel to Cu substrate

Figure 53. SEM micrograph of Sn-Pb-2.5%Ag alloy after TMF test.



Sn-5Sb, crack runs near Cu substrate, primarily at intermetallic-solder interface



Sn-5Sb, small crack near Cu substrate

Figure 54. SEM micrograph of Sn-Sb alloy after TMF test.

Table 13 lists the measurements made for samples failed in TMF tests. The size and volume % values were measured in the middle of the solder joint. Most of the samples experienced a large growth in the size of the intermetallic layer after the fatigue test.

Table 13. Summary of measurements made for SEM micrographs after TMF tests.

composition	average cycles to failure	intermetallic thickness (μm)	average diameter of Pb-phases (μm)	volume % of Pb-phases	coarsened band?
AMT 63Sn-37Pb	94.4	2.9	2.74	24.9 %	yes
HPM 63Sn-37Pb	116.0	3.8	1.99	29.5 %	yes
IEM 63Sn-37Pb	106	2.7	1.83	32.1 %	yes
AMT FRS	73	6.0	1.96	18.7 %	no
63Sn-34.5Pb-2.5Ni	173.0	10.3	3.61	36.1 %	yes
63Sn-32Pb-5Ni	265 +	16.0	1.85	20.7 %	no
63Sn-32Pb-5Cu	124.0	6.9	1.39	15.5 %	no
63Sn-34.5Pb-2.5In	68.0	4.5	1.37	24.6 %	slightly
63Sn-34.5Pb-2.5Ag	53.0	5.7	1.62	23.2 %	yes
95Sn-5Sb	280 +	7.5			
90Sn-3.2Ag-6.8Bi	164	5.3			

Table 14 lists where cracks were observed to form and grow for the thermomechanically fatigued samples examined by SEM.

Table 14. Crack propagation sites for samples failed in thermomechanical fatigue.

composition	alloy type	sites for crack initiation and propagation
AMT 63Sn-37Pb	eutectic Sn-Pb	in coarsened band
HPM 63Sn-37Pb	eutectic Sn-Pb	in coarsened band and at intermetallics-solder interface
IEM 63Sn-37Pb	eutectic Sn-Pb	in coarsened band
AMT FRS	near-eutectic	at intermetallics-solder interface
63Sn-34.5Pb-2.5Ni	dispersion strengthened	in coarsened bands
63Sn-32Pb-5Ni	dispersion strengthened	in intermetallics layer
63Sn-32Pb-5Cu	dispersion strengthened	initiate in intermetallics, propagates at intermetallics-solder interface, then runs through middle of joint
63Sn-34.5Pb-2.5In	solid solution strengthened	in coarsened band and at intermetallics-solder interface
63Sn-34.5Pb-2.5Ag	solid solution strengthened	in coarsened band
95Sn-5Sb	lead free, high melting temperature	at intermetallics-solder interface

The samples which contained coarsened band had about 10 % increase in the average diameter of Pb phases near the Cu substrate as compared to the middle of the joint sample. Moreover, all the samples with coarsened band also had at least a 10 % reduction in the volume percentage of Pb rich phases near the Cu substrate. This suggests that a Sn enrichment process is occurring in conjunction with the heterogeneous coarsening near the Cu substrate. One of the possible explanation to this is the diffusion of Sn from supersaturated Pb phase. The diffusion is assisted by the stress and temperature gradients during thermomechanical fatigue. Near the interface, stress concentrations exist due to the differences in the elastic moduli between these two materials[16].

The Sn enrichment can accelerate the failure of these samples. Because at 100 ° C, Sn is closer to its melting point ($T_m=0.74$). It is to be expected that the Sn grains will have worse creep resistance than the Pb grains whose melting point is higher than Sn. An EDS analysis showed that the grains in the Sn-enriched regions become moderately segregated into pure Sn and pure Pb grains. Therefore the temperature fluctuations associated with TMF tests may create a large amount of strain incompatibility between the purified Sn and Pb phases which can result in the formation of cavities at their interfaces. These cavities can interconnect to form cracks , which would spread throughout the coarsened regions.

In summary, dispersion strengthened and lead free alloys had the longest lifetimes followed by eutectic Sn-Pb. The solid solution strengthened compositions had the lowest lifetimes. The dispersion strengthened solders with larger volume fractions of dispersoids were effective in impeding the formation of heterogeneously coarsened areas. In the case of Sn-Pb and solid solution strengthened alloys, heterogeneously coarsened areas form because of strain and temperature assisted diffusion. Sn enrichment of coarsened areas contributes to the failure of the solder joint.

5.5 Straddle Board Tests

Straddle board testing was conducted to obtain information which can be correlated to an actual SMT joint. Straddle board tests involved making assemblies of different types of devices on FR-4 boards using solder pastes and subjecting these boards to thermal cycling in the temperature range from -55 ° C to +125 ° C at a rate of one cycle per hour.

A straddle board test was initiated by Army Research Center and conducted at Electronics Manufacturing Productivity Facility (EMPF) , Indianapolis. In this test, LCC devices were assembled on FR-4 boards at EMPF. The alloy composition of solders used in this study and their evaluation are summarized in Table 15. Typical reflow profiles of solders used in this study are shown in Figures 55 to 57. Electrical continuity tests were carried out by Army research Laboratory (ARL).

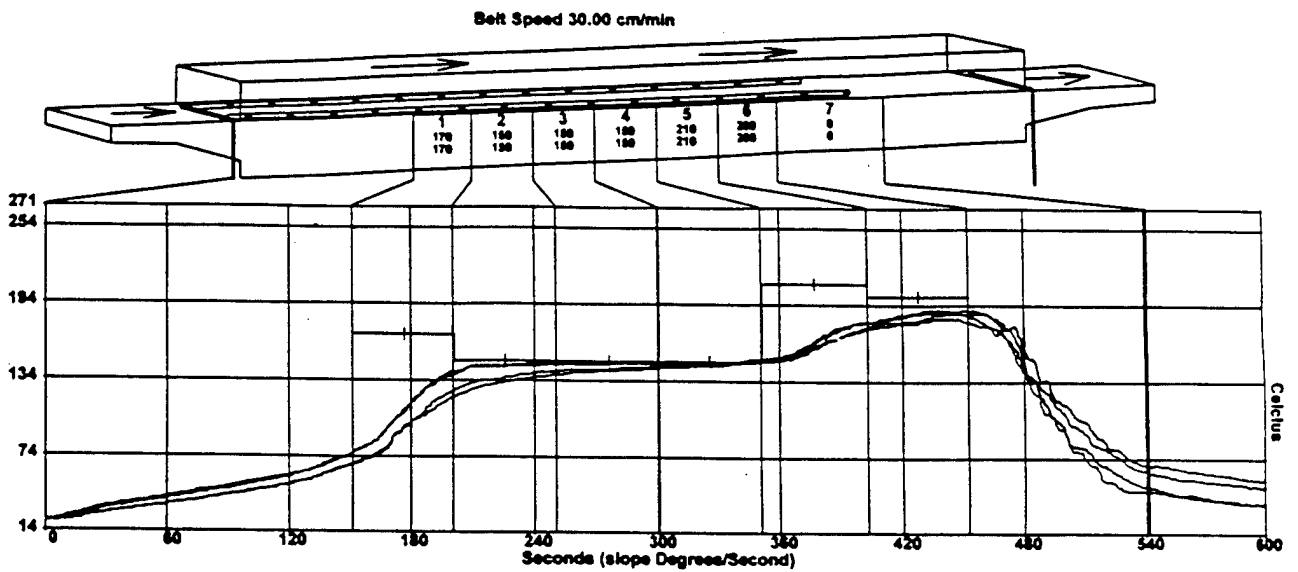
Table 15. Solder compositions used in the straddle board testing.

SURFACE MOUNT TECHNOLOGY Visual Inspection

LOT NO.	ALLOY COMPOSITION	REFLOW TEMPERATURE PROFILE	COMMENTS ON THE SOLDER JOINTS
95	HPM 63Sn-37Pb	mid-range	good wetting, solder balls, shiny joints nice fillets
92	HPM 63Sn-32Pb	mid-range	good wetting, solder balls, shiny joints nice fillets
90	5Cu HPM 63Sn-32Pb 5Ni	mid-range	rough and dull appearance, did not wet as as good as #95 and #92, solder pooling, LCC at U1 misaligned
91	HPM 63Sn 34.5Pb-2.5Ni	mid-range	less roughness, more shiny appearance, some voids on some pads. Pin holes, solder-balls observed. In general wetting is good.
93	HPM 63Sn 34.5Pb-2.5In	mid-range	Capillary flow-up. Shiny appearance, solder balling
94	HPM 63 Sn 34.5Pb-2.5Ag	mid-range	Grainy appearance. Solder balling. Cracking on some pads. Pitting.
96	HPM 43Sn 57Bi	low-range	wetting good. Grainy, shiny, solder balling
97	HPM 43Sn 52Bi-5Cu	low-range & mid-range	Did not reflow at both temperature ranges
98	HPM 43Sn 52Bi-5Ni	low-range & mid-range	Did not reflow at both temperature ranges
94A	HPM 63Sn 34.5Pb-2.5Ag	high-range	Grainy and dull appearance, pin-holes, solder balls, stress lines from fillet area. Good wetting.
87	HPM 90 Sn 3.2 Ag-6.8 Bi	high-range	Dull appearance. Fine Grains. Good wetting. Solder balls.
88	HPM 90 Sn 3 Ag-4.2 Bi 6.8 In	high-range	Dull appearance. Fine Grains. Wetting OK. Dewetting on some pads. Solder balls.
89	90 Sn - %Sb	mid-range	Shiny appearance. Dewetting, Solder balls, Pooling on pads. One device is bad because it failed in continuity test.
C	63Sn-37 Pb Control	mid-range	Good fillets. Shiny. Grainy appearance. Did not wet till the end of the pads. Solder balls. One solder ball seen with naked eye.

File FUSION2.PRF
 Date Time Tue 03/07/95 05:44:43
 Start Time Tue 03/07/95 05:38:45
 Postprint Time Tue 03/07/95 05:44:43

KIC Prophet™
 Process Monitoring System
 San Diego, CA (619)773-6555



Position	Max
1=icc68	183.3
2=icc28	190.0
3=icc68	187.8
4=icc28	188.4

SURFACE MOUNT TECHNOLOGY
Electronic Manufacturing Productivity Facility
REFLOW PROFILE

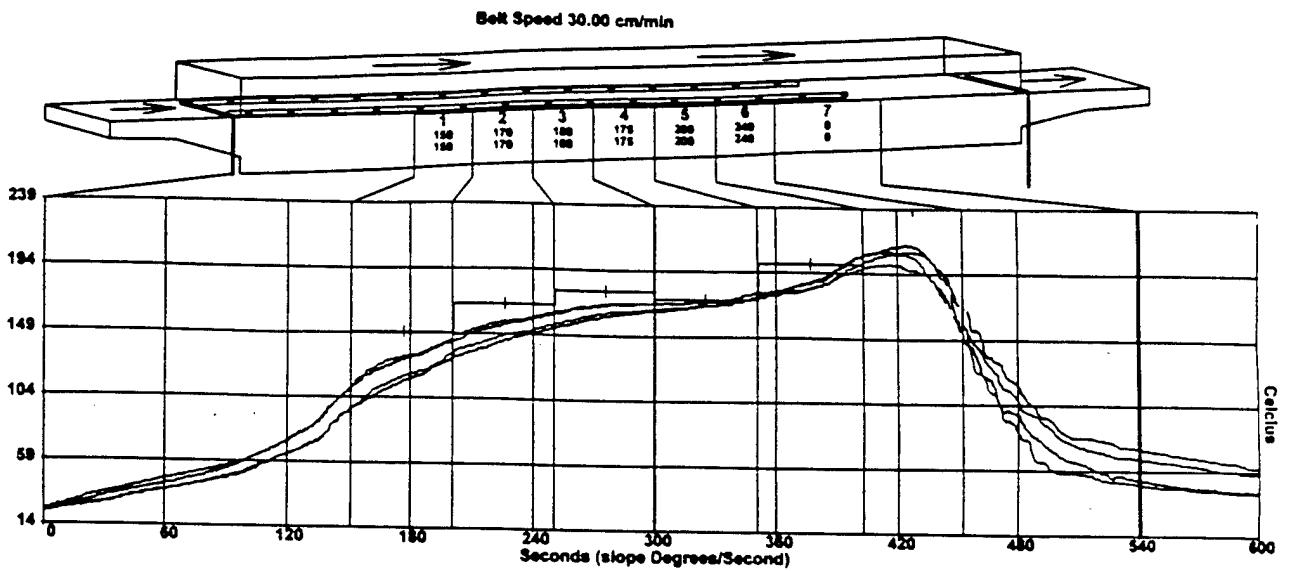
● low-range

Experiment Name _____
 Setup Profile _____
 Furnace Temp _____
 Preheat Temp _____
 Oven Size _____
 Experiment Start Time 03/07/95 05:38:45
 Input Name FUSION2.KDF File 21632

Figure 55. Typical reflow profile of low range solder paste.

File PUSK001.KDF
 Data Time Thu 02/23/96 11:49:43
 Start Time Thu 02/23/96 11:36:39
 Postprint Time Thu 02/23/96 11:49:43

KIC Prophet™
 Process Monitoring System
 San Diego, CA (619)773-6666



Position	Max
Profile	
1-loc68	201.1
2-loc28	210.0
3-loc68	208.4
4-loc28	214.8

SURFACE MOUNT TECHNOLOGY
Electronic Manufacturing Productivity Facility
REFLOW PROFILE

● mid-range

Experiment Notes

Standard Test Lead Profile

PROCESS NAME

PROCESS NAME

OVER

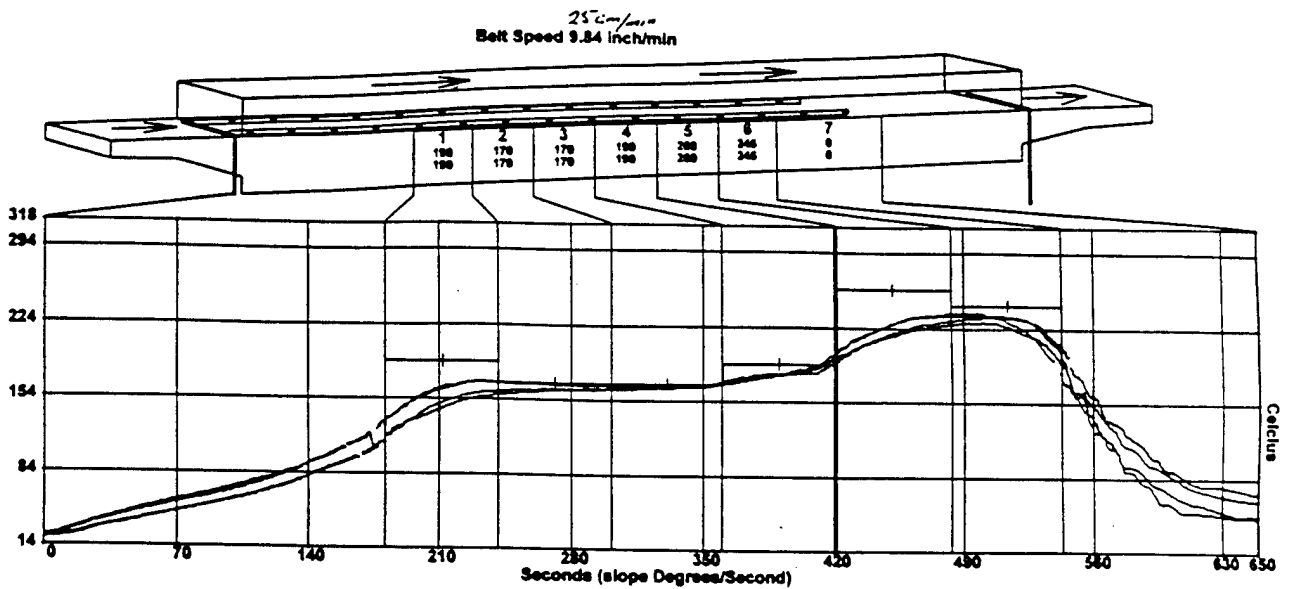
Experiment Start Time 02/23/96 11:36:39

Input Name PUSK001.KDF Pwr 21168

Figure 56. Typical reflow profile of mid range solder paste.

File FUSK0N3.PRU
 Data Time Tue 03/07/96 11:58:10
 Start Time Tue 03/07/96 11:58:10
 Footprint Time Tue 03/07/96 11:58:10

KICProphet™
 Process Monitoring System
 San Diego, CA (619) 573-0000



Position	Max
1-loc08	230.0
2-loc28	238.3
3-loc68	236.0
4-loc28	236.7

SURFACE MOUNT TECHNOLOGY
Electronic Manufacturing Productivity Facility
REFLOW PROFILE

● high-range

Department Name _____
 Title/Shift Profile _____
 PROGRAM NAME _____
 PROGRAM NUMBER _____
 DATE 1996 _____
 Department Start Time 03/07/96 11:58:10
 Input Name FUSK0N3.KICP Pwr 20004

Figure 57. Typical reflow profile of high range solder paste.

For the thermal cycling test conducted at EMPF, the temperature extremes were +125 ° C and -55 ° C with a complete cycle time of 60 minutes. The hot dwell was set for 17 minutes and cold dwell for 21 minutes with a positive ramp of 12 minutes and negative ramp of 21 minutes. An envirotronics chamber , model EV33-2-705-RS was used for thermal cycling the assembled boards and a computer software HP-VEE was used to monitor the data.

The electrical resistivity measurements were made in approximately 30 minute intervals, at the extremes of the oven temperature ranges. When a solder joint failed, the resistance reading would increase to an infinite number indicating an open circuit. In addition, resistance values which were higher than 300 % of the nominal value were considered hard failures. The test ran from between 900 and 1000 cycles and 11 of the 96 components did not fail before the test was stopped. During the test there was a power failure (between measurements 160 and 170). Therefore some of the data collected during that period is considered bad and can not be used for evaluation. Table 16 summarizes the results of the thermal cycling tests of straddle boards assembled using solder pastes of different solder alloy compositions.

Table 16. Results of the thermal cycling tests of the straddle boards.

	<u>U1</u>	<u>U2</u>	<u>U3</u>	<u>U4</u>	<u>U5</u>	<u>U6</u>	<u>U7</u>	<u>U8</u>		
C	171	236	420	204	**	**	**	1385		
87	20	24	63	47	1278	**	**	**		
88	37	27	77	54	724	174	734	1789		
89	171	171	xx	170	1080	1372	1372	1391		
90	88	137	33	169	784	727	1148	892	**	= No Failure
91	171	171	171	170	703	495	609	530	xx	= Internal component failure
92	39	171	171	170	**	1183	1483	1440		
93	171	171	81	108	1420	1387	**	1311		
94	171	171	171	170	1188	1464	**	826		
94a	38	20	398	37	655	1138	**	1391		
95	171	170	324	507	1389	1524	**	**		

The results from the Table 16 indicate that, the control eutectic Pb-Sn solders performed better than the alloy solder compositions. These results are quite contrary to the results observed in thermomechanical fatigue testing of lap-shear joints. The dispersion strengthened solder alloys are much superior to the conventional Pb-Sn eutectic and solid solution strengthened alloys in the TMF tests of lap-shear joints. The results of thermal cycling tests at EMPF may not be conclusive because of the following reasons.

- (i) During reflow of HPM solder paste the oxygen level was much higher than that maintained for reflow of control sample.
- (ii) There was a power failure during thermal cycling test at EMPF. Soon after the power was restored, most of the components failed within a cycle or two. The sudden failure of components soon after restoration of power raises doubts on the validity of the results.
- (iii) Our results of the Thermo Mechanical Fatigue (TMF) tests conducted on the lap shear joints made using HPM solder pastes with IEM flux (The paste prepared at IEM-Fusion Inc.) , show that the life times are significantly higher in nickel and copper containing solders than in the control sample.

Because of the above uncertainties, HPM proposed to conduct an additional thermal cycling test. This involved using one solder paste composition per 6" x 4" FR-4 board and different types of devices including two LCCs with 68 pads and two with 28 pads per board. Boards were made at EMPF and thermal cycling tests were performed at Trace Laboratories , 4633 N.Olcott, Chicago, IL 60656. The solder pastes were made at IEM Fusion Inc., using solder powders supplied by HPM Inc.

The boards were assembled at EMPF. The manufacture of assemblies consists of three major steps. They are screen/stencil printing, picking and placing of components and reflowing. A MPM Ultraprint 2000 series screen/stencil printer was used for screen printing. In this step, the solder paste is basically smeared onto the board uniformly. The board has the necessary locations for different components and after screen printing , the board is ready for the actual components to be placed on them. A Mydata UFP-11 pick and place system was used to pick and place the components. This equipment is a versatile and fully automated unit which is programmed to pick the desired components and place exactly on the required location of the board.

An Electrovet OmniFlo 7 convection oven was used to reflow the solder on the boards ensuring the soldering of components onto the boards. This oven has got 7 zones and is preprogrammed for required temperature and rate of heating. The solder characteristics determines the reflow profile to be used. After the assemblies were made the boards were evaluated for quality by (i) a visual inspection of the boards for bridging or any damage (ii) a closer inspection for any other defects such as voids under a low magnification microscope and (iii) checking for a good electrical connection using a multi meter.

The assembled board at EMPF consisted of three types of components . They are (i) LCC's of different sizes (ii) BGA's and (iii) Fine pitch (BQFP) . The different types of components used in the present study add versatility and provides a wider range of data for the performance of the solder alloys in different types of applications.

Before the assemblies were made, the melting temperatures of all the solder paste and flux volatilization were determined using Differential Scanning Calorimetry (DSC) using Thermogravimetric analysis (TGA) respectively. This information was used to develop reflow profiles. Table 17 lists the flux activation temperatures and melting temperatures of various solder pastes used in the study.

Figure 58, shows the drawing of the straddle board with assembled devices. There were components on all the locations except U4 and U14. LCC's were assembled on locations U1, U5, U6, U16, U15 and U11. The fine pitch BQFP devices were assembled on locations U2 and U1 and the BGA devices were assembled on U3, U7, U 17 and U13. Figure 59 shows the test set-up of the thermal cycling test conducted at Trace Laboratory. Using a 4 point digital ohmmeter the electrical resistance was measured. The board temperatures were monitored by thermocouples in the chamber. Thermal mapping was carried out to ensure that all the devices were receiving the same temperature environment and were tracking with respect to the required temperature profile. The temperature cycling consisted of maintaining the devices at 125 ° C for 21 minutes and cooled to -55 ° C at the rate of 8.5 ° C per minute. The boards were held at -55 ° C for 7 minutes and ramped up to 125 ° C in 11 minutes. The entire cycle lasts for 60 minutes. A 1000 cycles were completed and the devices were monitored during thermal cycling. The information of increases in the resistance was stored on a computer hardware. Table 18 summarizes the thermal cycling test data for various solder compositions.

Table 17. Flux activation and melting temperatures of solder pastes and alloy solders.

Material Tested	Flux Activation Temperature	Alloy Melting Temperature
HMPI-1	120 °C - 130 °C	184.78 °C
HPMI-2	120 °C - 130 °C	184.93 °C
HPMI-3	120 °C - 130 °C	183.90 °C
HPMI-4	120 °C - 130 °C	184.42 °C
HPMI-5	120 °C - 130 °C	186.39 °C
HPMI-6	120 °C - 130 °C	183.79 °C
HPMI-7	120 °C - 130 °C	181.35 °C
HPMI-8	120 °C - 130 °C	237.77 °C
HPMI-9	120 °C - 130 °C	206.62 °C
HPMI-10	120 °C - 130 °C	181.09 °C
HPMI-11	120 °C - 130 °C	213.00 °C
HPMI-12	120 °C - 130 °C	184.59 °C

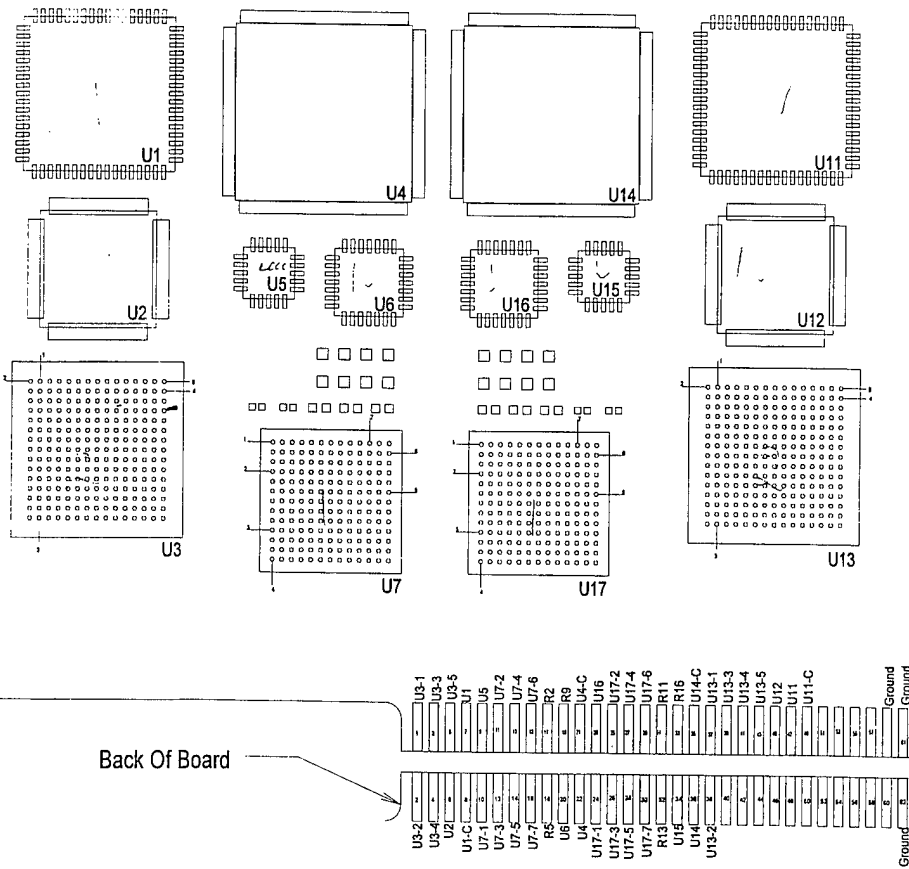


Figure 58. Drawing of the straddle board with various devices.

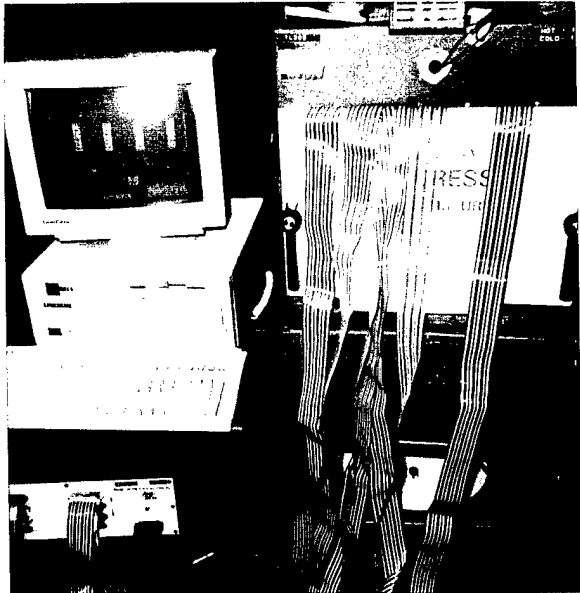


Figure 59. The test set-up used in thermal cycling of straddle board.

Table 18. Summary of the results of thermal cycling test.

Alloy	U1	U5	U6	U11	U15	U16
HPM 6337	204, 234	773, 593	612, NF	288, 170	791, 748	977, 920
AMT 6337	81, 61	719, 649	883, 889	288, 282	656, NF	814, 564
AMT FRS	182	662	942	260	743	797
HPM -Pb-Sn- 2.5%Ni	117, 125	601	935, 338	150, 203	689, 352	377, 305
HPM -Pb-Sn- 5%Ni	77, 74, 107	813, 566, 615	567, 356, 84	74, 15 14	673,578, 822	328,564, 639
HPM -Pb-Sn- 5% Cu	155, 162	947, 609	883, 794	89, 154	792, 904	599, 949
HPM -Pb-Sn- 2.5%Ag	288, 225	582, NF	927, 767	143, 101	NF 883	730, 897
HPM -Pb-Sn- Ag-Bi-In	122	652	NF	97	NF	555
HPM -Pb-Sn- Ag-Bi	32	NF	369	29	NF	409
HPM Sn-Pb -2.5%In	198	662	734	263	758	696
IEM 6337	269	734	NF	131	NF	981

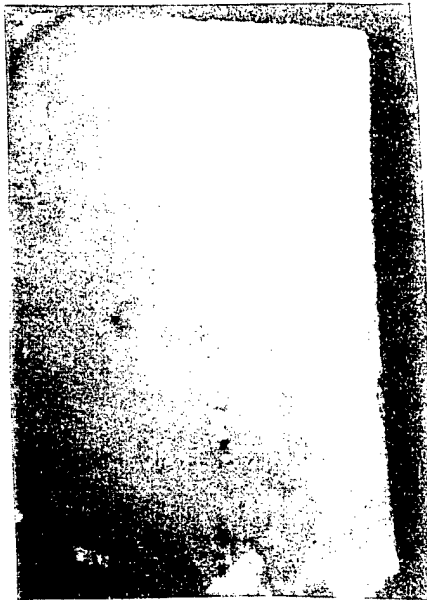
NF=No Failure

After 1000 cycles, components U1, U5, U6, U11, U15, and U16 failed, The other devices did not fail for any of the composition tested. As indicated from Table 18, eutectic solder compositions showed better life time values than dispersion strengthened alloy solders. The dispersion strengthened solder compositions may not have performed better than eutectic solder because of the following reasons.

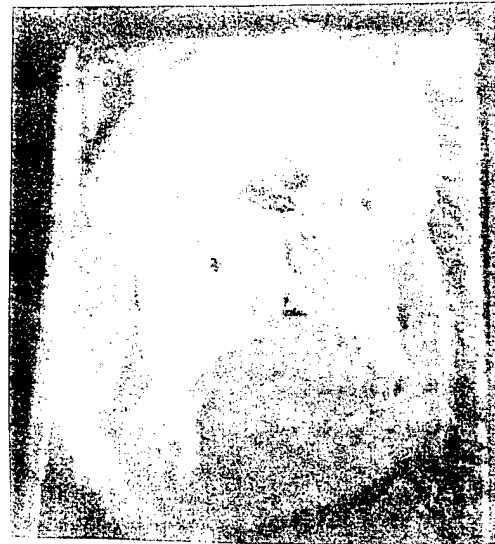
(i) The wetting of dispersion strengthened alloy solder paste may not be as good as eutectic solder paste. Improper wetting of the devices by dispersion strengthened alloy solder paste may have resulted in mechanically weak assemblies. While making assemblies using dispersion strengthened alloy solder pastes, it was observed during the reflowing stages that , gold was still showing in castilations of LCC 68s. This is an indication that, the devices are not strongly attached to the boards. Therefore, a higher reflowing profile was used for some of the alloy solder pastes to improve the wetting marginally. But this marginal improvement may not be satisfactory to result in mechanically strong devices as in the case of eutectic solder pastes.

(ii) The flux used by IEM, for making solder paste for various solder compositions was same. The flux used by IEM may be satisfactory for the eutectic compositions. But the flux may not be suitable for alloy solder compositions.

(iii) In the thermomechanical fatigue testing of lap-shear joints, the joints were prepared in very good vacuum. As a result the lap-shear joints were of high quality without any oxygen contamination. On the other hand, the boards were assembled at EMPF in nitrogen atmosphere. Therefore the conditions of specimen preparation were not the same between the lap-shear joint preparation and the assembly of boards. It has been observed that [9], the degree of vacuum can play a significant role in the quality of joints obtained. Figures 60 (a) and (b) show the fracture surfaces of joints made in high vacuum (a mechanical pump and a diffusion pump) and a low vacuum (only a mechanical pump). It is clear that voids are more in the joints made in low vacuum.

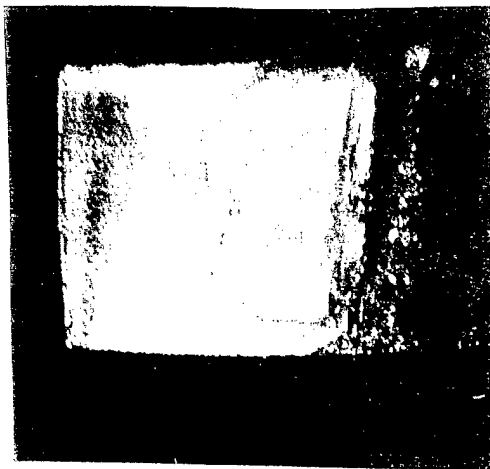


AMT 63Sn-37Pb

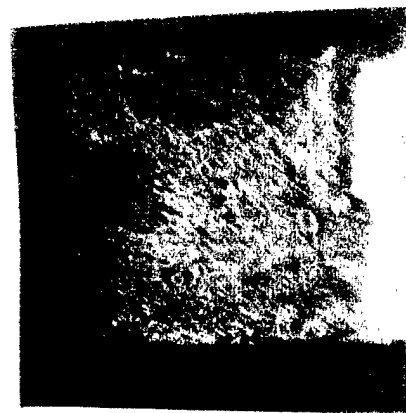


Sn-Pb-5Ni

(a)



HPM 63Sn-37Pb



Sn-Pb-5Ni

(b)

Figure 60. Fracture surfaces of joints made in (a) high vacuum and (b) low vacuum.

5.6 Scaling Up Of HPM's Powder Production Facility To 500 Lbs Per Batch

The powder production equipment was scaled in capacity up from 100 lbs per batch to 500 lbs per batch. The lay out of the 500 lbs powder production equipment is shown schematically in Figure 61.

Scale-up to Commercial Production Level of 500 lbs.

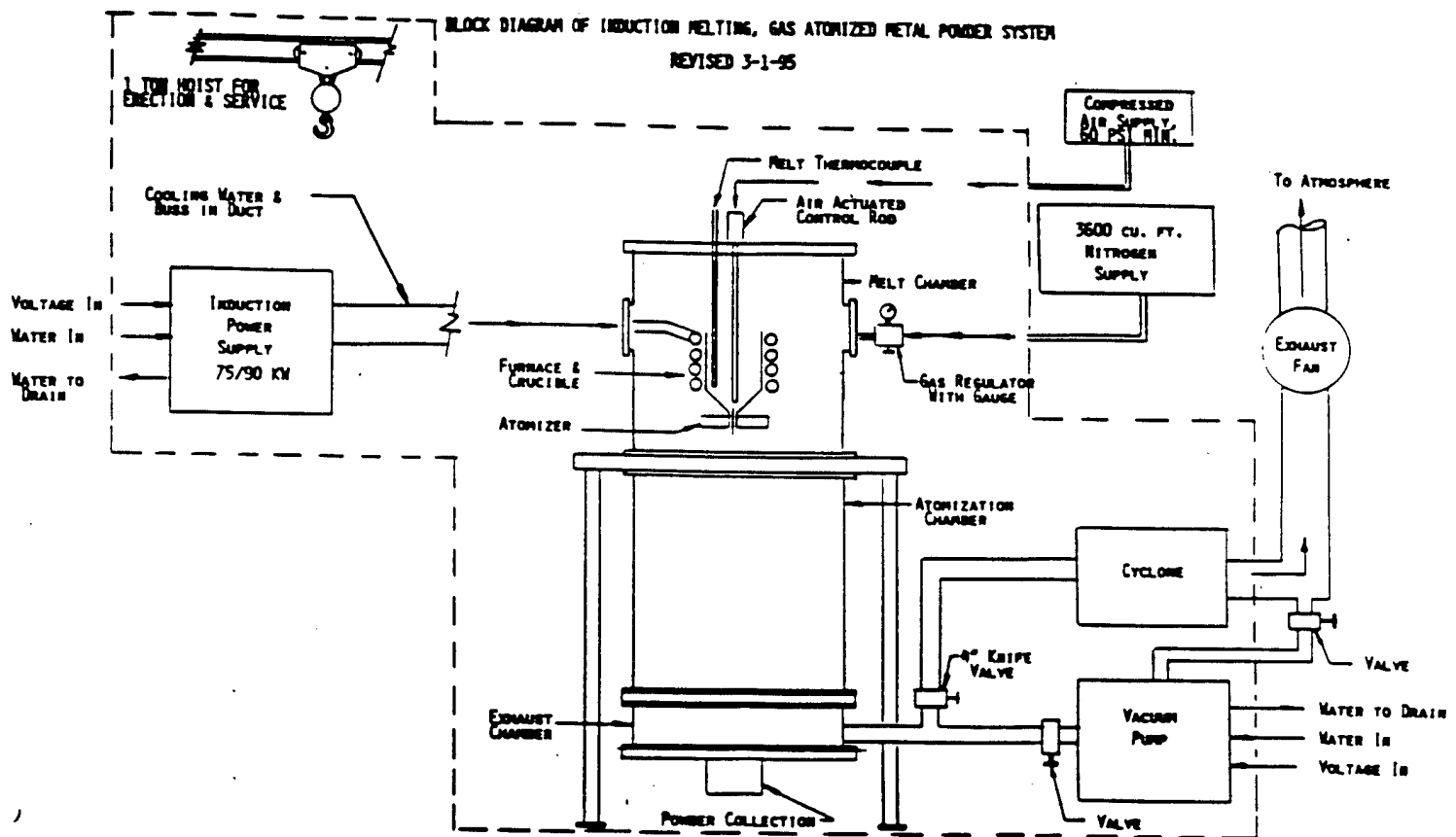


Figure 61. Lay out of HPM's 500 lbs per batch powder production equipment.

The primary consideration in the design of 500 lbs per batch powder production equipment was to make it make more economical in production by increasing the yield of quality powders. In this direction, the atomizer was redesigned. The number of holes in the stainless steel atomizer were increased from 12 to 18. The earlier design of convergent-divergent type was modified to convergent type and the throat area of the atomizer was reduced. These design changes are based on gas flow dynamics and is meant to reduce the gas consumption and also to increase the effective gas pressure at the atomization nozzle. The melting chamber was also redesigned. Figure 62 shows the schematic of the new 500 lbs chamber with new atomizer.

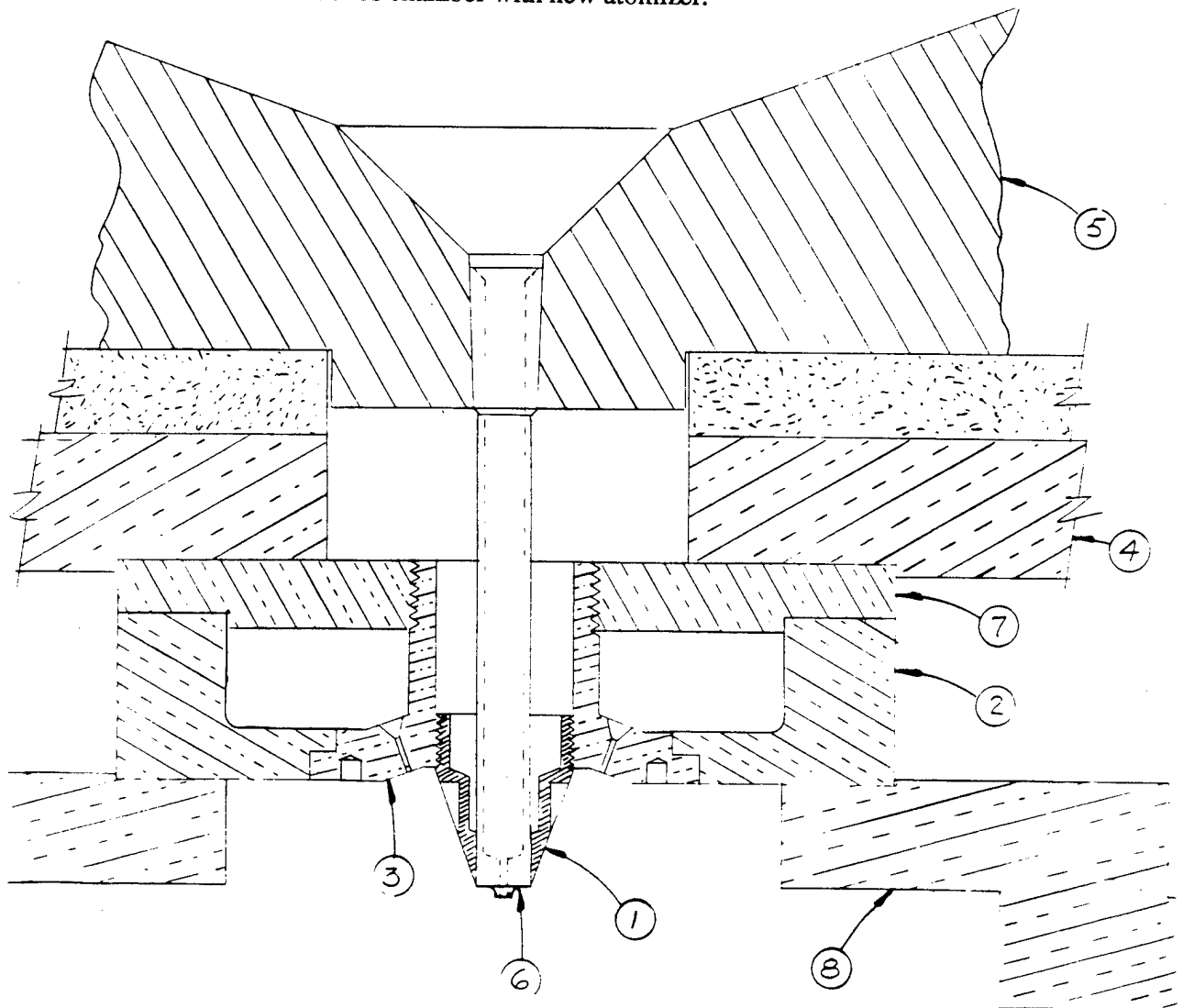


Figure 62. The schematic diagram of new convergent type atomizer.

Figure 63 shows the stainless steel guide tube assembly redesigned for 500 lbs per batch powder maker. The guide tube assembly was modified several times to ensure a steady stream of molten alloy without melt freeze up. Several experiments were performed to optimize the design. A graphite tip of varying diameters at the end of guide tube was introduced as a new feature and was used to vary the metal stream diameter.

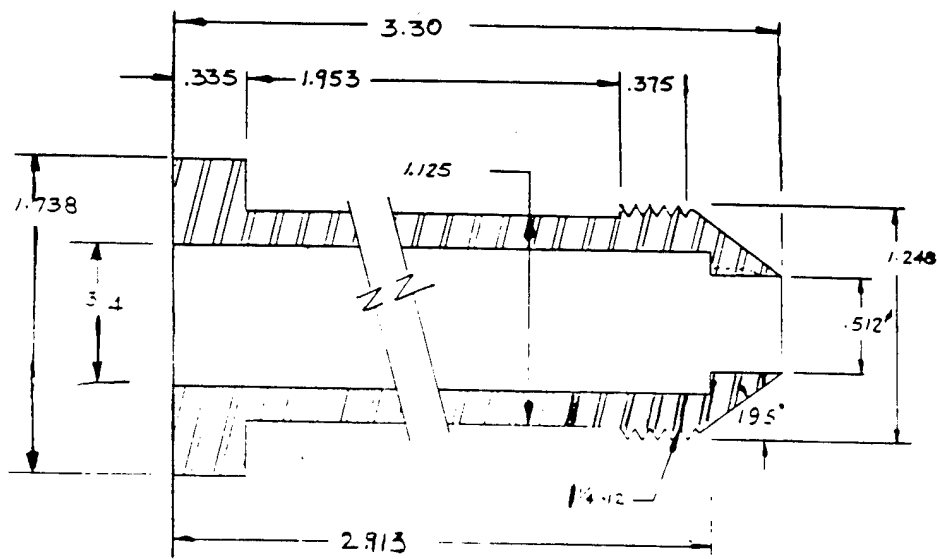


Figure 63. Schematic diagram of modified guide tube assembly.

The chamber frame stairs and landing for the 500 lbs powder production equipment is shown schematically in Figure 64. The flight distance for the atomized droplets has to optimum to get free flowing powders at the end of atomization run. Therefore an atomization chamber of suitable height was chosen. Figure 65 shows the drawing of the chamber frame built for 500 lbs powder maker.

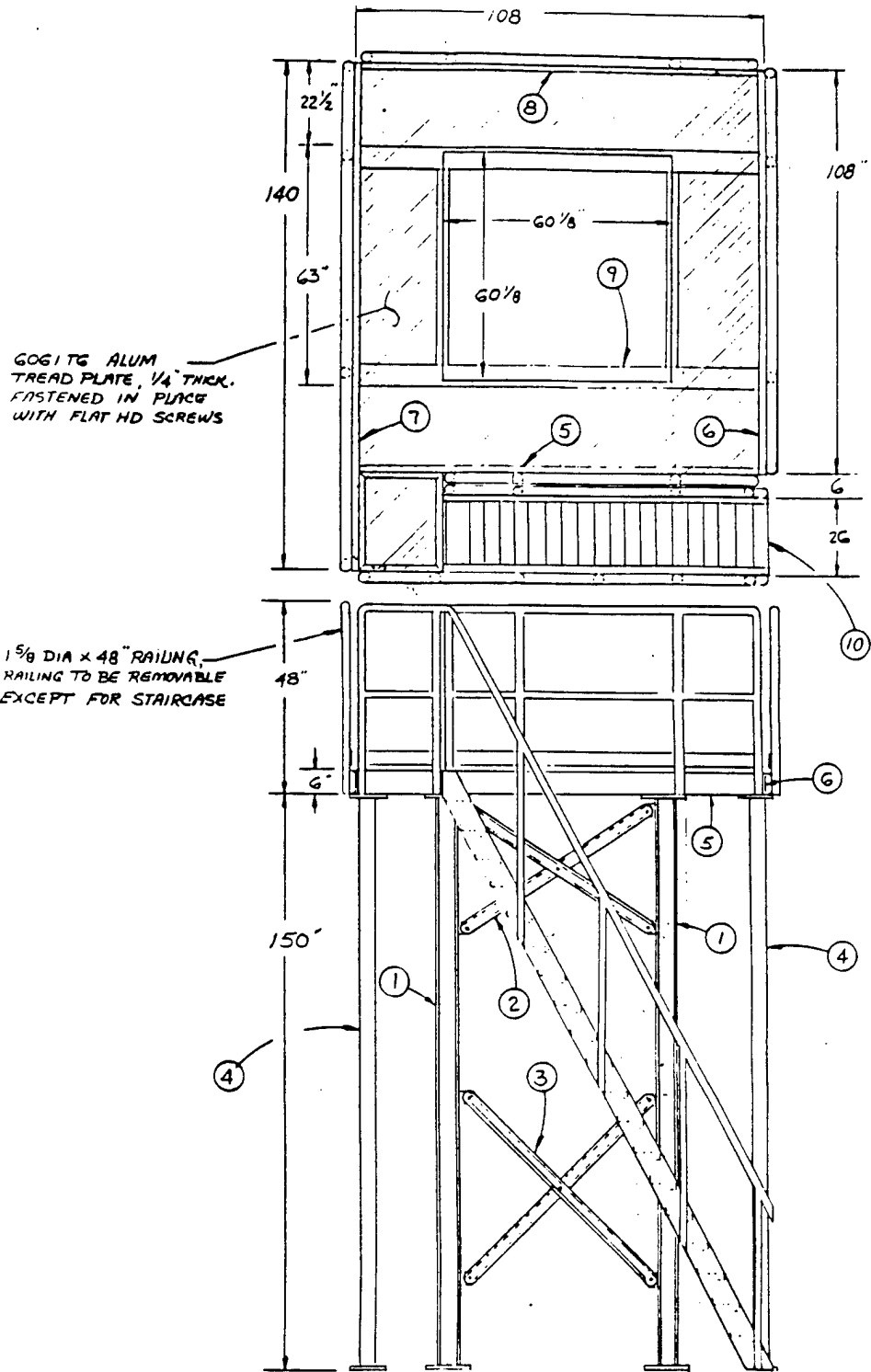


Figure 64. Stairs and landing drawing of the 500 pounds per batch powder production equipment.

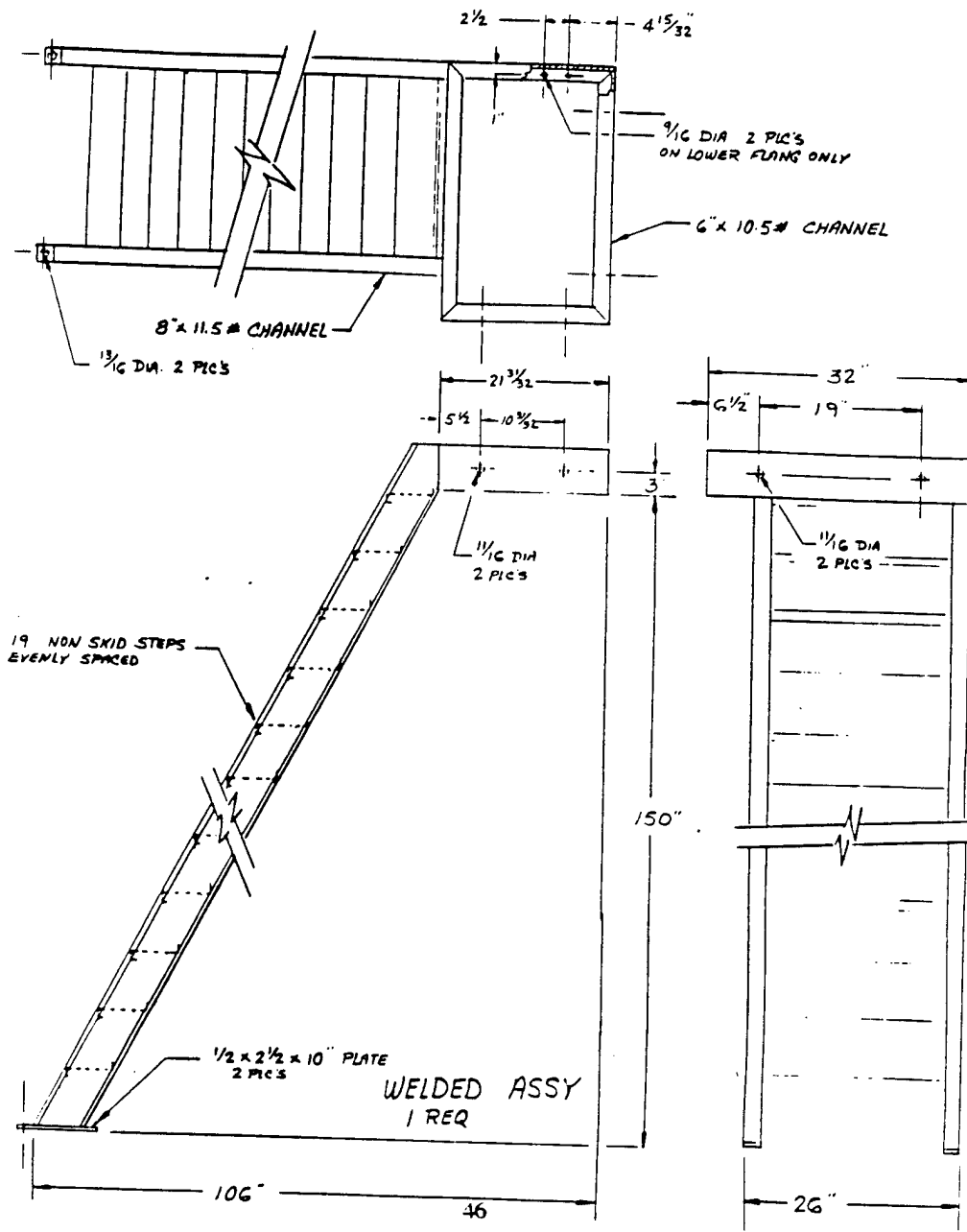


Figure 65. Engineering drawing of the 500 pounds per batch powder production equipment (a) top view and (b) side view.

A new cyclone with a capacity of 800 CFM was used in the 500 lbs powder production equipment .

5.6.1 Production of eutectic lead-tin and composite lead-tin powders.

The 500 lbs per batch powder production equipment was successfully used to produce 30 lbs batches of eutectic and composite solder powders. The process parameters used typically for processing eutectic solder powders, are shown in Table 19. The powder size distribution obtained after sieving in a mechanical sieve shaker for 20 minutes is shown in Table 20. The percentage yield of 25-44 μm powders is 66.73 % .

Table 19. Process parameters used for processing eutectic solder powders.

Process Parameters	Values
Gas Pressure	400 psi
Exit hole diameter	2.75 mm
Melt temperature	500 ° C

Table 20. Powder size distribution for eutectic solder powders.

Size	Weight percent
< 25 μm	0.9%
25-45 μm	66.73%
45-75 μm	26.28 %
75-106 μm	4.05%
106-212 μm	0.10 %
212-425 μm	0.19%

Figure 66 shows a SEM micrograph of the eutectic solder powder after sieving. The powders are spherical with smooth surface and devoid of any satellites.

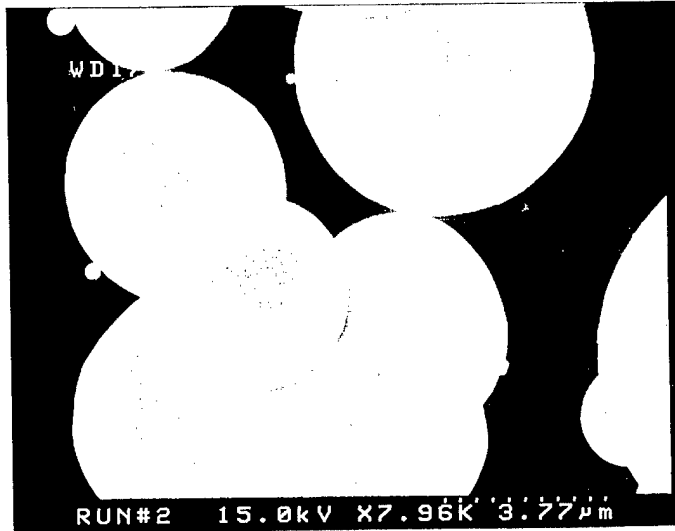


Figure 66. SEM micrograph of sieved eutectic solder powders.

5.6.3 Production of composite Pb-Sn -1 % WC₃, Pb-Sn-1% SiO₂, and Pb-Sn-1% Al₂O₃ powders.

The 500 lbs capacity powder production equipment was used to produce 30 lbs batches of composite solder powders. The process parameters maintained for the three production runs, to produce composite solders containing 1wt% WC₃, 1 wt % SiO₂, and 1 wt % Al₂O₃ are shown in Table 23. In each of these production runs, the additives WC₃, SiO₂ and Al₂O₃ were added in the form of powders along with the lead and tin charge into the crucible. The charge was heated to a temperature of 900 ° C and allowed to stabilize at that temperature for 30 minutes. All these additives have a very high melting points. Therefore, at melt temperatures of 900 ° C, these additives are in the solid state. Since the density of WC₃ is higher than lead-tin liquid alloy, WC₃ powder settled down at the bottom of the crucible. During the atomization, these powders did not create problems of obstructing a free flow of molten metal. But the WC₃ powders did not mix well with molten solder metal. Table 24 shows the size distribution of Sn-Pb-1wt% WC₃ powders after mechanical sieving for 20 minutes. The percentage yield of 25 µm size powders is about 67 %.

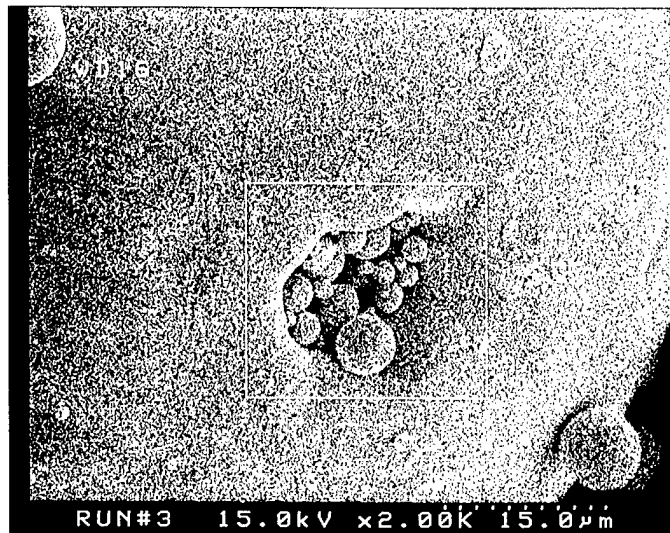
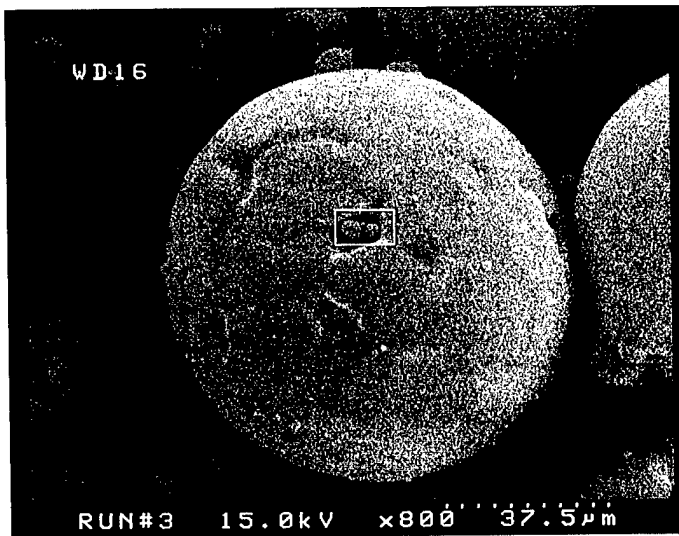
Table 21. Process parameters maintained for production of composite solder powders.

Process Parameters	Values
Gas Pressure	300 psi
Exit hole diameter	2.75 mm
Melt temperature	800 ° C

Table 22. Sieve analysis of Pb-Sn-1 wt% WC₃ powders.

Size	Weight percent
< 25 μm	3.5%
25-45 μm	18.05%
45-75 μm	48.95%
75-106 μm	19.05%
106-212 μm	8.8%
212-425 μm	1.67%

Figure 67 shows the SEM micrograph of the Pb-Sn-1wt% WC₃ powders along with the EDAX analysis of an area. As confirmed by the EDAX analysis, the WC₃ powders segregated in the composite solders since they are not mixed well in the liquid metal.



Chi-sqd = 0.82 Livetime = 189.0 Sec.

Standardless Analysis

Element	Relative k-ratio	Error (1-Sigma)	Net Counts	Error (1-Sigma)
Sn-L	0.58965	+/- 0.12388	120	+/- 25
Pb-L	0.00000	+/- 0.00001	0	+/- 0
W -L	0.39479	+/- 0.39479	11	+/- 11
C -K	0.01556	+/- 0.01556	1	+/- 1

Adjustment Factors	K	L	M
Z-Balance:	0.0000	0.0000	0.0000
Shell:	1.0000	1.0000	1.0000

PROZA Correction Acc.Volt.= 15 kV Take-off Angle=32.45 deg
 Number of Iterations = 4

Element	k-ratio (calc.)	ZAF	Atom %	Element Wt %	Wt % Err. (1-Sigma)
Sn-L	0.52036	1.119	50.77	58.21	+/-12.23
Pb-L	0.00000	1.149	0.00	0.00	+/- 0.00
W -L	0.34840	1.108	21.74	38.60	+/-38.60
C -K	0.01373	2.323	27.50	3.19	+/- 3.19
Total			100.00	100.00	

Figure 67. SEM micrograph of the sieved Sn-Pb-1 wt% WC₃ solder powders.

While processing Pb-Sn-1 wt % SiO₂ and Pb-Sn-1 wt % Al₂O₃ composite solders, the SiO₂ and Al₂O₃ powders being lighter than liquid Pb-Sn alloy, floated at the top. Even the stirring action of induction heating did not help to achieve a good mixing of Sn-Pb alloy and the additives. But the additives did not interrupt the flow of molten metal and the atomization was achieved without any problems. After the production runs, it was observed that some amount of SiO₂ and Al₂O₃ powders were left as a residue in the crucible. Table 23 shows the sieve analysis of the Pb-Sn-1 wt % SiO₂ and Pb-Sn-1 wt % Al₂O₃ composite solders, after mechanical sieving for 20 minutes. Figures 68 and 69 show SEM micrograph of Pb-Sn-1 wt % SiO₂ and Pb-Sn-1 wt % Al₂O₃ composite solders. The powders are spherical and the SiO₂ and Al₂O₃ are segregated in the powders without any uniform distribution in the powders.

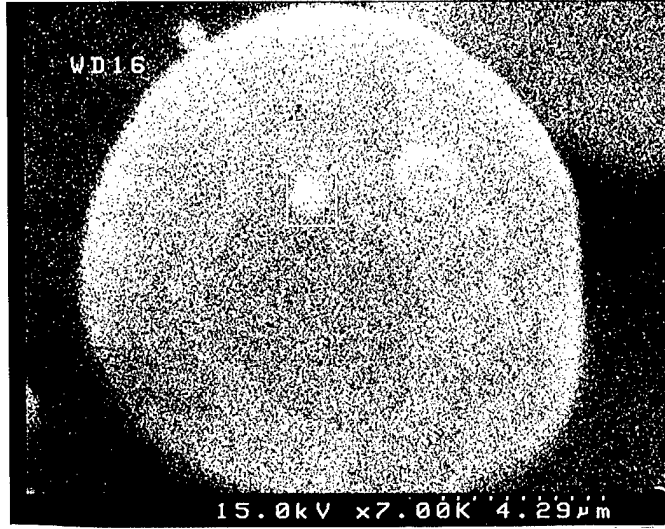
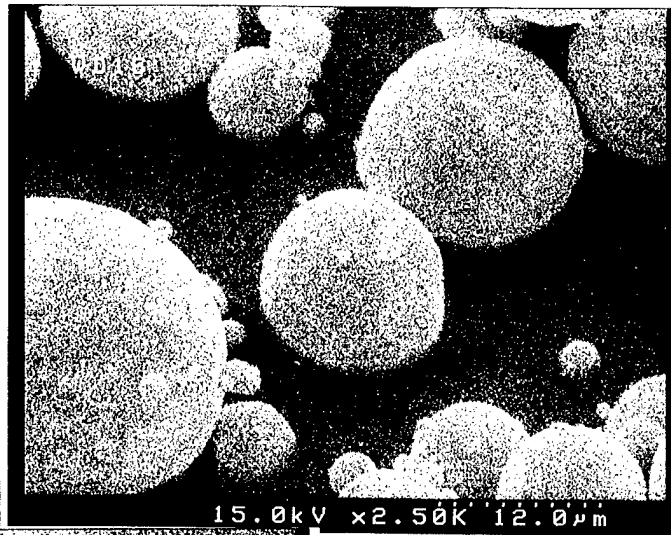
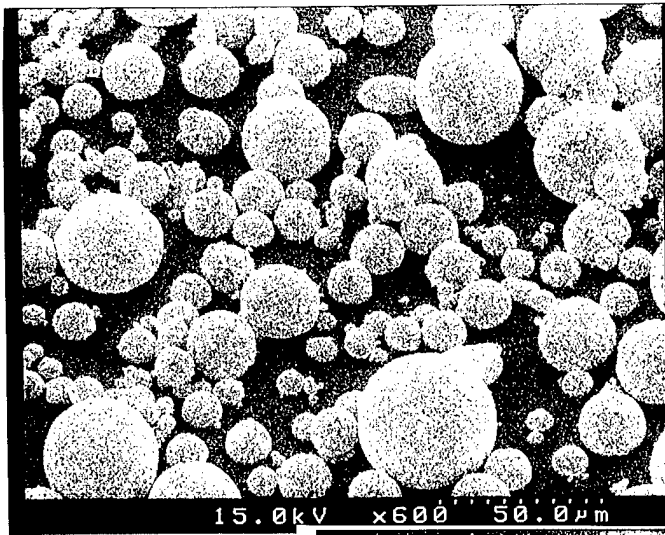
Table 23. Sieve analysis of Pb-Sn-1 wt % SiO₂ and Pb-Sn-1 wt % Al₂O₃ composite solders.

Pb-Sn-1 wt% SiO₂

Size	Weight percent
< 25 μm	0.21%
25-45 μm	37.24%
45-75 μm	32.41 %
75-106 μm	17.78%
106-212 μm	11.15 %
212-425 μm	0.81%

Pb-Sn-1 wt% Al₂O₃

Size	Weight percent
< 25 μm	0.39%
25-45 μm	40.15%
45-75 μm	32.24%
75-106 μm	15.42%
106-212 μm	11.05%
212-425 μm	0.6%



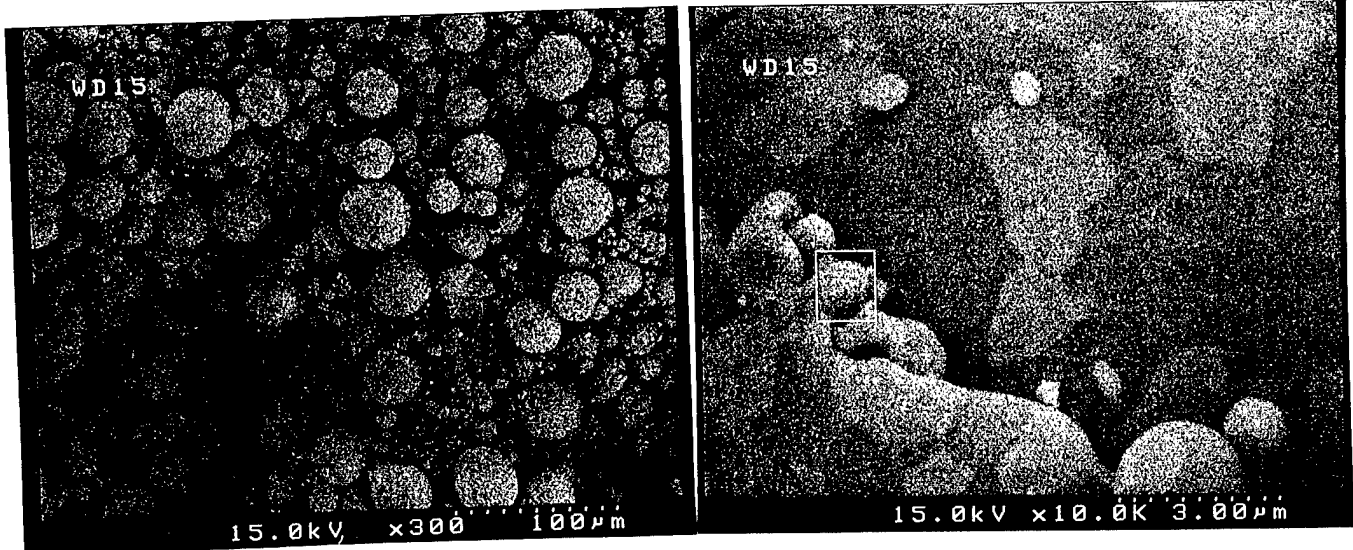
Element	Relative k-ratio	Error (1-Sigma)	Net Counts	Error (1-Sigma)
O -K	0.03895	+/- 0.01558	5 +/-	2
Pb-L	0.00000	+/- 0.00001	0 +/-	0
Sn-L	0.94085	+/- 0.22616	105 +/-	25
Si-K	0.02021	+/- 0.01347	6 +/-	4

Adjustment Factors	K	L	M
Z-Balance:	0.0000	0.0000	0.0000
Shell:	1.0000	1.0000	1.0000

PROZA Correction Acc.Volt.= 15 kV Take-off Angle=31.26 deg
 ** Warning ** Proza Model Limits Exceeded.
 Increase Accel. Voltage and/or Lower Tilt Angle
 Number of Iterations - 5

Element	k-ratio (calc.)	ZAF	Atom %	Element Wt %	Wt % Err. (1-Sigma)	Stoichiometry
O -K	0.03157	4.861	55.30	15.34	+/- 6.14	24.000
Pb-L	0.00000	1.237	0.00	0.00	+/- 0.00	0.000
Sn-L	0.76263	1.080	40.01	82.37	+/-19.80	17.366
Si-K	0.01638	1.395	4.69	2.29	+/- 1.52	2.036
Total			100.00	100.00		

Figure 68. SEM micrograph of the sieved Sn-Pb-1 wt% SiO₂ solder powders.



Chi-sqd = 0.77 Livetime = 134.7 Sec.

Standardless Analysis

Element	Relative k-ratio	Error (1-Sigma)	Net Counts	Error (1-Sigma)
O -K	0.72317 +/-	0.72317	1 +/-	1
Pb-L	0.00000 +/-	0.00001	0 +/-	0
Sn-L	0.00000 +/-	0.00001	0 +/-	2
Al-K	0.27683 +/-	0.55366	1 +/-	2

Adjustment Factors

	K	L	M
Z-Balance:	0.0000	0.0000	0.0000
Shell:	1.0000	1.0000	1.0000

PROZA Correction Acc.Volt.= 15 kV Take-off Angle=31.26 deg
 ** Warning ** Proza Model Limits Exceeded.
 Increase Accel. Voltage and/or Lower Tilt Angle
 Number of Iterations = 8

Element	k-ratio (calc.)	ZAF	Atom %	Element Wt %	Wt % Err. (1-Sigma)	Stoichiometry
O -K	0.47078	1.550	82.01	72.99	+/-72.99	24.000
Pb-L	0.00000	2.019	0.00	0.00	+/- 0.00	0.000
Sn-L	0.00000	1.411	0.00	0.00	+/- 0.00	0.000
Al-K	0.18022	1.499	17.99	27.01	+/-54.02	5.266
Total			100.00	100.00		

Stoichiometry results are based upon 24 Oxygen atoms

Figure 69. SEM micrograph of the sieved Sn-Pb-1 wt% Al₂O₃ solder powders.

6. CONCLUSIONS

- The capacity of the HPM powder production equipment was increased from 10 lbs per batch to 100 lbs per batch. Suitable modifications in the design of the powder production equipment were implemented and several test runs were performed to optimize the production unit. The 100 lbs per batch powder production equipment was used successfully to produce the eutectic and all other ternary and quaternary solder alloy compositions.
- The powders produced from 100 lbs per batch powder production equipment were consolidated and extruded to make bulk tensile test specimens. The mechanical properties such as, tensile strengths, high cycle fatigue and low cycle fatigue properties and creep properties at room and elevated temperatures were determined. The properties were consistent and comparable to those of the powders and compacts made from 10 lbs powder maker. Thus the quality of the powders are maintained even though the production was scaled up.
- A single lap-shear geometry was used as the joint configuration for mechanical property testing of eutectic and other solder alloy compositions. A systematic study of the mechanical properties, such as tensile strengths, low and high cycle fatigue properties, creep properties at room and elevated temperatures and thermomechanical fatigue properties of the lap-shear joints was conducted. Several specimens were tested under the same conditions for reproducibility. A detailed and systematic evaluation of the failed specimens was conducted using optical microscopy, stereo microscopy, SEM and EDS to understand the mechanism of failure.

The dispersion strengthened solder alloy compositions exhibited the best tensile strengths, creep resistance and high cycle fatigue behavior at room and elevated temperatures among lead containing alloys. The dispersion strengthened solder alloy and lead free alloys had the longest life times in the thermomechanical fatigue tests. In the thermomechanical tests, the solid solution strengthened alloys had the lowest life times while the eutectic alloys exhibited life times which were in-between.

Creep results of the lap-shear joints showed that solid solution strengthened and eutectic alloys deformed by dislocation climb. The presence of large threshold stress was observed for dispersion strengthened solder alloys indicative of dispersion strengthening remaining effective at higher temperatures.

In the dispersion strengthened solder alloys, the heterogeneous coarsened regions were not observed unlike eutectic and solid solution strengthened solder alloys during thermomechanical tests. The cracks were observed to initiate and propagate in the heterogeneous coarsened band leading to failure in the solid solution strengthened and eutectic alloys. The obstruction to formation of the heterogeneous bands in the dispersion strengthened and lead free solder alloys resulted in longer life times during thermomechanical tests.

- Two straddle board tests were conducted by subjecting the components on the board to a thermal cycling between -55°C to 125°C , for 1000 hours. The first straddle board tests were conducted at EMPF, Indianapolis and the results were not conclusive. Therefore, the straddle board tests were repeated and carried out at Trace laboratories in Chicago. The eutectic and solid solution strengthened solder alloys showed higher lifetimes than dispersion strengthened and lead free alloys. These results do not agree with those obtained in the thermomechanical tests. The poor performance of the dispersion strengthened and lead free alloys in the straddle board tests may be attributed to (i) unsatisfactory wetting properties of the alloy solder compositions during mounting of components, (ii) absence of good vacuum during reflowing and (iii) use of an unsuitable flux during paste making of these alloy solders.
- The 100 lbs per batch powder production equipment was scaled up to 500 lbs per batch. Several design modifications were implemented and a few test runs were conducted to optimize the powder production. The 500 lbs powder production equipment was successfully used to produce the eutectic solder powders and composite solder powders containing 1wt% Al_2O_3 , 1wt% SiO_2 and 1wt% WC_3 . The powder size distribution of the powders is narrow and the percentage yield of 25-44 μm is about 65 %.

REFERENCES

- [1] S.W.Hinch, Handbook of Surface Mount Technology, John Wiley and Sons, Inc., New York, NY, 1988
- [2] D.S.Steinberg, Vibration Analysis for Electronics Equipment, 2nd ed., Wiley, New York, NY, 1988.
- [3] High Performance Materials ,Inc., Advanced Composite Solders For Microelectronics, Contract No. DAAL02-92-C-0012, Final Technical Report to Harry Diamond Laboratories, Adelphi, MD, September 30, 1992.
- [4] J.Dunkley, Producing Metal Powders, Metals and Materials, p.361, 1990.
- [5] A.Unal, Materials Science and Technology, Vol.3, p.1029, 1989.
- [6] S.Hariprasad, D.Sc.Thesis, Washington University, January 1995.
- [7] Chih-Wei G. Kuo , D.Sc.Thesis, Washington University, August 1994.
- [8] Steven Bayhnam, M.S.Thesis, Washington University, August 1995.
- [9] Brett Goldstein, M.S.Thesis, Washington University, May 1996.
- [10] Solomon,H.D., Solder Joint Reliability, ed. J.H.Lau, Van Nostrand Reinhold,New York, p. 406, 1991.
- [11] Pinizzotto,R.E., Y.Wu, E.H.Jacobs and E.A.Foster, Proceedings of Technical program NEPCON West , Vol.3, p.1284, 1992.
- [12] J.K.Tien, B.C.Hendrix,A.I.Attarwala, Solder Joint Reliability, ed. J.H.Lau, Van Nostrand Reinhold,New York, p. 279, 1991.
- [13] Frear,D.R, N.R.Sorenson,J.S.Martes, Fatigue of Electronic Materials, ASTM STP 1153, eds, S.A.Schroeder and M.R.Mitchell, ASTM, Philadelphia, p. 95,1994.
- [14] S.M.L.Sastry, D.R.Frear, C.G.Kuo and K.L.Jerina, The Mechanics Of Solder Alloy: Wetting and Spreading., eds. F.M.Hosking and D.R.Frear, Van Nostrand Reinhold, New York, p.299, 1993.
- [15] C.G.Kuo, S.M.L.Sastry and K.L.Jerina, Proc. on Microstructures and Mechanical Properties of Aging Materials,The Minerals,Metals and Materials Society, Warrendale, PA, p.417, 1993.
- [16] Clough, R.B., A.J.Bayba, A.J.Shapiro and G.K.Lucey, First ASME International Electronic Packaging Conference, (SUNY, Binghamton, NY, Oct.1993), ed. P.Engel, ASME, 1993